MARSOL

Demonstrating Managed Aquifer Recharge as a Solution to Water Scarcity and Drought

MAR to Improve the Groundwater Status in South Portugal

Deliverable No.	D4.5
Version	1.0
Version Date	31.01.2017
Authors	Teresa E. Leitão, J.P. Lobo Ferreira, Tiago Martins, Manuel M. Oliveira, Maria José Henriques (LNEC) Tiago Carvalho, José Martins de Carvalho, Rui Agostinho, Rita Carvalho, Raquel Sousa (TARH) José Paulo Monteiro, Luís R.D. Costa, Rui Hugman (UAlg) Rogério Mota, Elsa Mesquita, João Rogeiro, Maria João Rosa (LNEC)
Dissemination Level	PU
Status	Final

The MARSOL project has received funding from the European Union's Seventh Framework Programme for Research, Technological Development and Demonstration under grant agreement no 619120.

Contents

Figures

Tables

1. INTRODUCTION AND MAIN GOALS

This report integrates an update of all the relevant work done for WP4 “DEMO Site 2: Algarve and Alentejo, South Portugal”, previously reported. This Deliverable 4.5, together with Deliverable 4.4 concerning hydrogeological modelling at the South Portugal MARSOL demonstration sites, summarize all work performed in the Portuguese DEMO sites.

The main objectives of WP4 are to demonstrate how MAR can contribute as an alternative source of water, in the context of an integrated and inter-annual water resources management, as well as in solving groundwater quality problems caused by previous agricultural practices and wastewater discharges.

Three DEMO sites (Figure 1) have been chosen for WP4:

- PT1: Rio Seco and Campina de Faro aquifer system (Algarve)
- PT2: Querença-Silves limestone karstic aquifer system (Algarve)
- PT3: Melides aquifer, river and lagoon (Alentejo)

In PT1 – Rio Seco and Campina de Faro aquifer system (Algarve) – the main goal is to improve the groundwater quality heavily contaminated with nitrates (vulnerable zone), mainly due to agriculture bad practices.

In PT2 – Querença-Silves limestone karstic aquifer system (Algarve) – there are two main sub-areas and two goals: (1) develop a soil-aquifer-treatment (SAT) system to improve the water quality of treated effluents from a waste water treatment plant (WWTP) (PT2_4) at São Bartolomeu de Messines (SB Messines), which discharges into Ribeiro Meirinho river (PT2_5) that in turn recharges the karstic aquifer, and (2) increase groundwater storage at Cerro do Bardo karstic area using wet years surface water surplus to increase the water availability in dry years and facilitate downstream water supply.

In PT3 – Melides aquifer, river and lagoon (Alentejo) – the main goal is to use SAT-MAR to remove rice field pollutants prior to their discharge in Melides lagoon.

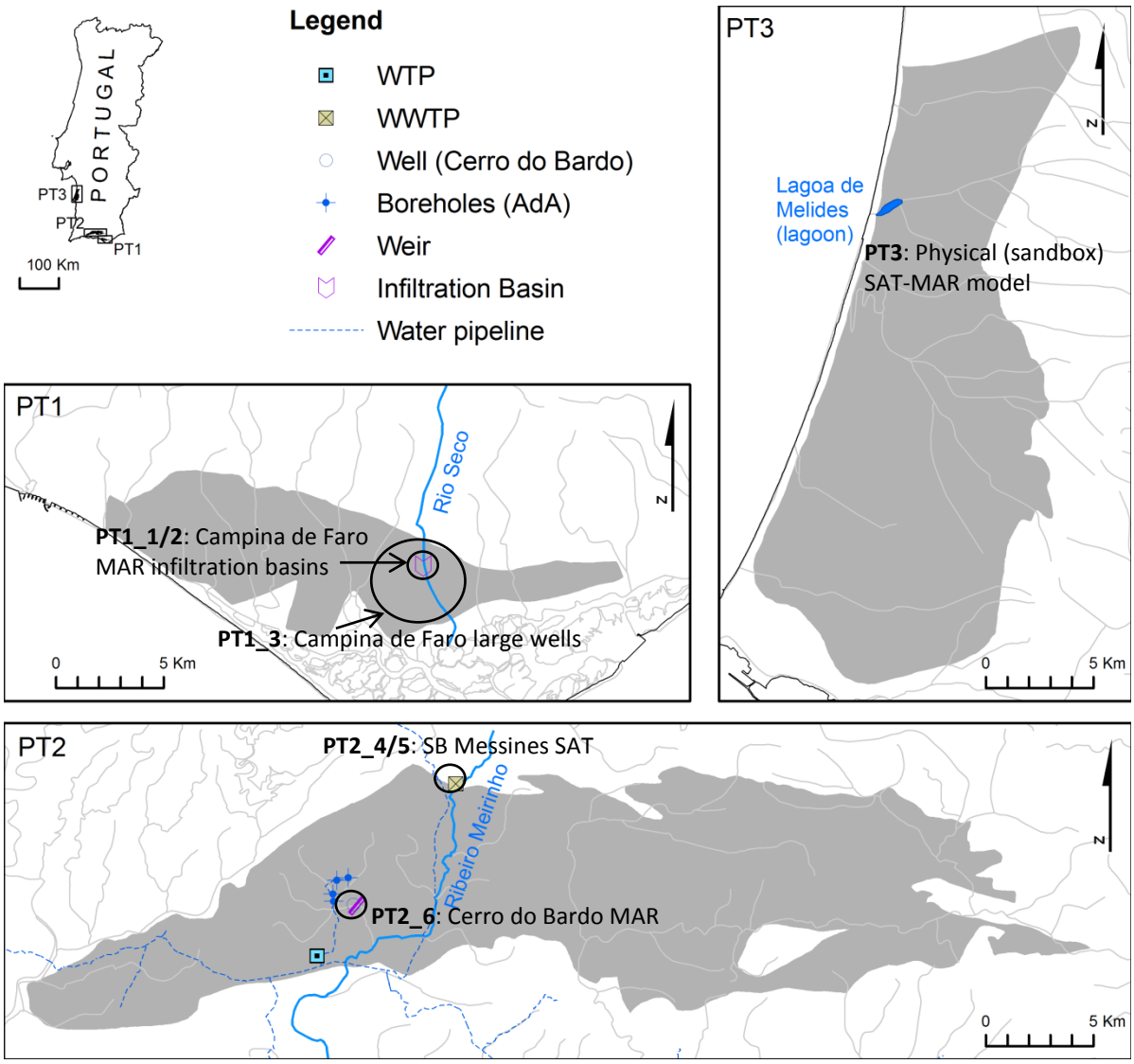

Figure 1 – PT MARSOL DEMO sites location (the aquifers boundaries are market in grey)

The work developed for the different DEMO sites was developed in the following tasks:

- Task 4.1: Recharge water availability
- Task 4.2: Developing the (MAR) infrastructures
- Task 4.3: Investigation and monitoring
- Task 4.4: Modelling

The results are being presented in five main deliverables:

- D4.1: Water sources and availability at the South Portugal MARSOL demonstration sites
- D4.2: South Portugal MARSOL demonstration sites characterisation
- D4.3: Monitoring results from the South Portugal MARSOL demonstration sites

- D4.4: Hydrogeological modelling at the South Portugal MARSOL demonstration sites
- D4.5: MAR to improve the groundwater status in South Portugal (Algarve and Alentejo)

This report presents the results from D4.3: Monitoring results from the South Portugal MARSOL demonstration sites.

2. MARSOL DEMO SITES CHARACTERISATION IN PORTUGAL

2.1 PT1: RIO SECO AND CAMPINA DE FARO AQUIFER SYSTEM (ALGARVE)

2.1.1 Introduction and objective

PT1, Rio Seco and Campina de Faro aquifer system (Algarve) aims to demonstrate that the aquifer water quality can be improved by means of managed aquifer recharge. For this purpose, infiltration basins constructed in the Rio Seco river bed are being tested and monitored, using either the basins constructed in 2006 during GABARDINE EU project (PT1_1), which were rehabilitated during MARSOL, or the new MARSOL basins (PT1_2) constructed in July/August 2014. Furthermore, infiltration in typical existing large-diameter wells (PT1_3) is being tested as a MAR facility to increase regionally the water recharge and improve the groundwater quality status, using the water collected in the greenhouses roofs during rain events.

2.1.2 Motivation for the site selection

Campina de Faro aquifer MARSOL case-study area was selected based on the following background considerations and advantages:

1. This is an area with a relevant environmental quality problem (agriculture groundwater nitrate contamination), requiring appropriate MAR INNO-DEMO solutions. As a matter of fact, a significant part of Campina de Faro aquifer system has been declared in 1997 as a nitrate vulnerable zone (Portaria nº 1037/97, 1st October), in the framework of the Decreto-Lei nº 235/97 (transposes EU Directive 91/676), which aims water protection from diffuse pollution caused by nitrates of agricultural sources (Figure 2).
2. A relevant amount of MAR knowledge and groundwater data is available, having been gathered on another EU sponsored project, the GABARDINE a 6th Framework Programme for Research, Technological Development and Demonstration - Specific Targeted Research or Innovation Project (Contract no.: 518118-1) (Lobo-Ferreira *et al.*, 2006a e b; Diamantino *et al.*, 2007; Diamantino, 2009).
3. A MAR/groundwater thematic PhD thesis was developed at MARSOL partner institution LNEC, i.e. DIAMANTINO (2016, cf. http://repositorio.ul.pt/handle/10451/1627). This PhD dissertation was carried out in the framework of GABARDINE Project. The Project was developed in Núcleo de Águas Subterrâneas (NAS) of Laboratório Nacional de Engenharia Civil (LNEC).
4. Several *in situ* MAR experiments have been applied to Campina de Faro unconfined aquifer. The main objective of those experiments was to estimate performances in terms of infiltration rates, to assess groundwater quality and quantity resulting effects, considering alternative sources of water (e.g. surface water surpluses), and to determine aquifer hydraulic parameters (e.g. hydraulic conductivities and groundwater velocities). These infrastructures intend to demonstrate the adequacy of such facilities in contributing to improve the water of a contaminated aquifer, which in the case of Campina de Faro's aquifer is due to agriculture diffuse water pollution.

5. Two groundwater flow and mass transport model (for both regional and local scales) have been developed, allowing simulating real time aquifer responses, after the incorporation of different MAR scenarios.

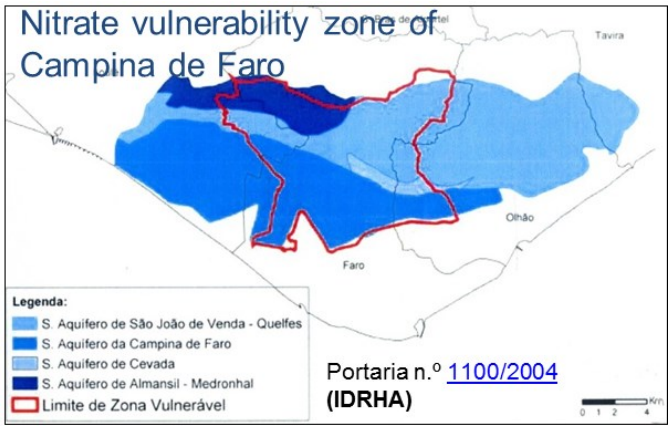

Figure 2 – Vulnerable Zone of Campina de Faro

2.1.3 Geological/hydrogeological setting

According to INAG (2000), Campina de Faro aquifer system has an area of around 86.4 km^2, being limited, in the North, by the less permeable deposits of Cretaceous, in the East, by S. João da Venda – Quelfes aquifer system, in the West, by the Quarteira aquifer, with a probable hydraulic connection between them, and in the South, by the sea. Figure 3 shows the identification of the aquifer systems in the Algarve coastal zone by INAG (2000), including also the aquifer system of Campina de Faro.

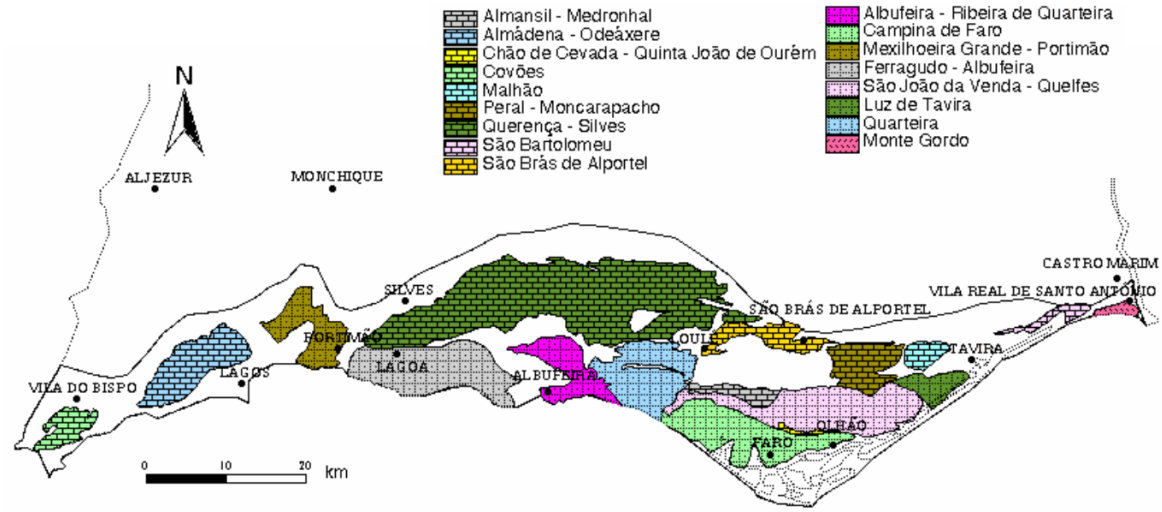

Figure 3 – Location of the aquifer systems in the Algarve region (Almeida *et al.*, 2000)

Figure 4 (Stigter, 2005) presents a hydrogeological section of Campina de Faro area. The oldest formations belong to the Jurassic gypsiferous material that locally outcrops near Faro and is related to diapiric activity.

According to Stigter (2005), the oldest aquifer system that occurs in the Campina de Faro area is the Cretaceous, formed by limestone layers separated by marls (Figure 4). They dip to the south (20º-

30º) and crop out in the NW part of the area. The top of the sediments is found at a depth below 200 m, near the city of Faro (Stigter, 2000). According to Manupella (1992, *in* Stigter, 2005) the thickness of Cretaceous aquifer is larger than 1000 m. A Graben-like structure was formed at the end of the Cretaceous where Miocene limestone and, later (sands and marls) were deposited in unconformity (Silva, 1988, *in* Stigter, 2000).

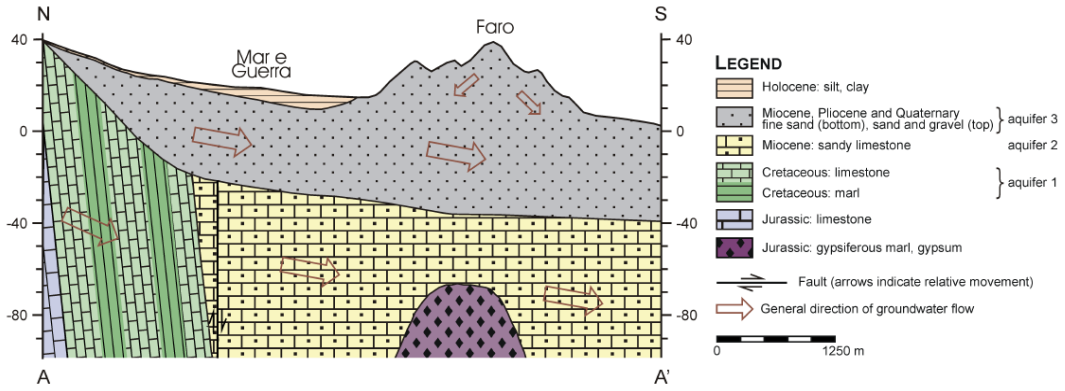

Figure 4 – Campina de Faro N-S hydrogeological section (Stigter, 2005)

Miocene fossil-rich sandy-limestone deposits constitute the second aquifer. It deeps to the East but, because of the presence of several N-S faults, a stepwise structure is present (Silva *et al.*, 1986 and Silva, 1988, in Stigter, 2000). There are few outcrops of Miocene limestones in Campina de Faro, also because they are covered by fine sand deposited during Miocene. The depth of the top of Miocene formations varies between 3 and 25 m below surface and the presence of marls seems to be very irregular (Silva, 1988 in Stigter, 2000). The topography of the top of the Miocene is irregular. Despite Miocene outcrops are very few and small, Miocene formations thickness is very large. It increases from north to south and exceeds 200 m near the coast. According to Antunes and Pais (1987, in INAG, 2000) a deformation might have affected the Miocene deposits and that could explain the apparent thicknesses, larger than the real ones. The carbonated fraction varies from 60% to 95% with a decreasing trend from the base to the top (Silva, 1988).

Covering the Miocene deposits, sands, clayey sandstones, gravels and conglomerates of the Plio-Quaternary are found ("Areias e Cascalheiras de Faro-Quarteira" formation), with a thickness very variable. They crop in the NW and also near the city of Faro. Stigter (2000) refers that its thickness varies between 8 and 50 m. According to Moura e Boski (1994, in INAG, 2000) this formation has a maximum thickness of 30 m. Silva (1998, in INAG, 2000) refers that the thickness of these deposits can reach, in some places, a thickness of 60 m.

The third aquifer system is formed by the fine sand of Miocene and also the Plio-Quaternary sand and gravels. This aquifer presents an average thickness of 50 m (Stigter, 2005). Despite being partly covered by Holocenic materials, this aquifer is still considered phreatic, because their thickness is often too small to give confined characteristics to the underlying aquifer. According to Silva (1988) the average thickness of this aquifer is 25 m, but reaching maximum values of 60 m and 65 m near Galvana and in Quinta do Lago, respectively.

Some authors refer the existence of a confining layer between the second and the third aquifers. According to Silva *et al.* (1986), that separation is made by several silty-clayey-sandy layers (Figure 5) with variable thickness and apparently with some lateral continuity. Nevertheless, one cannot

exclude the possibility of some hydraulic connection in sectors where that confining layers are absent (INAG, 2000). Furthermore, in some situations there is a hydraulic connection artificially established due to new wells built within old large wells with the aim of extracting water from the Miocene and confined aquifer. This connection facilitates the confined aquifer contamination coming from the overlying phreatic aquifer.

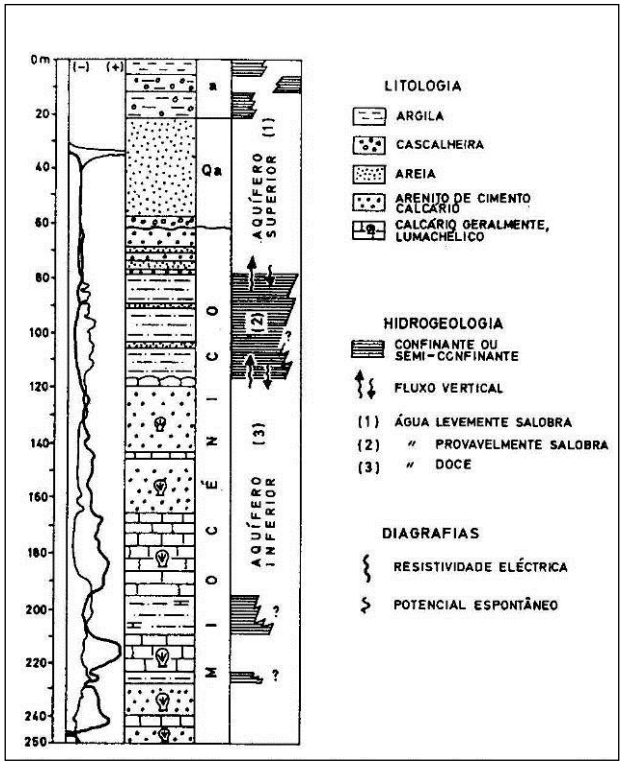

Figure 5 – Campina de Faro hydrogeological model, presented in JK15 well log (Silva *et al.*, 1986)

According to Stigter (2005), the general direction of groundwater flow is N-S (cf. Figure 4). There are preferential flow paths formed by the N-S trending faults but the NW-SE trending fault acts like a barrier, which is indicated by the steeper hydraulic gradient of the water table in the north.

Considering the aquifer area equal to 86 km^2, the average annual precipitation equal to 550 mm and a recharge rate (of the phreatic aquifer) between 15 and 20% of the precipitation, direct recharge has an approximate value of 10 hm^3/year (INAG, 2000). Oliveira and Lobo-Ferreira (1994) calculated the potential recharge of hydrogeological system ALG-5, that includes also Campina de Faro aquifer, and obtained a value of 36,3 hm^3/year (143 mm/year).

2.1.4 Developing the infrastructures

PT1_1: Rio Seco existing infiltration basins

The rehabilitation and modification of the structures inherited from the GABARDINE (2006) project in Rio Seco - Campina de Faro was carried out between 25 and 26 July 2014.

The existing structures were:

- Two infiltration basins - with approximately 20 m long, 5 m wide and 6 m deep. In the downstream infiltration basin (south) there is a perforated pipe with 1'' diameter and an effective depth of 5.50 m.
- Two piezometers, LNEC1 and LNEC2 (cf. Figure 6, Figure 7 and Figure 8), with a depth of approximately 20 m both cased in 3'' PVC. The piezometer LNEC2 is located between the two GABARDINE infiltration basins at a distance of 2.5 m from the boundary of each basin. LNEC1 piezometer is located approximately 2.5 m downstream of the south infiltration basin.
- A well (LNEC3, cf. Figure 7) with a depth of 40 m and an iron casing with 140 mm in diameter till 20 m. From 20 to 40 m it is not cased (limestones and sandstones). This well is located between the two GABARDINE infiltration basins at a distance of 2.5 m of each basin's limit.

Figure 6 – LNEC1 piezometer before rehabilitation

Figure 7 – LNEC2 piezometer and LNEC3 well before rehabilitation

Figure 8 – LNEC2 piezometer without ladle

The rehabilitation works were developed in three phases.

The first phase was the creation of the access to the GABARDINE project infrastructures. The work consisted of cleaning the river bed and access, including the removal of vegetation, through the levelling of the Rio Seco bed for a distance of about 300 m, from the place where EM518 crosses the riverbed to the location of the existing structures (Figure 9). The Rio Seco bed was in general in acceptable traffic conditions, with the exception of just a few points where levelling was necessary. This was carried out using solely the material of the river, ensuring the conditions for the movement of heavy machinery.

In a second phase, the GABARDINE basins were levelled and cleaned (Figure 10). This work was carried out with the minimum disturbance possible, avoiding to modify the outcome of the clogging test, which took place on July 1st, 2014. It included only a minor regulation, the clearing the vegetation and the necessary arrangements for the preparation of the downstream GABARDINE infiltration basin clogging test.

Figure 9 – Levelling of Rio Seco bed

Figure 10 – Levelling of GABARDINE basins

Before: April 2014 After: July 2014

Figure 11 – Rehabilitation of the existing infiltration basins, access and piezometers at PT1_1 Campina de Faro

The third phase of the rehabilitation processes consisted in developing the piezometer LNEC2 and the borehole LNEC3, using a special bailer to extract the sand. LNEC1 piezometer was found obstructed and was leaning, having proceeded to its recovery and rehabilitation (cf. Figure 10). The rehabilitation work took place between July 28th and August 1st, 2014, within the scope of the implementation of MARSOL piezometers.

Construction of the piezometers

The construction work related to the implementation of three MARSOL piezometers and rehabilitation of GABARDINE project piezometer in Rio Seco – Campina de Faro, took place between July 28th and August 8th 2014.

The location of the new boreholes was decided in the field in relation to the expected location for MARSOL infiltration basin. These infrastructures aim to control and monitor the planned injection tests later performed in Rio Seco, in MARSOL's and GABARDINE´s infiltration basins (dug in the upper aquifer), and to improve the geological knowledge of the MARSOL basin area.

Figure 12 – Piezometer and well development

The MARSOL piezometers reached depths between 20 and 30 m, and mostly crossed the Miocene Superior formations (clay and sand), superficially covered by more or less consolidated gravel. Their coordinates are shown in Table 1, and its location is show in Figure 13.

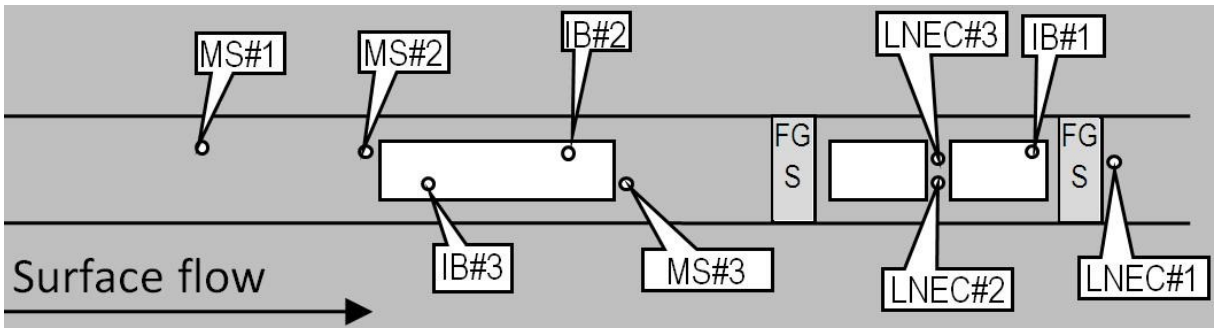

Figure 13 – Location of the piezometers and all infrastructures at Rio Seco

Table 1 – Coordinates of the new piezometers (EPSG: 20790; Hayford Gauss System; Lisbon Datum)

Name	M	P
LNEC1	219344	8555
MS3	219322	8626
MS1	219292	8691
MS2	219315	8646

The piezometers were drilled with a diameter of 8" with direct circulation method using sludges, until the depth of interception with the Miocene formation (lower confined aquifer) which was “hinted” with the presence of glauconitic minerals (see Figure 14).

Figure 14 – Rotation with direct circulation

During execution, material samples (cuttings) were collected every 2 m or whenever the crossed materials would significantly vary. This allowed to tune the placement of the screens, and to define the final depth of the piezometer (see Figure 15). A profile of these cuttings can be seen in the Figure 16.

Figure 15 – Regular sample collection of materials ("cuttings")

Figure 16 – Litostatigraphic profile of the piezometers

The piezometers were installed with 3'' PVC pipes. The screens (1 mm slot size openings) were covered with a thin net to prevent the entry of silt (see Figure 17) and were installed according to the location of the sand strata. The space between the casing and filter bed was filled with sorted gravel of size 3-5 mm (see Figure 18), up to the screen depths. The upper section (3 to 4 m) was filled with cement, with an intercalated sand layer, for total isolation.

Figure 17 – Screens covered with a net

Figure 18 – Filter material

All piezometers were clean and developed with air lift method, with intermittent pumping, focusing on the entire screen section. This process was carried out until the water was clean and almost with no turbidity (Figure 19).

At the end of the development a final drawdown was induced (with the air compressor) and the recovery was measured (Figure 20). Almost all piezometers seem to recover well and hence are monitoring accurately the aquifer characteristics; the exception is MS1, where the sand thickness was much thinner. The lithological and hydraulic results of the construction of the MS1 (Figure 16) were in fact, the main reason for the relocation of the MARSOL basin position, which was thought to be placed between piezometers MS1 and MS2, but due to the thick clay/silt level found, it was transferred downstream between piezometers MS2 and MS3.

Figure 19 – Water collection and turbidity check

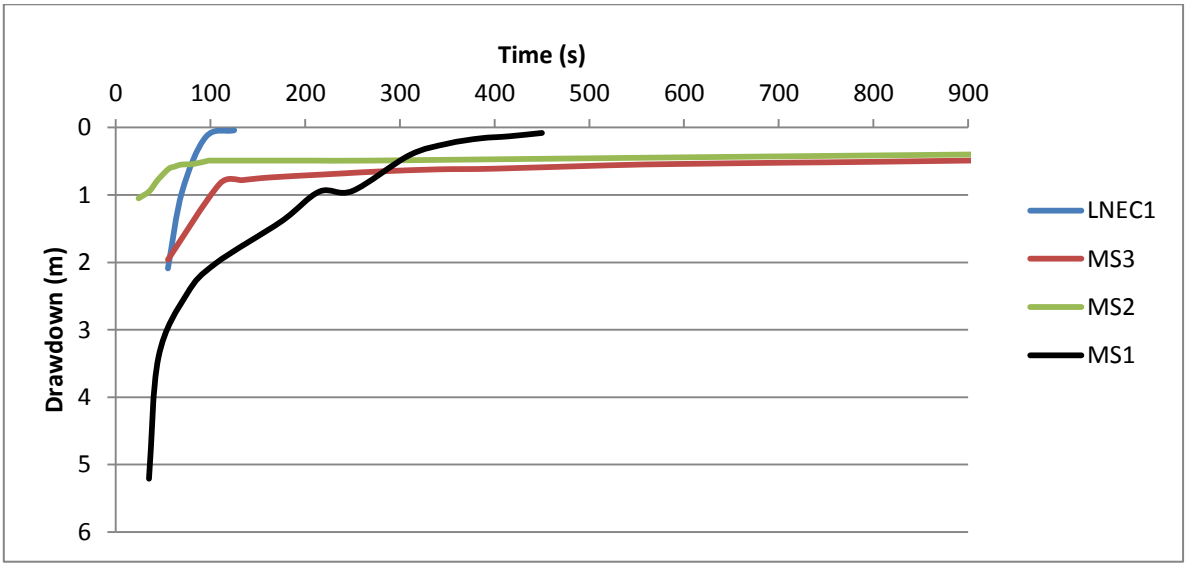

Figure 20 – Water level recovery after total drawdown

The piezometers were then developed for several minutes and left ready to be instrumented safely, by welding a hook on the cover where a CTD diver can be tied even with the cover closed. The logs of the piezometers are presented in Figure 21.

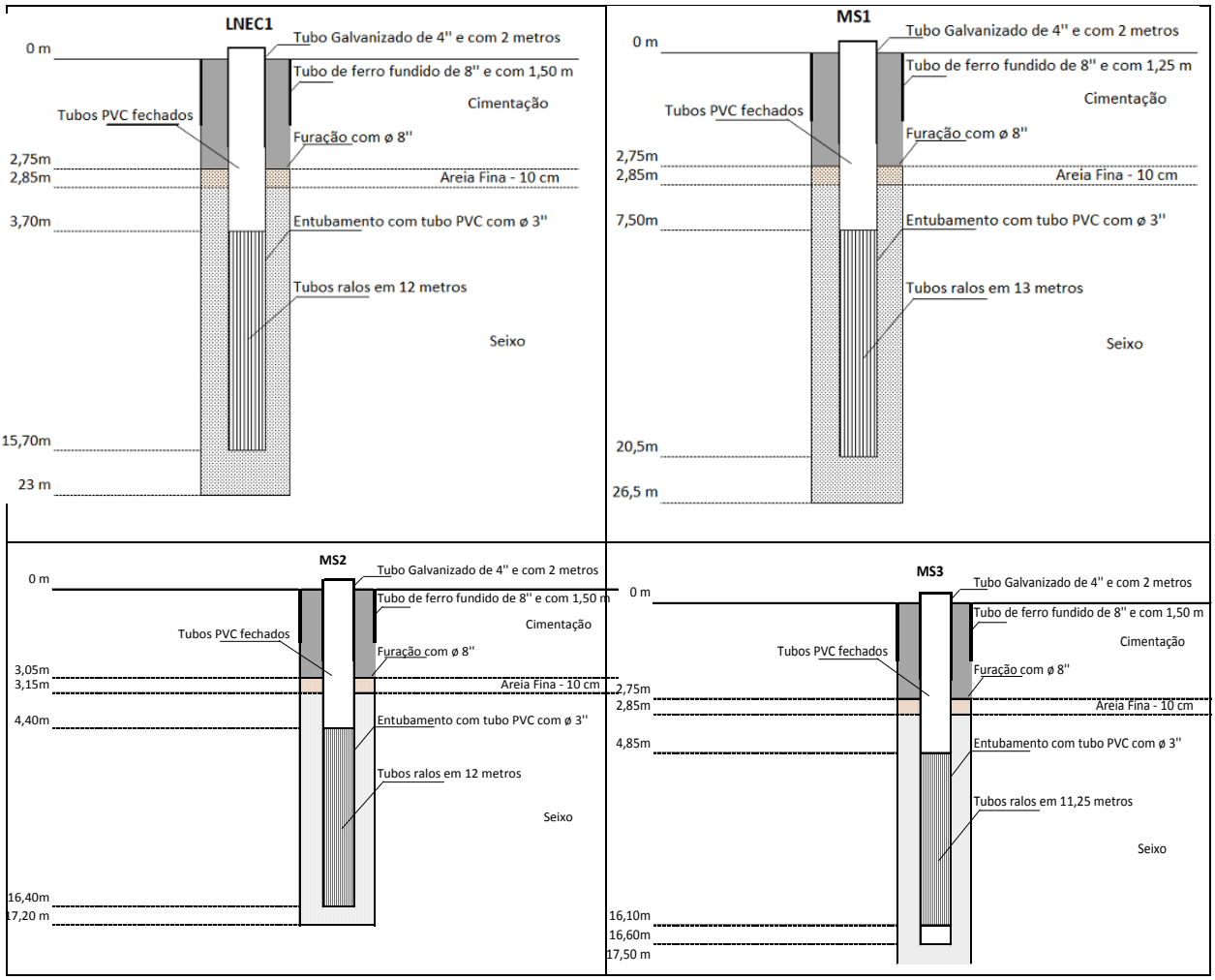

Figure 21 – Logs of the new piezometers

PT1_2: Rio Seco new MARSOL infiltration basins

The construction works for MARSOL new infiltration basin developed in Rio Seco - Campina de Faro, took place between August 12th and 29th, 2014. The site of the infiltration basin is depicted in Figure 22 and its coordinates are as follows: latitude N 37º02'35.88' and longitude 7º54'57.11 W' (WGS 84). In this figure, it is also possible to see GABARDINE project two basins, rehabilitated and modified during MARSOL.

Figure 22 – Location of the infiltration basins at Rio Seco

Preliminary knowledge of existing geological conditions at the site was gathered from the available information of GABARDINE project (piezometers, borehole two infiltration basins (approximately 20x5x7m), located roughly 100 m further downstream in the Rio Seco river bed. These infrastructures were implemented in 2006, under the EU project GABARDINE (Figure 22). This information was analysed and complemented with data from the execution of three geotechnical surveys (piezometers) implemented, both upstream and downstream of the planned site for construction of the MARSOL basin (see above). The geological and hydrogeological information obtained from these monitoring piezometers, allowed predicting and refining the ideal location and dimensions for the basin. For example, the stratigraphy and poor hydraulic performance of the MS1, called for a displacement of the basin more downstream, where the hydraulic permeability is higher.

Geologically, the MARSOL infiltration basin's site is composed of alluvial material comprising consolidated clays and gravel with very low permeability up to a depth of about 6 m. The aquifer is then composed by fine sands, intercalated with some clay/silt levels constituting the semi-confined Miocene superior aquifer.

The work was carried in three phases. The first phase of the construction work corresponds to dirt removal and excavation, and it took place between 12th and 18th August, having been excavated a volume of approximately 1350 m^3 of material (Figure 23). Excavation was carried on until reaching the aquifer's piezometric level, which was around 6.5 m deep, at the time.

River basin excavation: August 2014

River basin filling: August 2014

Figure 23 – Construction of a new infiltration basin (equivalent to 2 x old ones) and new monitoring piezometers at PT1_2 Campina de Faro

A visual observation of the pit slopes in depth allowed identifying four major lithological levels with different thicknesses and lithology, as can be seen in Figure 25 diagram and in Figure 24.

Figure 24 – Lithological levels identified during the excavation of the MARSOL basin

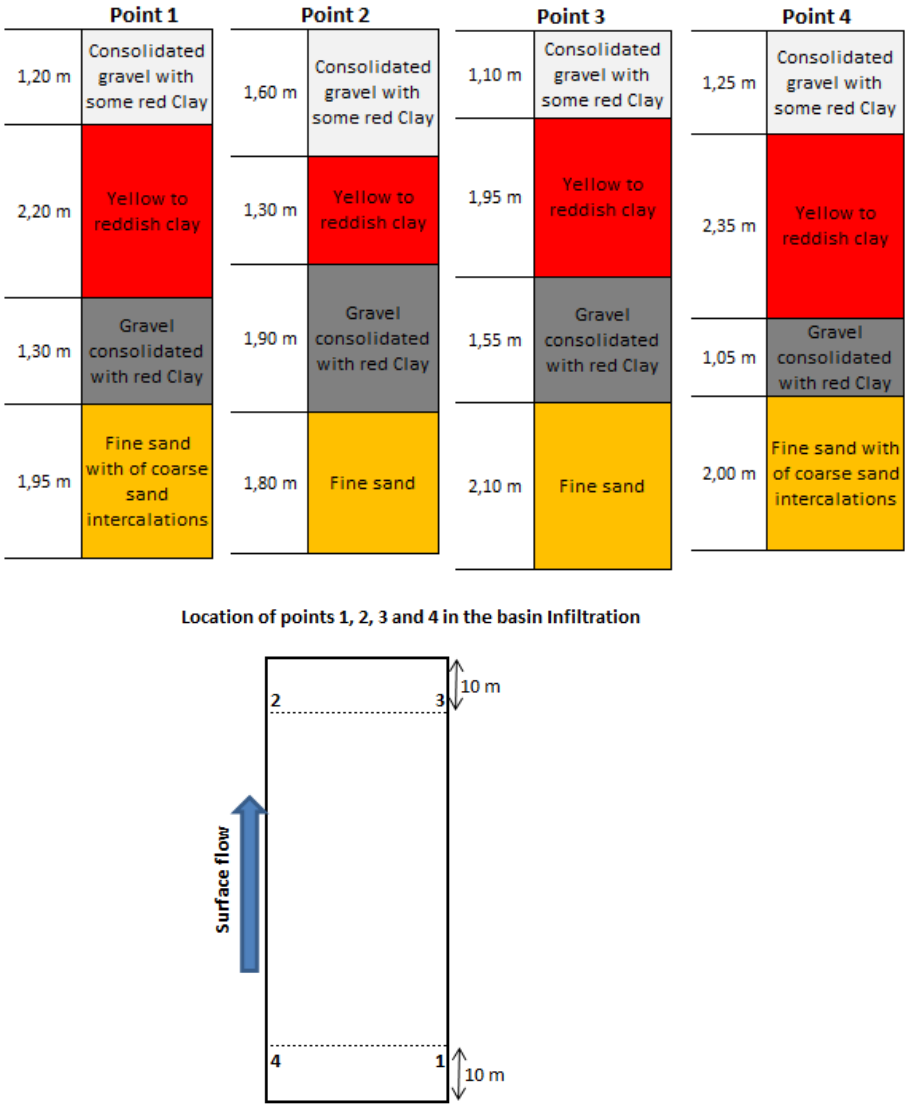

Figure 25 – Profile and location of points 1, 2, 3 and 4 in the infiltration basin. Point 1 and 4 (east and west) are located downstream and point 2 and 3 are located upstream (west and east)

During the excavation, several soil samples were taken at 2 m, 4 m, and at the very bottom of the infiltration basin, and were sent to the lab for sieve analysis. The objective will be to have a rough idea about the hydraulic permeability in space (looking for possible heterogeneities), determine the variation in depth, and to compare with the experimental values from the infiltration experiments in the basin.

In a second phase, between 18th and 28th August, the filling of the basin was carried out, with about 1800 tons of siliceous coarse gravel material, until reaching the river bed surface. The selection of siliceous over calcareous material was due to its low solvability (particularly in acid environment) and precipitation potential.

On the last day of construction work (29th August), the basin surface was levelled. Two perforated tubes (IB2 and IB3) with 1'' diameter were placed up to the bottom of the basin, to assess the water

level in the basin, and another six iron bars were installed to mark the basin limits. The top of the basin, coincident with the height of the Rio Seco bed, was slightly lowered by approximately 20 cm in order to keep a height of water in the basin and to avoid losses during the infiltration tests.

The constructed basin has an average depth of 6.7 m, a total length of 33 m and occupies the entire cross section of the river, with an average width of 6.1 m at the surface (cross-section of the river varying between 5.5 to 6.2 m). This basin has a surface area of 201 m^2 (33 m x 6.1 m). Vertically it presents a perfectly rectangular configuration (vertical slopes) across its lateral extent.

2.1.5 Field experiments conducted

Introduction

Upon the completion of the infiltration basins work, several tests were performed in order to evaluate the performance of the basins in terms of clogging, infiltration rates and its local influence in the groundwater quality. Besides, a test was conducted in a large diameter well to assess its infiltration rate capacity.

PT1_1: Clogging test in one GABARDINE basin, 1st July 2014

General description

In this test, an 18 m^3/h flow rate was obtained from a pump installed at about 30 m deep in the well (LNEC3). This pump is connected to a water supply system that has a split hydraulic "T" equipped with flow control valves, where three PEAD pipes come out. Two of them had the function of water distribution across the basin (and were therefore perforated) and the third test tube rejected the excess flow of the water stream, when necessary.

After saturating the basin with water, a constant level of about 20 cm was kept using a system of valves which diverged the surplus water to a discharge point, where the flow was measured with a 200 l barrel. The inflow of the basin was calculated through the difference from the original outflow (18 m^3/h) and the outflow during steady state conditions.

The monitoring was performed during and after the test, using automatic multiparametric probes (recording water pressure, temperature and conductivity) installed in the piezometers upstream and downstream the basins and in the perforated tubes placed within the basin, with manual control.

Figure 26 shows some aspects of the test layout.

The test may be divided in the 4 stages depicted in Table 2.

Figure 26 – Infiltration test at Rio Seco infiltration basin (PT1_1 Campina de Faro) to access clogging from 2007-2014

Table 2 – Discharge control during the infiltration test

Stage	Time	Stage
1	9:15 – 14:28	Water input into the infiltration basin until saturation (average water input in the infiltration basin = 17.98 m^3/h)
2	14:28 – 15:43	Raising the level from 0 cm till 20 cm above the infiltration basin surface
3	15:43 – 19:15	Keeping the water level at 20 cm head above the infiltration basin surface by controlling water leaving the basin
4	19:15 – 21:25	No water input in the infiltration basin and measuring water level decreasing

Figure 27 represents the values of depth of the water level below the infiltration basin (IB) surface measured during the test (in relation to the ground level that corresponds to the surface of the IB). The same picture depicts the calculated differences (variations) of the water level. The 1 minute variation is the variation from the previous measurement to the actual one. As these changes oscillate up to 4 cm from one measurement to the next one, a 5 minute average variation was calculated in order to smooth the variation curve. This curve is also represented in Figure 27. The 5

minutes variation curve is the average variation of the last five minutes (i.e. the difference [actual value of depth – the value of depth five minutes before] divided by 5 minutes).

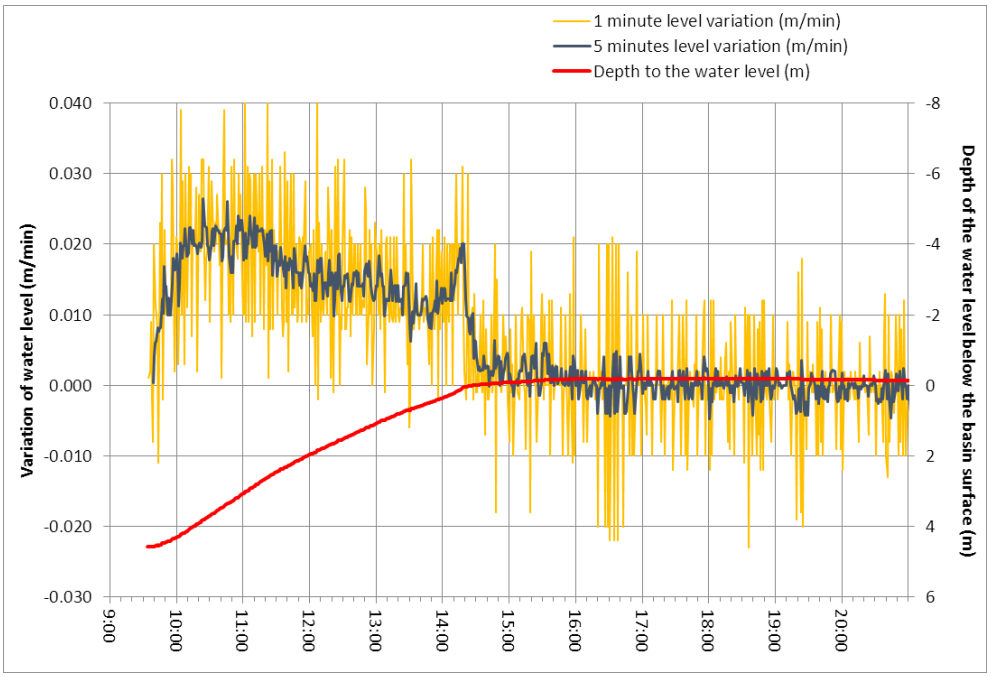

Figure 27 – Depth of the water level below the basin surface, and 1 minute and 5 minutes average variations of the water level

In order to lower the level oscillations, all the curves were smoothed by considering that at each time the depth to the water level is the average of the level itself and of the two levels measured before and after the actual time. This means that at a specific time the depth to the level represents a 5 minutes average of the depths to the levels. The 1 minute and 5 minutes level variations were again calculated as in Figure 27. The results are shown in Figure 28 and it can be seen that the variations are now much smaller. Figure 28 also represents the stages presented in Table 2.

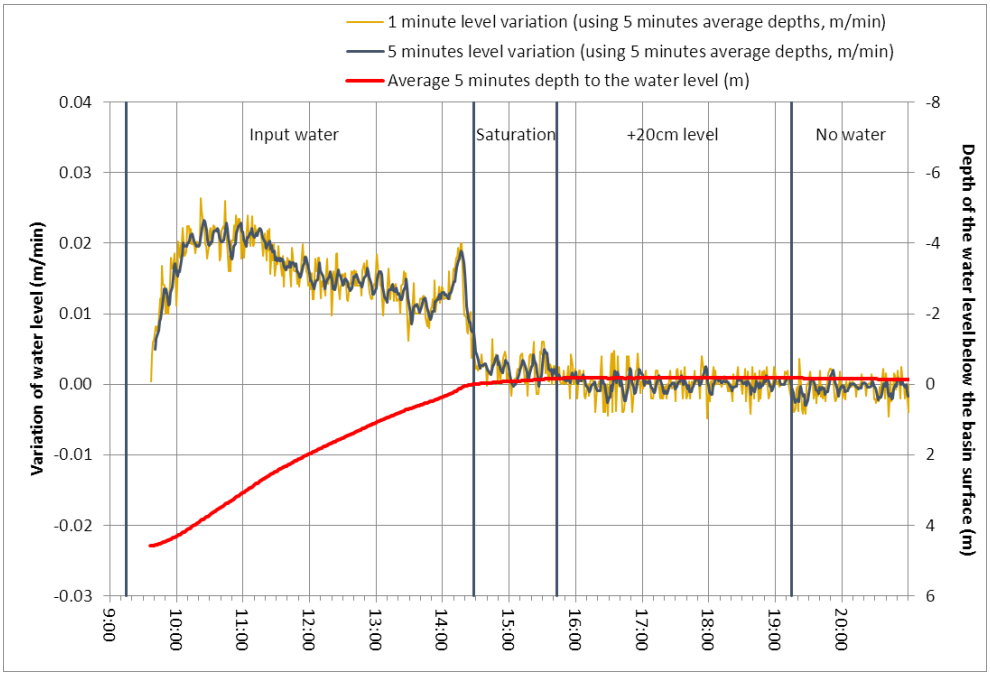

Figure 28 – Average 5 minutes depth of the water level below the basin surface, and 1 minute and 5 minutes average variations of the water level

Filling stage

During the filling stage, several behaviours can be detected concerning average level variations (Figure 29):

- initially during about 32 minutes from 9:41 until 10:13, there is a constant increase in the rate of change of the water level in the infiltration basin – each minute the level change increases 0.00045 m/min; this may be related with the fact that initially the water fills the smaller voids of the infiltration basin from top to bottom, and only when these are progressively filled the water fills the bottom voids of the infiltration basin and the levels start to increase progressively more, as all the water is used to increase the voids corresponding to the effective porosity of the medium; this process must be considered in conjunction with the preferential flow paths that may exist in the basin;
- then, from 10:13 until 11:15 (1h02min), there is a quasi-stabilisation in the change of the water level, meaning that the increase in the water level is approximately constant, with a value of 0.021 m/min; this may be related to the balance between the input water, the raise in the water level and the infiltration rate of the basin;
- a new period in which the rate of change of the water level is decreasing, from 11:15 till 11:38 (23 minutes), in an approximately constant rate of -0.00022 m/min per minute of inputting water; due to the raise in the water level inside the basin, and the associated head increase, there is an increase of the infiltration rate in the basin and the corresponding reduction of the rate of change of the water level;
- a new break in this decreasing change to about -0.00004 m/min of inputting water, from 11:38 until 14:02 (during 2h24min); the reason could be the same as the previous one, the

reduction of the rate of change of the water level could be associated with higher infiltration conditions;

- with the approximation of the filling of the infiltration basin, since 14:02 until 14:17 (15 minutes), the variation on water level suddenly increases, in the order of 0.00047 m/min per minute; this increase may be related to the proximity of the ground surface, that can be slightly more compressed due to clogging (at 14:02 the water level is 33 cm below ground and at 14:17 is 9 cm below ground);
- finally, in the near end of the filling period, the last 11 minutes from 14:17 until 14:28, again the rate of change of the water level decreases with time, at a rate of -0.00121 m/min, and this should be related with the transition to the open air, with the reduction of the solid phase, which means more empty space and less pebbles, thus inducing, for the same water input, a lower increase of the water level with time.

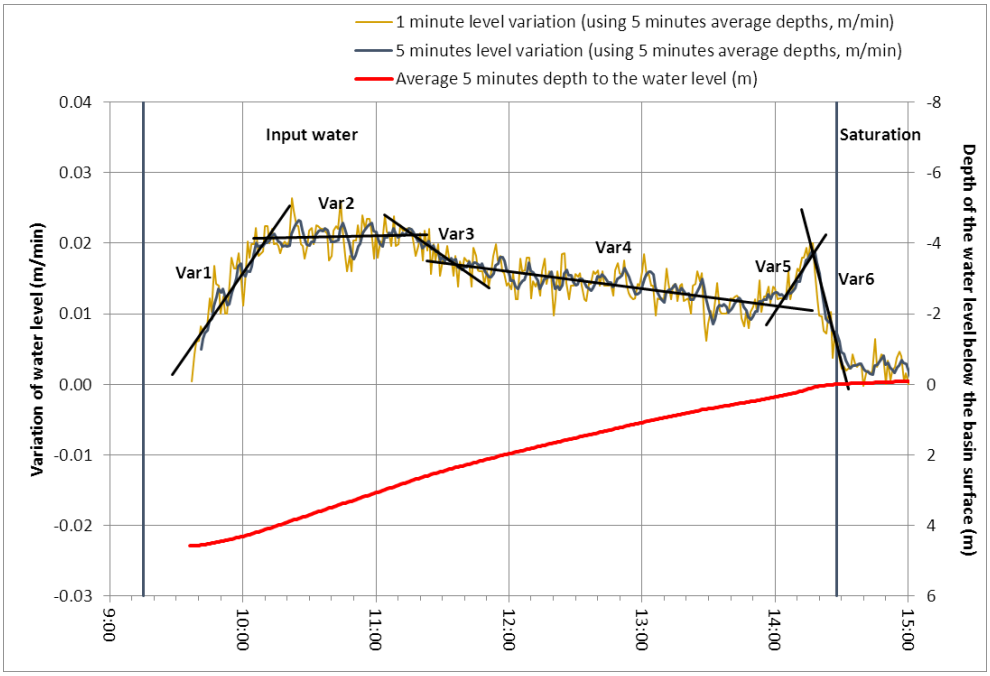

Figure 29 – Indication of the change on the variation of the water level during the filling stage (Input water) of the infiltration basin

Increasing surface storage above infiltration basin stage

Concerning the period between saturation and the +20 cm of water, when water input was increasing storage above the infiltration basin or infiltrating to the aquifer, a similar analysis can be performed (Figure 30). Despite the fact that the level behaviour is not steady, it is possible for this entire period, from 14:28 until 15:43, to adjust a straight line, whose slope is almost null, which means (in average) a constant relation between water change and time. In this case the rate of change of the level is about 0.002 m/min. This situation is quite adequate to infer the infiltration rate below the infiltration basin. In this period of time, infiltration may be estimated by the difference between water input and the variation of surface storage above the ground. Total input water is 17.98 m^3/hour, which means a total volume of input water between 14:28 and 15:43 (1h15min) of

22.475 m^3. The variation of surface storage corresponds to filling the height of water, which in fact, in this period was 0.163 m (instead of 0.200 m). This times 100 m^2 (the surface of the area) corresponds to 16.3 m^3 of water stored at surface. This represents an infiltration of 22.475 m^3 – 16.3 m^3 = 6.175 m^3 of water during 75 minutes = 0.08233 m^3/min = 118.56 m^3/day = 1.19 m/day.

It can be seen in Figure 31 that the determination of the infiltration rate along time calculated by the difference between the input of water since the beginning of the saturation until the represented time and the level variation used to calculate the variation of storage in the same period, provides initially lower values of infiltration rate, and only around 15:04, 36 minutes after storage is completed, when the water level above ground is about +8 cm the infiltration rate stabilises around the final value of 1.19 m/d, despite at this time an oscillation of about +-20 cm is still observed.

The same Figure 31 also depicts a complementary situation: by computing the infiltration rate along time by the difference between the input of water since the current time until the beginning of the +20 cm water height stage] and the level variation used to calculate the variation of storage in the same period], an opposite situation occurs. When using only the later values that correspond to higher water levels infiltration rates increase to more than 2 m/day (for instance after 15:35).

This can also be observed in Figure 32 that represents the same infiltration rates but as a function of water level height.

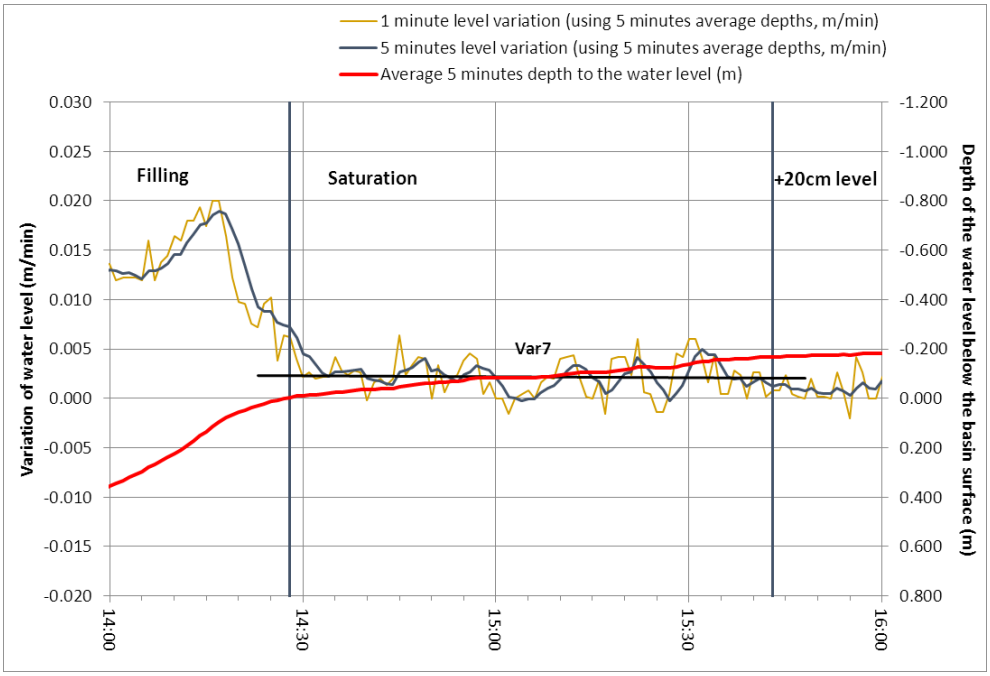

Figure 30 – Indication of the change on the variation of the water level during the completion of the +20 cm storage above the infiltration basin

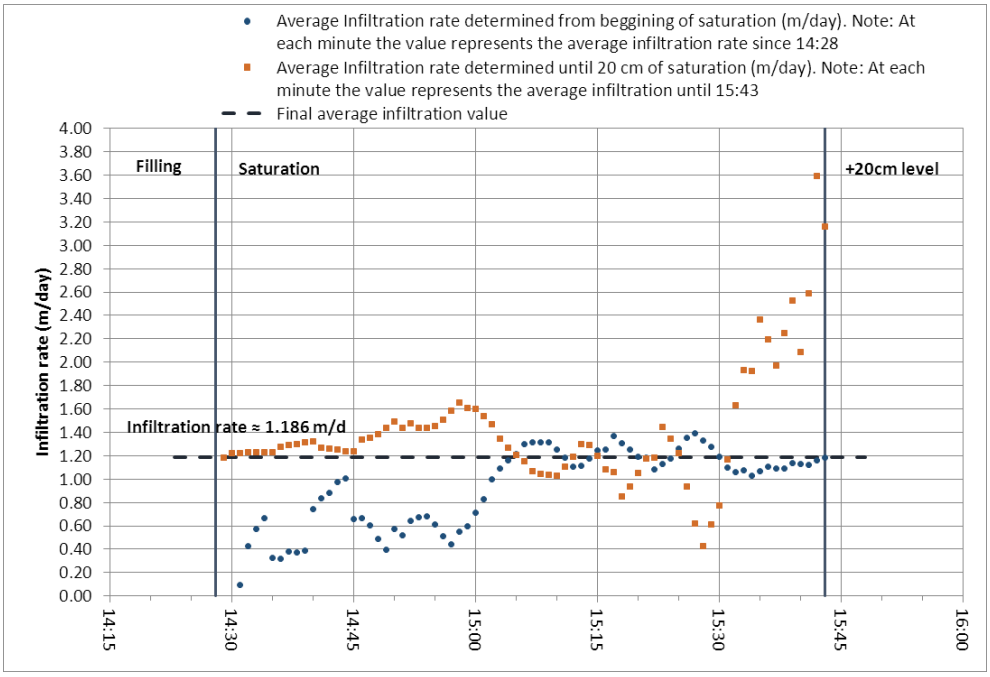

Figure 31 – Average infiltration rate computed at each time since the beginning of saturation of the infiltration basin or until the beginning of the +20 cm of water stage

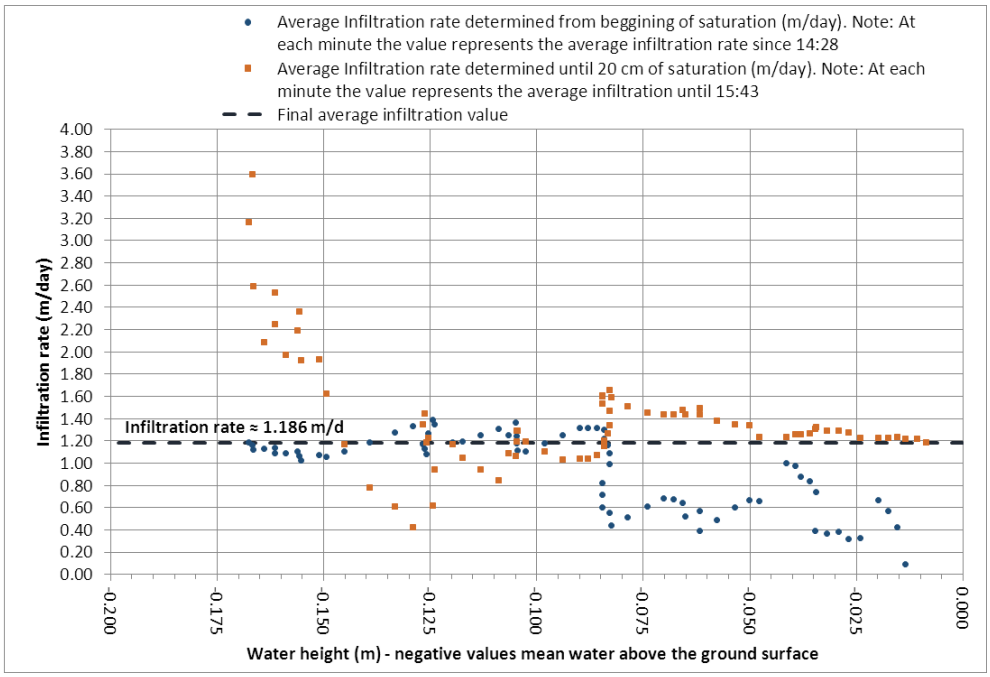

Figure 32 – Average infiltration rate computed at each time since the beginning of saturation of the infiltration basin or until the beginning of the +20 cm of water stage as a function of water height

Keeping surface storage above infiltration basin stage

At this stage the objective was to control outflow discharge to the river so that the water level above ground surface of the infiltration basin could be kept at an approximated value of +20 cm. Changes in water level can be seen in Figure 33. Figure 34 shows the variations of flow along time. It was decided that during the last period, from 18:20 until 19:03, equilibrium was achieved, at an average level of +0.189 m above ground, with the level oscillating between +0.185 m and +0.192 m. For this level water input to the infiltration basin was determined as 4.29 m^3/h = 102.96 m^3/day or 1.03 m/d infiltration rate.

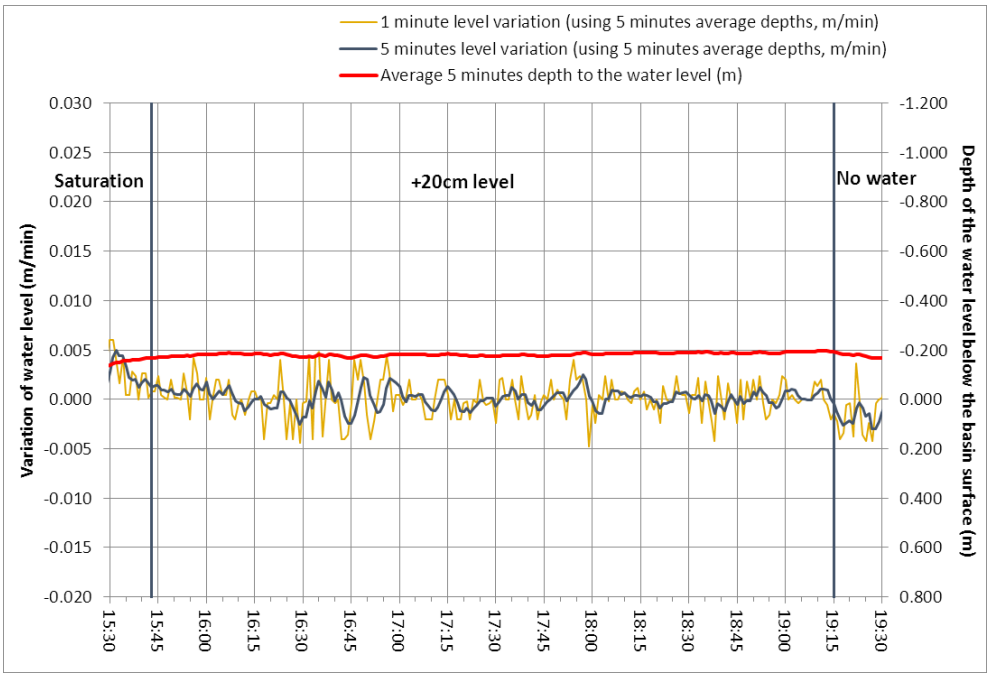

Figure 33 – Indication of the change on the variation of the water level during the period of maintaining a constant level above the infiltration basin

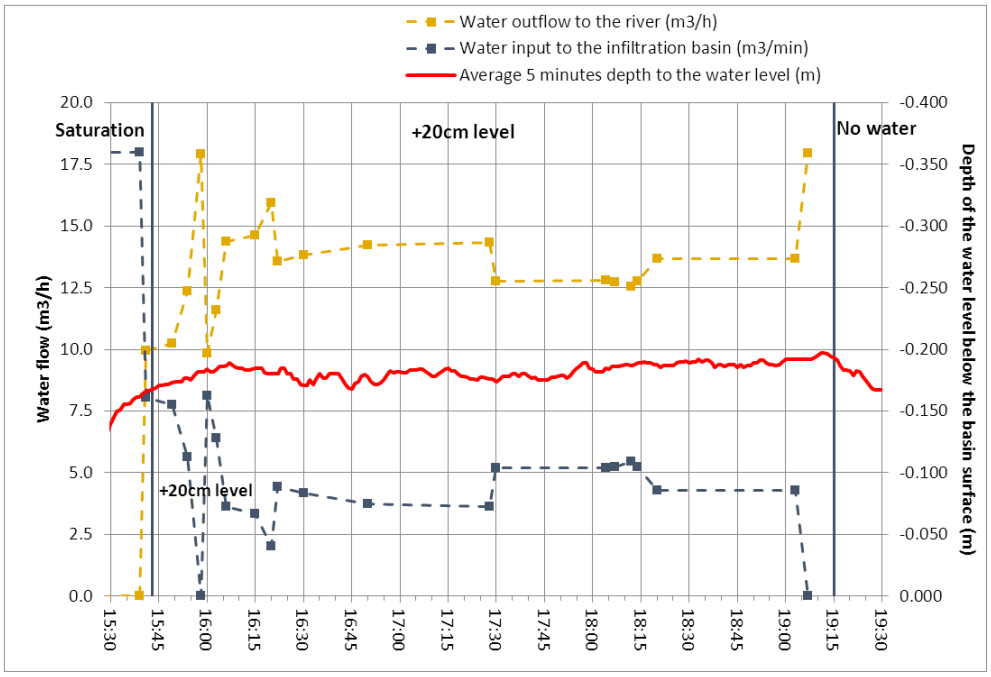

Figure 34 – Indication of the change on the variation of the water level and the controlled flows into the infiltration basin and out to the river during the period of maintaining a constant level above the infiltration basin

No input water stage

This may be the best situation to determine the infiltration rate of the infiltration basin. After water input is stopped the variation of the level as a function of time, while the level is above the ground surface is a direct estimator of the infiltration rate. Figure 35 represents the measured levels since 19:15 until 21:23 when automatic measurements of the test stopped. It also represents the level variations in 1 and 5 minutes interval. Considering the measured levels a best fit line is calculated. The slope (or derivative) of this line is the infiltration rate, which is determined to be 0.641 m/day.

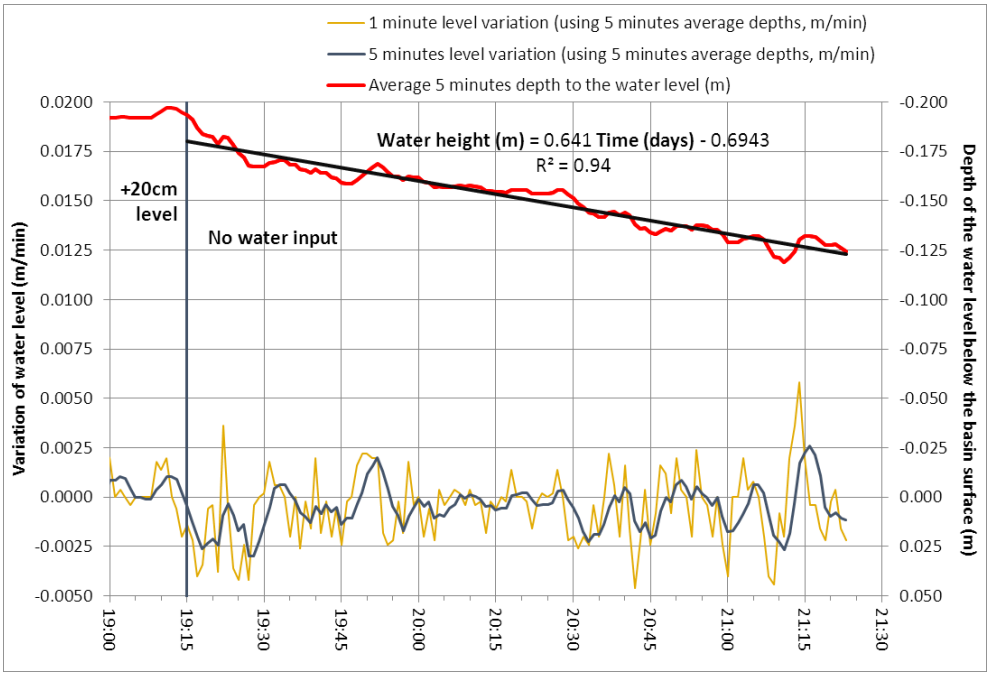

Figure 35 – Indication of the change on the variation of the water level during the period of no water input in the infiltration basin

A different analysis is carried out by considering the rate of change of the water level along time Figure 36. It can be seen that there is a general decrease of the infiltration rate as time increases. This may be due to the fact that the water height is diminishing. Figure 37 shows the same infiltration rate data projected against the water height. Note that each point represents the relation between the level changes since 19:15 until the time that the point represents divided by this time difference. As it can be observed, for larger water heights above the ground the infiltration rate is quite variable, but when the levels drop to about +0.155 m above ground this relation tends to stabilise between 1.0 m/day and 0.73 m/day.

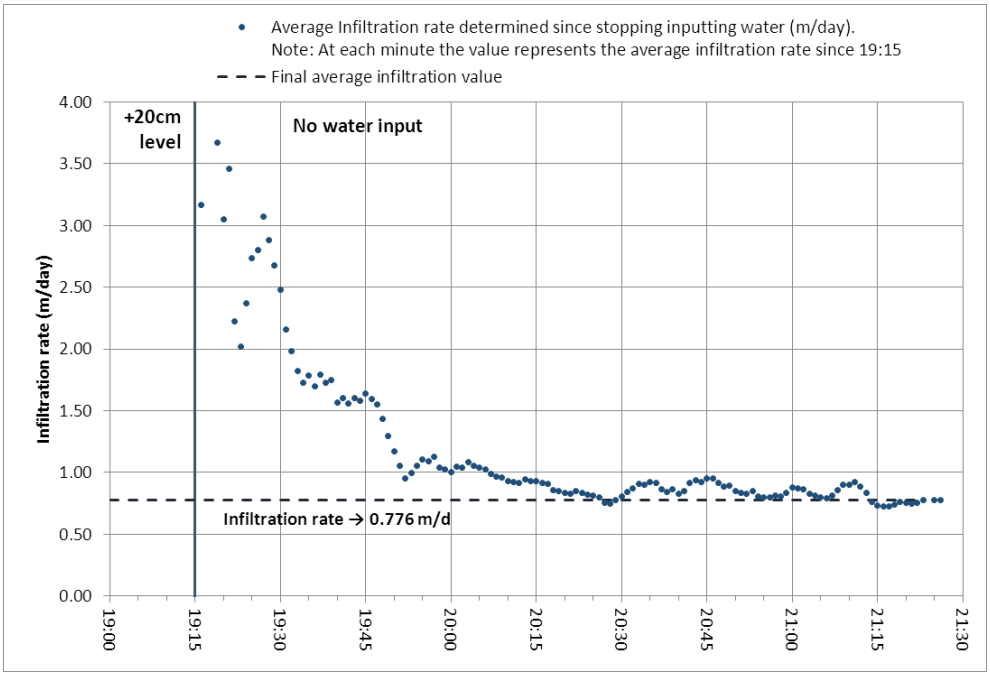

Figure 36 – Average infiltration rate since the beginning of stopping inputting water in the infiltration basin

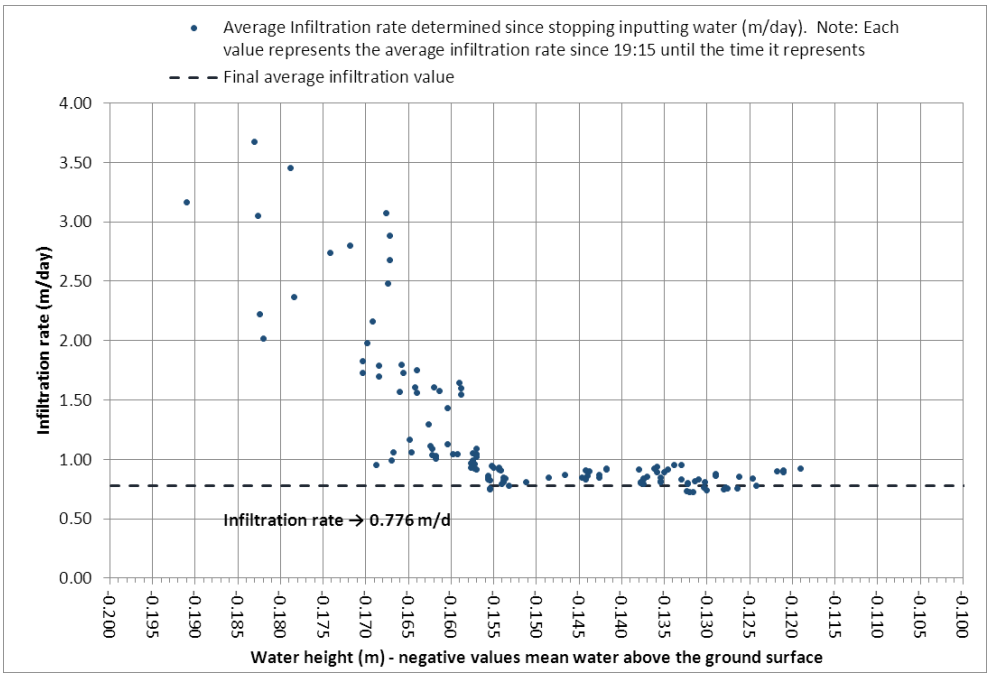

Figure 37 – Average infiltration rate since the beginning of stopping inputting water in the infiltration basin as a function of water height

Porosity

Initially as the material was incorporated in a dry condition into the IB, when filling the IB with water the relation between water incorporated in the IB and the total volume of IB (solids+voids)

corresponds to the porosity of the medium. This value is determined only when the IB is saturated (i.e., when the water level is at the surface), and not as a function of time. This single determination (instead of time dependent) is made because the totality of the input volume of water is not immediately incorporated in the bottom part of the IB but will partially fill some of the pores that will retain water instead of draining it into the bottom part of the IB. Another part of the input water will follow preferential paths and will immediately fill the bottom of the IB.

The (total) porosity of 15.6 % is estimated by excess using the calculations depicted in Table 3.

Table 3 – Estimation of the total porosity of the infiltration basin

Variable	Value	Units
Initial time	9:15	
Final time	14:28	
Time lapse	313	min
Water rate input in the IB	17.98	m^3/h
Input volume of water until saturation	93.8	m^3
Depth of the infiltration basin (IB)	6	m
Area of the IB	100	m^2
Volume of the IB	600	m^3
Total porosity (value calculated by excess)	15.6	%

Infiltration rate and clogging

Different parts of the test allow different estimates of infiltration rate. Table 4 summarises the results. It seems that the infiltration rate varies in relation to the water height in the infiltration basin. When the basin is full and the water level is more than 16 cm above the ground surface the infiltration rate is higher, and can go up to values of more than 1.19 m/day (as can be inferred in Figure 31, Figure 32, Figure 36 and Figure 37). For lower values of water height, the infiltration rate may be as low as 0.64 m/day and these values may become lower with decreasing water height.

Table 4 – Infiltration rate as determined using different stages of the infiltration test in the GABARDINE basin

Period of the test	Methodology	Infiltration rate
Increasing surface storage above infiltration basin	difference between water input and the variation of surface storage above the ground	1.19 m/day
Keeping surface storage above infiltration basin	control outflow discharge to the river so that the water level above ground surface of the infiltration basin could be kept at an approximated value of +20 cm	1.03 m/day
No input water	slope of level drawdown vs. time linear fit	0.64 m/day
	relation between long term level drawdown and time	0.78 m/day

The increasing rate of water level variation recorded near the end of time of the test filling stage, may be an indication of a clogged stratum inside the infiltration basin. This stratum (the basin material filled with fine particles) is located between 33 cm and 9 cm below ground.

PT1_1 and PT1_2: Infiltration test in all three basins, 29-30th September, 2014

Test description

This infiltration test aimed to determine the infiltration potential of the whole MAR river bed infiltration basins system.

The test was carried out during 38 hours using the water from a nearby well (around 130 m) with a flow rate of 31,3 m^3/h, and distributing it in the MARSOL and GABARDINE infiltration basins. The water was evenly sprinkled on the basins with the help of perforated tubes. A system of valves was in place in order to regulate the flows (Figure 38). The control of the inflow in the basins was calculated through the difference from the pumped flow rate to a discharge point, where the flow was measured with a 200 L barrel.

Figure 38 – System of valves to regulate the flow

It took 34 hours to fill the basins and to keep the water level constant above the basin level.

Methodology for determining the infiltration potential

Two different methods were used to determine the infiltration potential: i) during the final stages of pumping the water was rising at a slower pace due to the high infiltration. Since the pumping volume is known as the predicted level variation in a basin with same area but no permeability, it was possible to calculate the infiltration rate using the volumes calculated with the measured level variation; ii) the calculation of the volume variation through time using the level decrease (after pumping has ceased) in the two basins.

Results

The maximum infiltration capacity value for the three basins was estimated to be between 19.0 and 21.6 m^3/h, accordingly to the two methods above described.

Considering that MARSOL basin could infiltrate 15.65 m^3/h (as measured in the qualitative test on 13th and 14th October, see below) and the downstream GABARDINE 4.29 m^3/h (measured in the clogging test, see above), this could mean that the upstream GABARDINE basin has an infiltration capacity up to 1.66 m^3/h [1.66 m^3/h = 21.6 m^3/h (all basins) - 15.65 m^3/h (MARSOL basin) - 4.29 m^3/h

(downstream GABARDINE). However it is important to mention that this infiltration rate depends on the piezometric level, and can be augmented if this level is high.

The different behaviour between the basins is clear. Figure 39 shows the water level (measured first with the divers, and later with manual probes) in the infiltration basin tubes. It is clear that the basins weren't filled at the same pace, due to uneven water level dropping rates on the top. The IB1 (Figure 13) in the GABARDINE basin didn't come down to NHE as fast as the IB2 and IB3 in the MARSOL basin. These results could be related with the higher hydraulic conductivity of the basin filling material (newer), to the hydraulic conductivity of the aquifer material, or to the higher infiltration area due to its vertical slopes. However, the possibility that the IB1 was influenced with the water input upstream (from the MARSOL basin) shouldn't be disregarded.

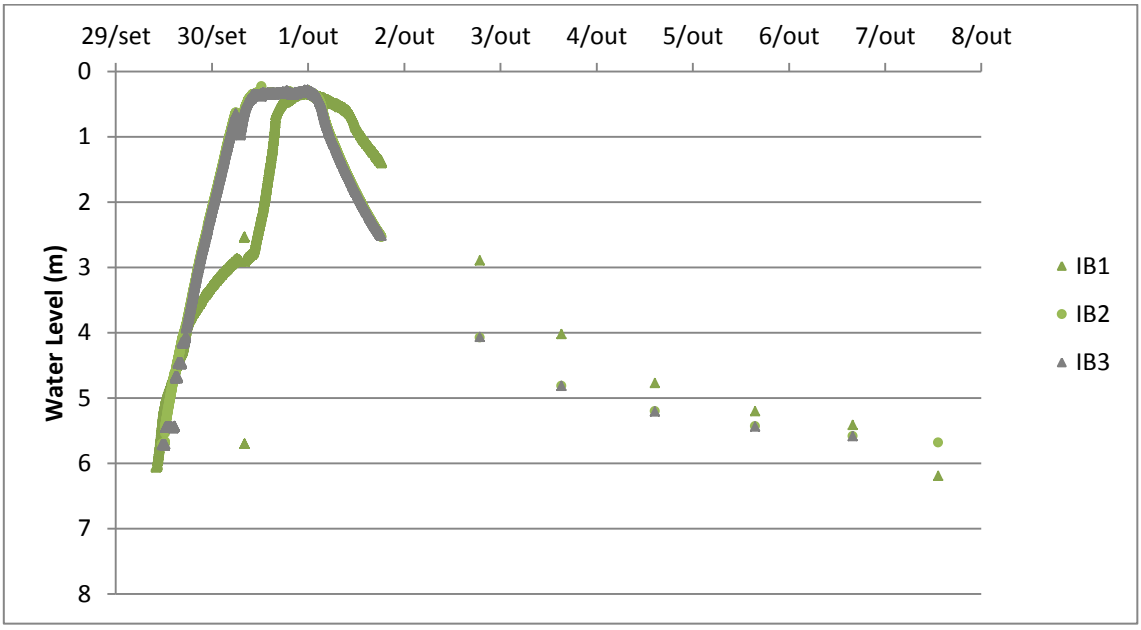

Figure 39 – Water level in the tubes in the basins during the quantitative experiment

PT1_2: Tracer test in MARSOL basin, 13-14th October, 2014

Test description and methodology

A NaCl tracer test was conducted in MARSOL basin between 13th and 14th October, 2014 in order to determine the infiltration capacity of this basin alone, as well as the velocity and dispersion in the aquifer. The salt was inserted into the infiltrated basin at 10:30 on 13/10/2014, which coincided with the time the infiltration basin became saturated with the injected water.

The infiltration rate value was calculated through the same steady-state injection/pumping method, i.e. the injected water into the basin is set to a value at which no water level variations are seen in the infiltration basin and all injected water in the basin is being infiltrated into the system. It is important to take into consideration the fact that the injection was ceased between 20:00 of the 13th and 08:25 of the 14th, for security reasons, and that during this period a heavy rainfall event occurred, which in total summed 19 mm. This rainfall event may have influenced somewhat the dispersion of conductivity.

Results

The infiltration rate value reached 15.65 m^3/h (1.87 m/d, considering the area of 201 m^2, see section 2.1.4), after fixing the water level around 20 cm above the basin floor.

Considering this value and the rate of the water level rise in the basin, the porosity of the basin filling material was calculated and should average 12,6%, a value that might change in time with the arrangement of the material inside the basin and fine particles potential clogging effect. It is worth mentioning that the top 20 cm of the basin seems to have a different porosity (slower water level rise) than the rest of the material (Figure 40). This can also be due to the compression of the filling materials of the basin, once the lower materials are subjected to a higher compressing level as opposed to the top of the basin.

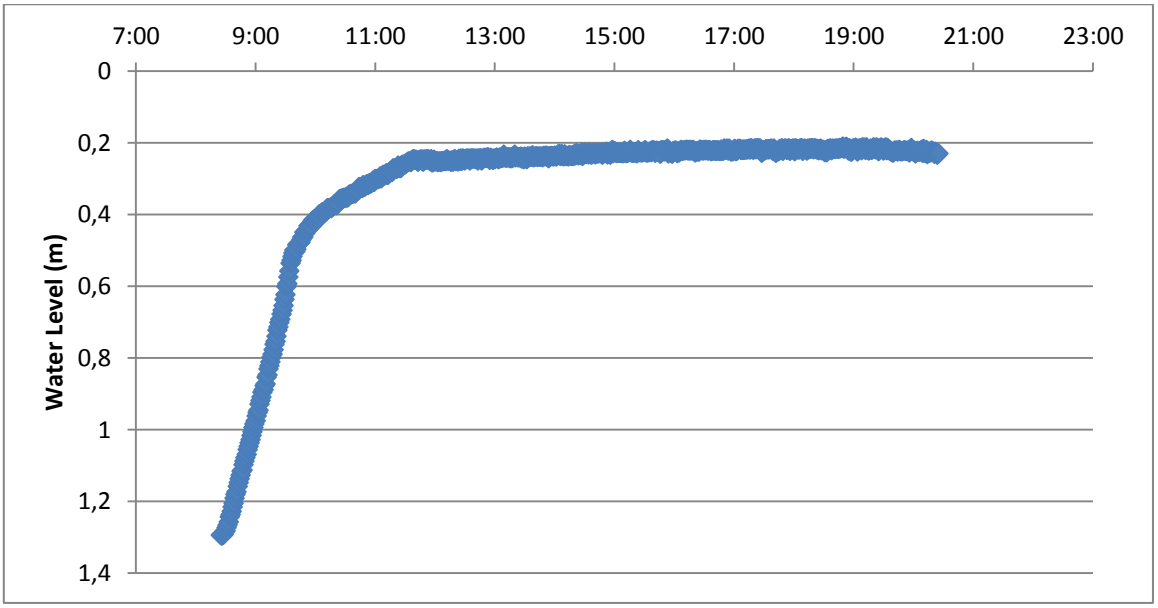

Figure 40 – Water level rise on the 14/10/2014 (average of IB2 and IB3)

Returning to the quantitative test (29th and 30th of September), during the drawdown, the infiltration volumes through time were calculated and compared to the average water level height above the hydrostatic level. The results were different for the GABARDINE and the MARSOL basins, and are shown in Figure 41 and Table 5. The scatter plot between the water level and the injection flow rate shows a trend with a logarithmic fit distribution and from this distribution, it can be seen that the MARSOL infiltration basin has a much higher infiltration capacity than the GABARDINE infiltration basins in general.

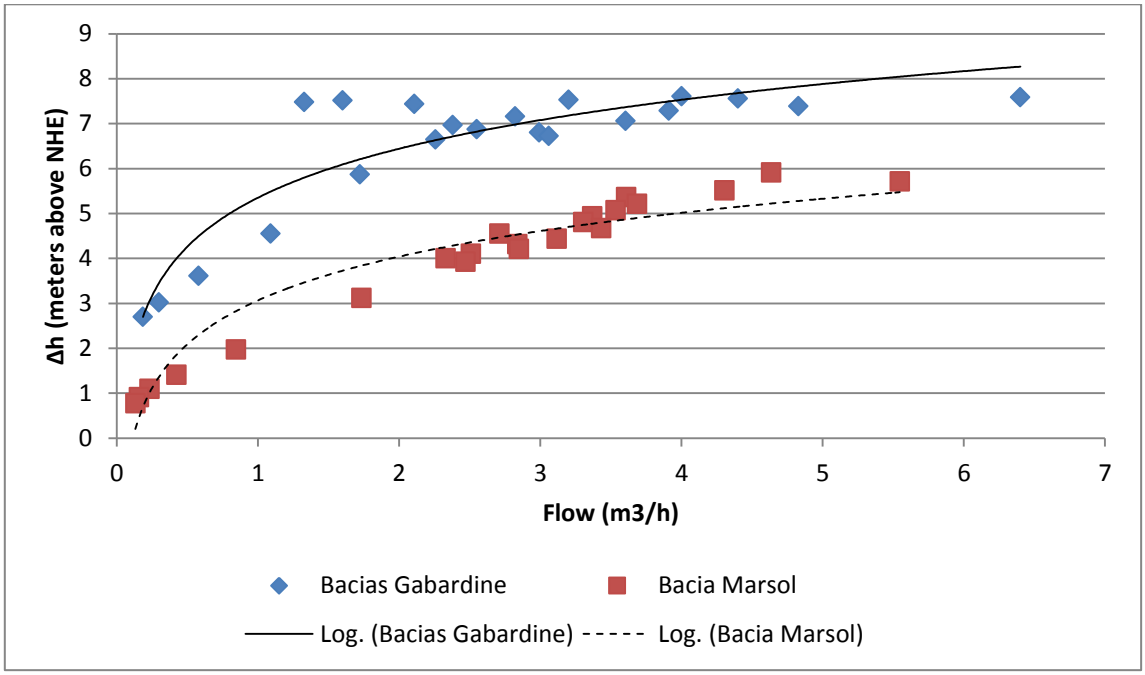

Figure 41 – Infiltration flows vs water height above the hydrostatic level in the MARSOL and GABARDINE basins in Campina de Faro

Table 5 – Infiltration of the Campina de Faro basins, accordingly to the vertical gradient

	Flow (m^3/h)		
Δh (m)	MARSOL	GABARDINE	Total
1	0.2	0.1	0.3
2	0.5	0.1	0.6
3	1.0	0.2	1.2
4	1.9	0.4	2.4
5	4.0	0.8	4.8
6	8.1	1.5	9.6
7	16.4	2.9	19.3

The location of the monitoring points is presented in Figure 42. The results on the piezometers are presented in Figure 43 (MS3), Figure 44 (MS2), Figure 45 (MS1), Figure 46 (LNEC1), Figure 47 (LNEC2), Figure 48 (LNEC3), considering only the period during the experiment, with various flow rates. To facilitate comparison between all monitoring points and for a period of a week, a representation of the groundwater level at all piezometers is shown in Figure 49 and all the records for electrical conductivity are comprised on Figure 50.

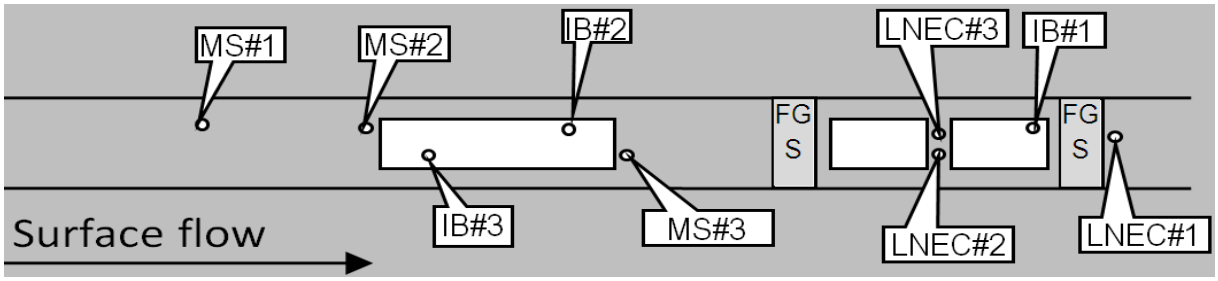

Figure 42 – Schematic location of the monitoring points used during the tracer test

The data show a significant positive response from most of the piezometers. MS3 is the piezometer with the clearest response, showing the influence of the injection immediately when the pumping started to fill the basin. This can also be seen with the restart of the pumping on the morning of 14/10/2014 and with the maximum level of about 3.6 m depth to water level being achieved during the injection of water. Groundwater level recovery appears to be about 5 days after the test at about 5.30 m. Also, this was the only piezometer which appeared to present a stable groundwater level, particularly during the first day of the test, before interrupting the injection pump. From the data is also clear that the rainfall on the night of the 14/10/2014 did produce a slight increase in the groundwater level.

MS2 also showed a quick response to the injection test, though the maximum level (around 5.6 m) being achieved at approximately 4 hours after the end of the test (which occurred at 20:00 of 14/10/2014), at midnight of the 15/10/2014. The groundwater level recovered to 6 meters 3 days after the injection test.

Piezometer MS1 does appear to show a residual response, with maximum level being achieved 8 hours after the end of the injection test (4:00 of the night of 15/10/2014). It is not clear if this influence is due to the injection test but the fact that the piezometer level decreases up to 10 cm in one day after 4:00 of the 16/10/2014 suggests the injection test influenced the levels of this piezometer.

In the case of LNEC1 it is important to take into consideration the fact that, during the interruption of the pumping, which coincided with a heavy rainfall event, the depth to water level at LNEC1 had a sharp peak, increasing from 5.5 to 3.75 m in 3 hours. This peak is clearly an effect of the rainfall event and not of the injection test. This is confirmed by the decrease on EC value after this event (Figure 50). Anyway, there is a clear decreasing groundwater level trend 7 hours after the end of the test, at 3:00 of the 15/10/2014. This peak being an influence of the test suggests the maximum depth groundwater level was about 5.35 and during the following 4 days groundwater level returned to 5.65 m.

In the case of LNEC2 it is not clear if there is an injection test influence on groundwater levels. There is a slight peak in groundwater level at 6 am of 15/10/2014 at 6.15 m, which appears to drop 2-3 cm during the next 6 hours. LNEC3 as well does not show a clear response to the test, since in this case a peak was not detected and groundwater levels kept increasing residually during the monitoring period. Considering LNEC3 is located in the confined unlike all the other piezometers, this increase in groundwater level could be associated to an effect of leakage recharge from the top aquifer.

The influence of the test was felt also 50 m upstream the MARSOL basin in MS1, 30 hours after the end of the experiment.

The piezometer LNEC 2 also showed a 50 cm rise, 8 hours after the end of the test. LNEC3 well, in the confined aquifer, didn't react. This fact suggests there is no hydraulic connection between the upper unconfined aquifer and the lower confined aquifer in the area around the infiltration basins.

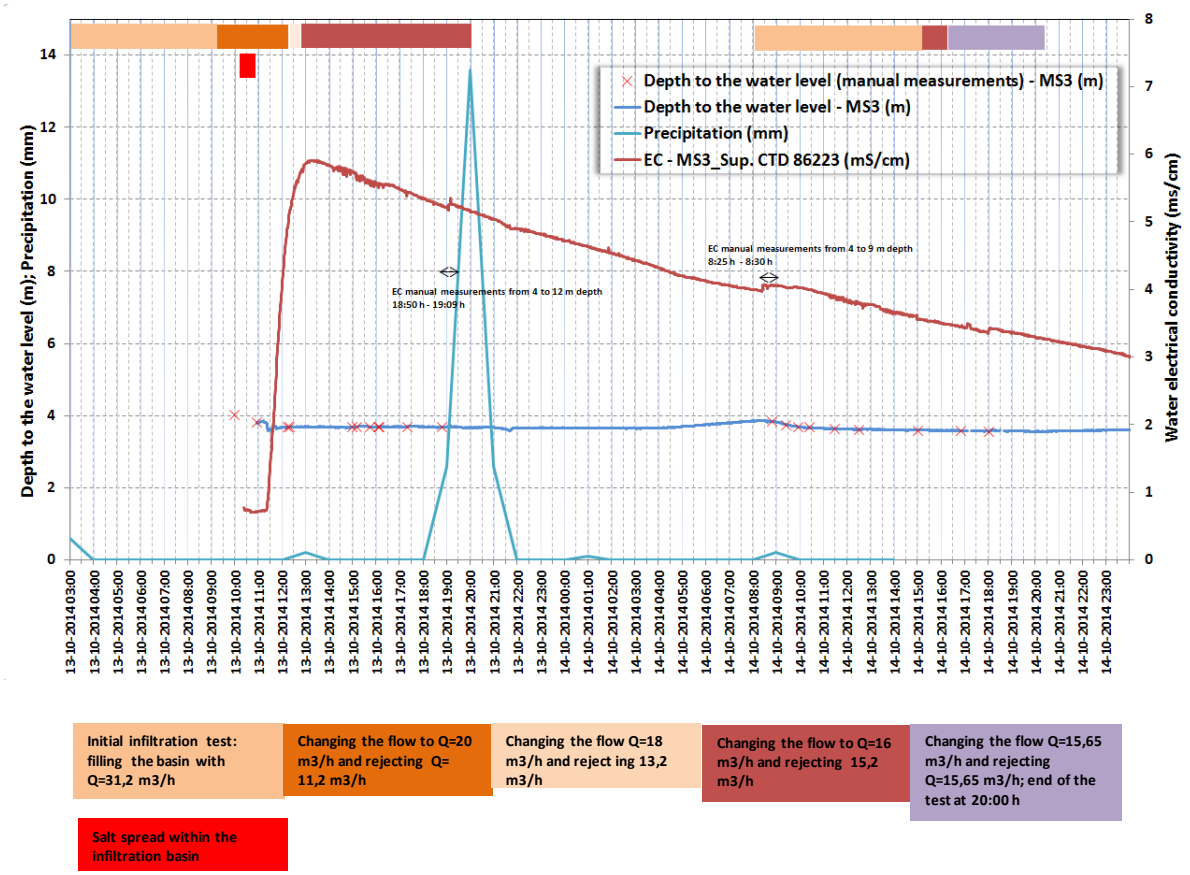

Figure 43 – Changes in EC and piezometric level in MS3 piezometer during the tracer experiment

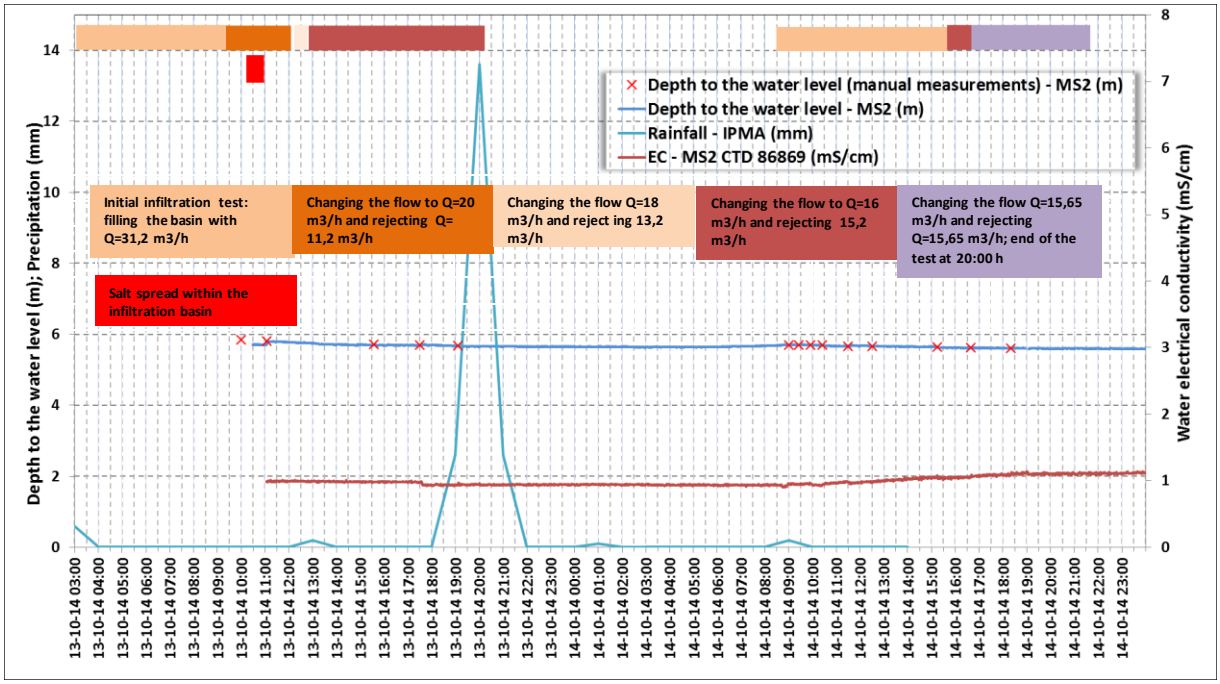

Figure 44 – Changes in EC and piezometric level in MS2 piezometer during the tracer experiment

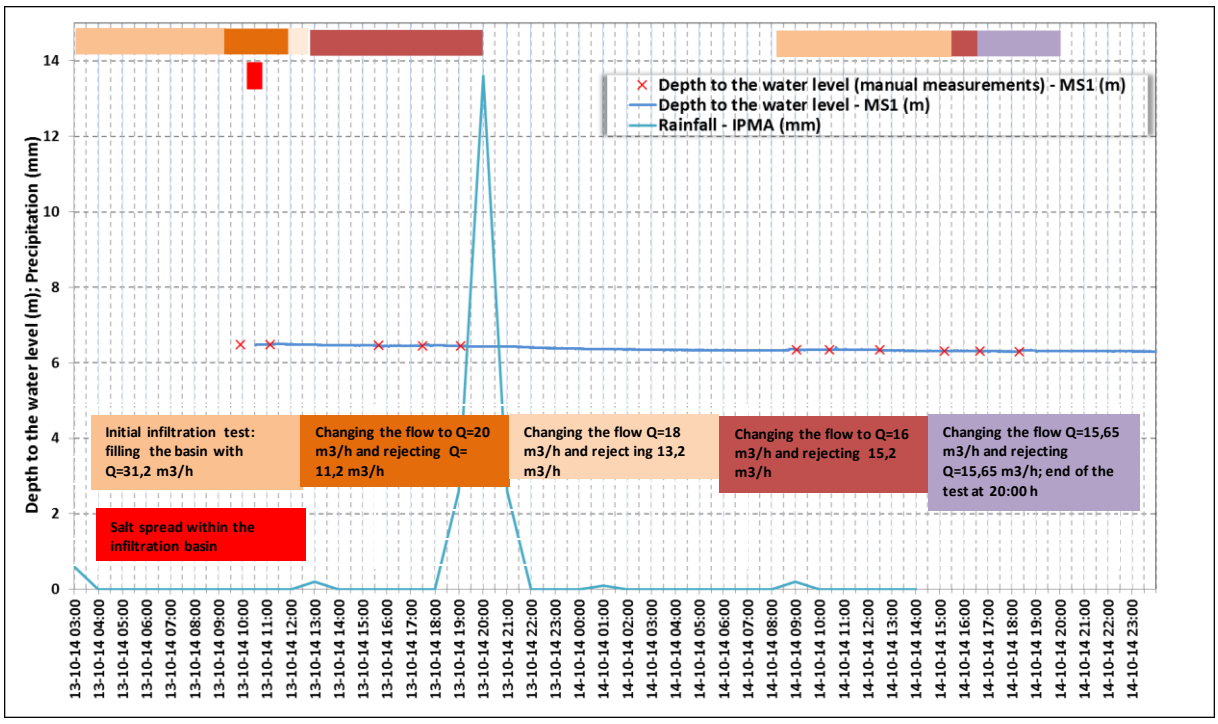

Figure 45 – Changes in piezometric level in MS1 piezometer during the tracer experiment

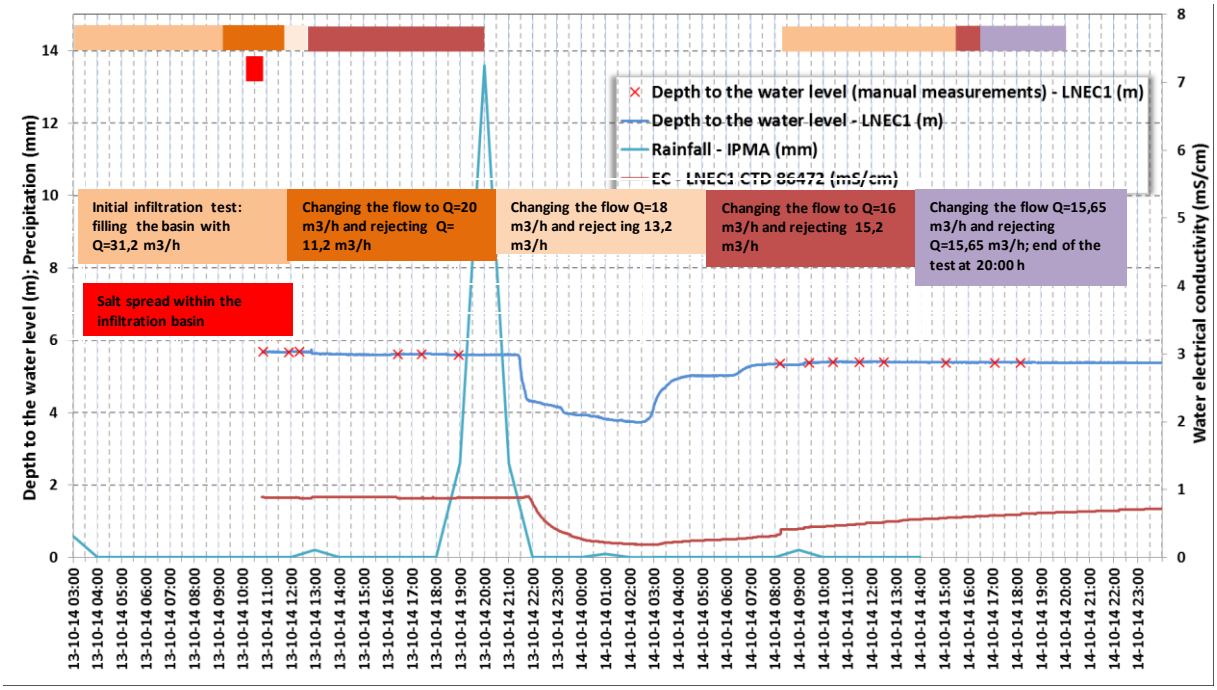

Figure 46 – Changes in EC and piezometric level in LNEC1 piezometer during the tracer experiment

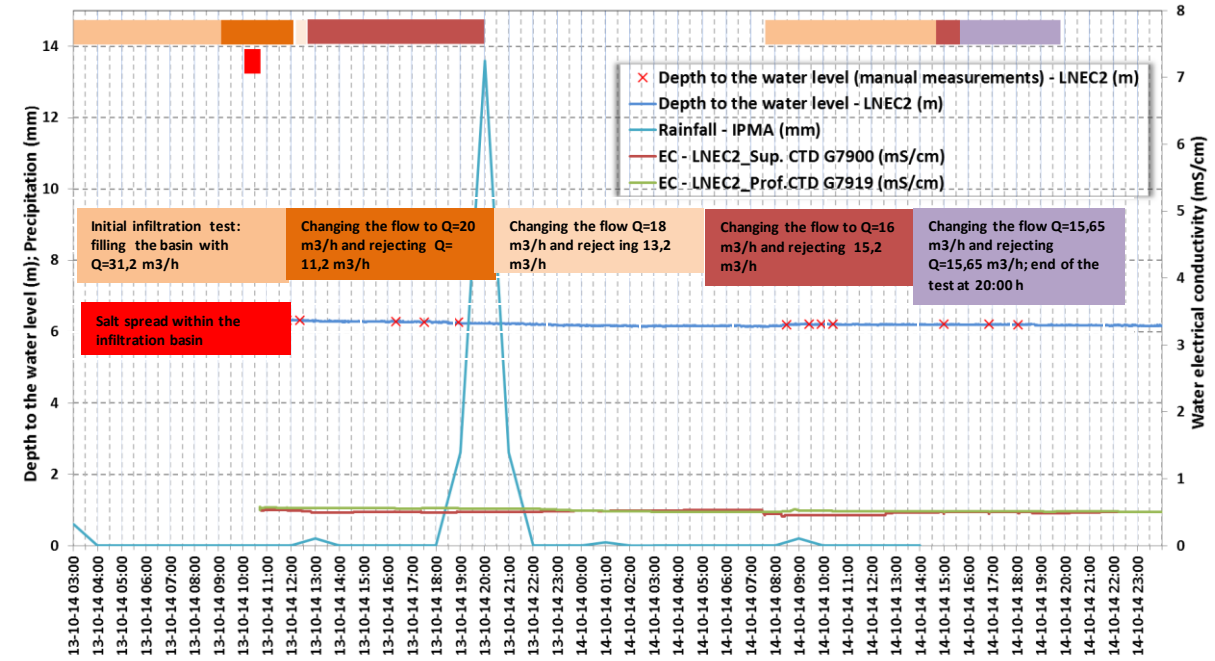

Figure 47 – Changes in EC and piezometric level in LNEC2 piezometer during the tracer experiment. Two divers were installed on different levels, at approximately 8 meters (LNEC2_SUP) and 20 meters (LNEC2_Prof)

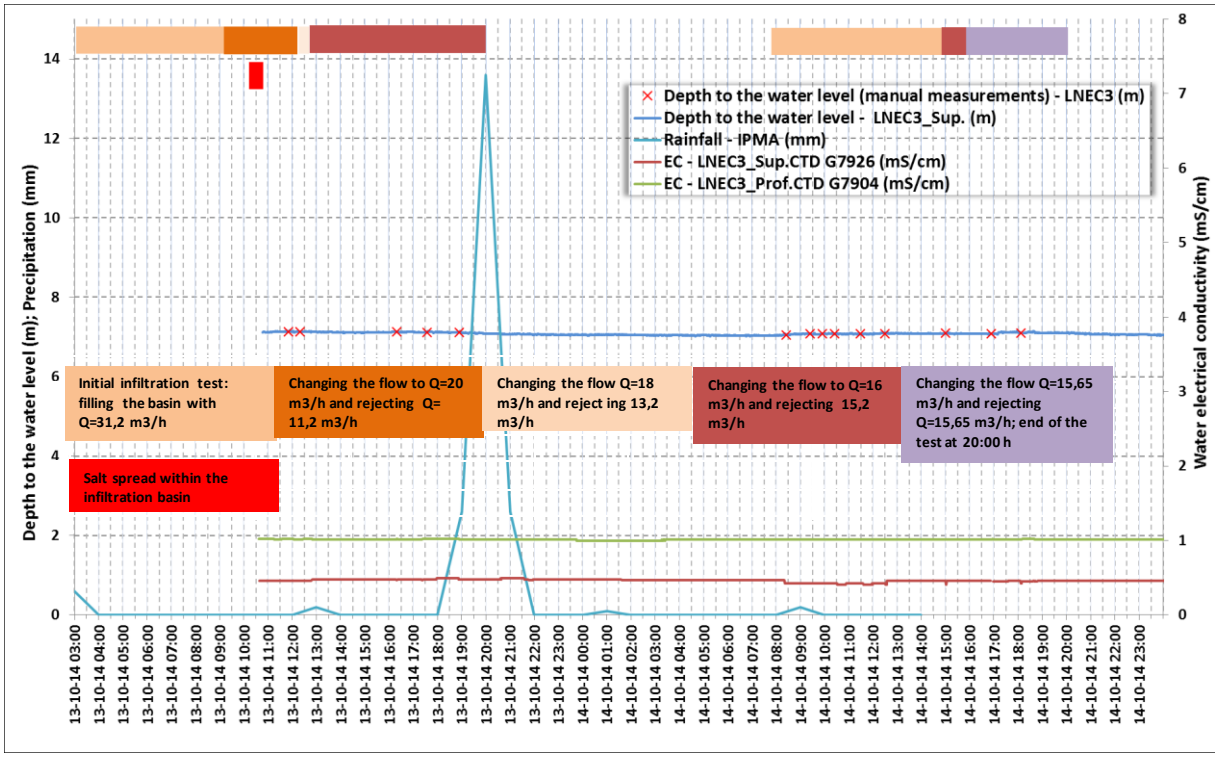

Figure 48 – Changes in EC and piezometric level in LNEC3 piezometer during the tracer experiment. Two divers were installed on different levels, at approximately 10 meters (LNEC3_SUP) and 35 meters (LNEC2_Prof)

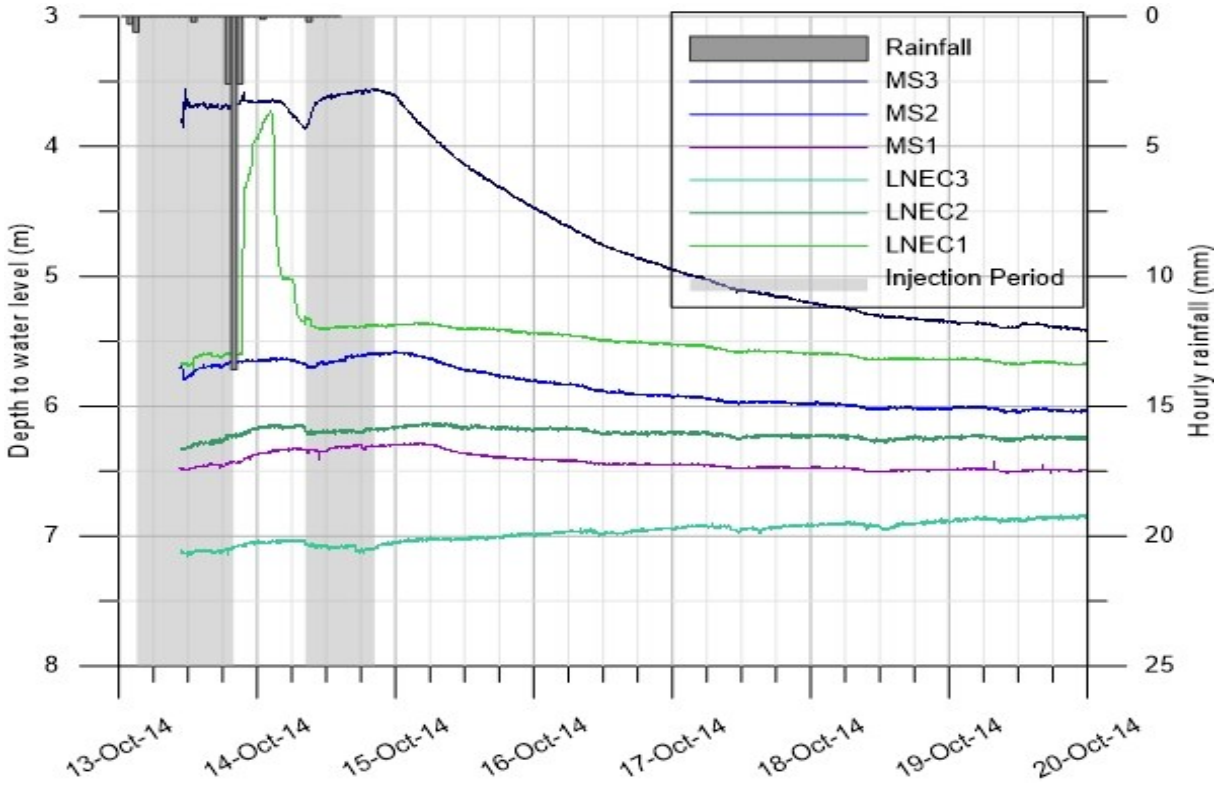

Figure 49 – Depth to water level at all monitoring wells

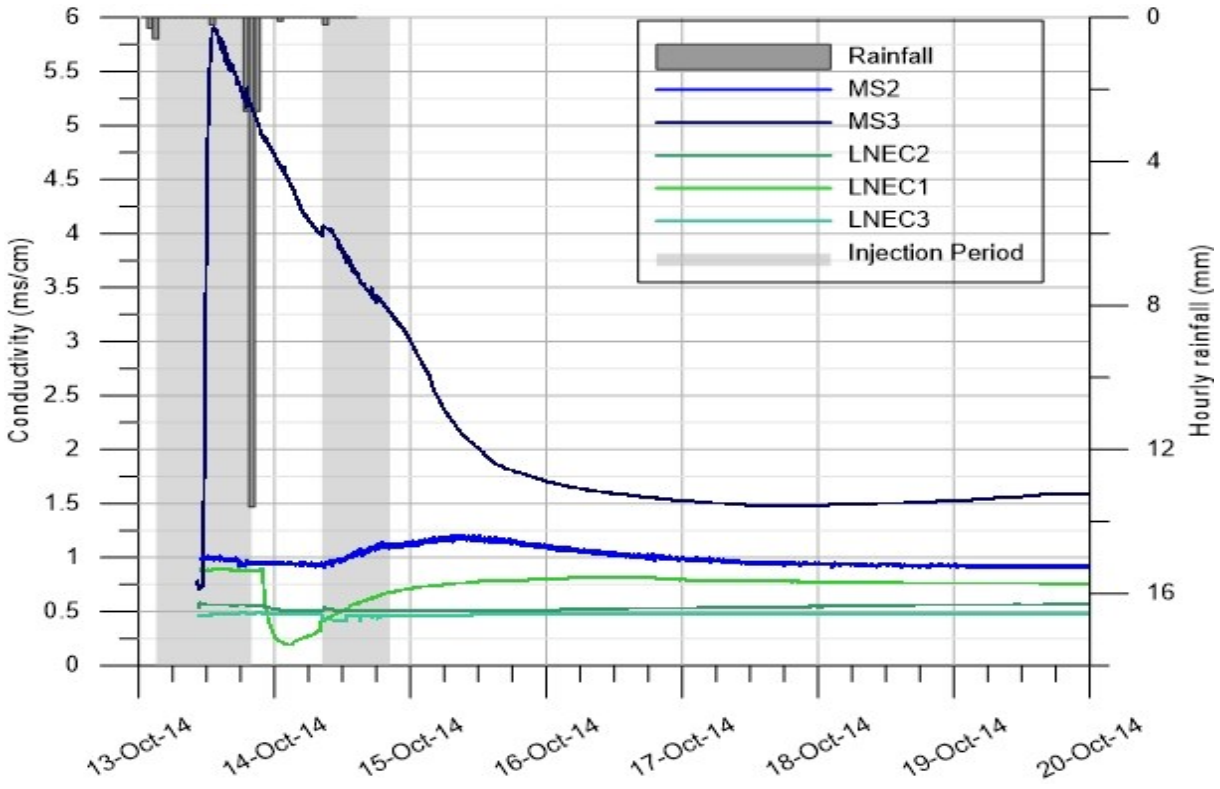

Figure 50 – Electrical conductivity at all monitoring points

Regarding the effect of the salt tracer on the electrical conductivity at the monitoring points, the piezometer immediately downstream to the infiltration basin had a quick and clear response achieving the peak breakthrough 3 hours after the introduction of the salt in the basin, at 13:30 of the 13th, and with an increase in electrical conductivity from around 0.7 mS/cm to 6 mS/cm. The peak breakthrough happened before the interruption of the injection of water between the night of 13th and 14th. Anyway, the heavy rain episode that occurred contributed to the washout of the tracer even though there was no injection of water during a period of nearly 12 hours (injection stopped at 20:15 on the 13th and restarted at 08:25 of the 14th). In fact, when the injection restarted on the 14th, electrical conductivity at MS3 had decreased from 6 to 4 mS/cm already.

As for MS2, located immediately upstream the infiltration basin, a small increase in electrical conductivity can be noted from 0.9 to 1.2 mS/cm, with a peak occurring approximately 12 hours after the interruption of the injection (around 10:00 of the 15th). This shows that, at some extent, the infiltrated water may have created a groundwater mound effect, in which water flows radially in the infiltration basin, therefore proportioning an increase of groundwater level all around the infiltration basin, but moving in the flow direction. This is the reason why the electrical conductivity peak is much sharper downstream, showing the main direction of the groundwater flow.

In the remaining monitoring points, the influence of the tracer was not so easy to identify, maybe due to the heavy rain that occurred between the nights of 13th and 14th October. LNEC3 didn't show any significant changes as expected due to its location on the lower confined aquifer. LNEC2 has showed a mild increase in electrical conductivity of about 0.1 mS/cm before the interruption of the

injection, which is then countered by the rainfall event resulting in a slight decrease. Still, after the restart of the injection on the morning of the 14th, this piezometer shows an increasing trend long after the end of the test, but it is not clear if there has been a peak breakthrough. This indicates that at some extent, this piezometer might be subject to some degree of confinement from the infiltration basin groundwater formation. In the case of LNEC1, once again there was a strong influence of the rainfall episode, which produced a decrease of the electrical conductivity from 0.9 to 0.2 mS/cm. On the other hand, a peak can be observed at around 12:00 of the 16th of October, 40 hours after the end of the injection period, and 73 hours prior to the injection of the tracer.

Considering the peaks observed at MS3 and LNEC1, and the distance between both, it is possible to have a rough estimate of the tracer velocity between these two monitoring points. The necessary data for these calculations are presented on Table 6.

Table 6 – Data for the calculation of the velocity of the tracer dispersion between monitoring points MS3 and LNEC1

	Peak breakthrough time after injection of salt (hours)	Distance from MARSOL Infiltration Basin (m)
MS3	3	0.5
LNEC1	73	82

Considering the data on the previous table, the distance between monitoring points MS3 and LNEC1 is 81.5 m and the time between peaks at both points was 70 hours, which results in tracer groundwater velocity of 1.16 m/h. Though there is an increase in MS2, located upstream the infiltration basin, this effect is due to the mound effect of the recharge in the infiltration basin and not due to the main flow direction of the infiltrated water. It can thus be concluded that the main direction of groundwater flow is south, in the river downstream direction.

Some pictures of the tracer test are presented in Figure 51, in which it is possible to see the filling of the infiltration basin, the spreading of the salt and the infiltration basin filled with water.

Figure 51 – Tracer test at Rio Seco MARSOL infiltration basin (PT1_2 Campina de Faro)

PT1_2: Small infiltration test during Mid-Term meeting, 24th June, 2015

Test description

On 24th June 2015 a minor infiltration test was performed on the upstream GABARDINE infiltration basin (20 m long, 5 m wide and 6 m deep). Water injection started at 9:00 with a flow of 20 m^3/h and water level in the basin was at 1.72 m (Figure 52). After 3 hours, at 12:00, water started to reach the basin surface and injected flow was changed to 9 m^3/h and was kept like this until 18:00 in order to keep a column of water of about 20 cm above the infiltration basin.

Results

The monitoring results of this test are presented in Figure 52.

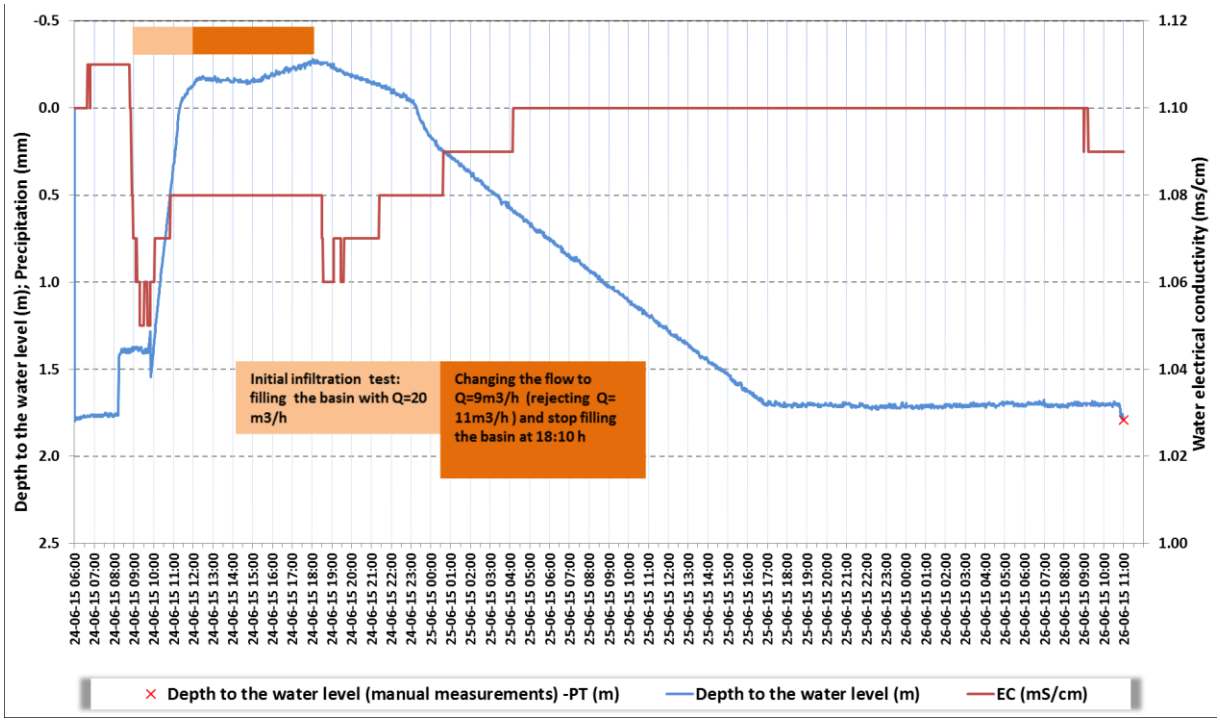

Figure 52 – Groundwater level and electrical conductivity measured on the infiltration basin

During this test it was possible to identify a thin clogging clay layer of about 25 cm close to the surface, which is expressed by a steeper groundwater level variation gradient after the injection period between 23:00 of 24/06/2016 and 00:00 of 25/06/2016.

Prior to stopping the water injection, at 18:10 on 24/06/2016, groundwater took approximately 1 day (at 17:00 on 25/06/2016) to decrease to the initial level observed at the beginning of the test (1.72 m).

Regarding electrical conductivity values, these have slightly decreased from 1.10 mS/cm to 1.06-1.08 mS/cm during the injection period, which is due to the injected water having lower electrical conductivity than the existing water in the infiltration basin. Anyway, after the injection period, the electrical conductivity of the water in the infiltration basin slowly increased to 1.10 mS/cm.

During this test, a stable water column level above the infiltration basin wasn't achieved; therefore it is not possible to estimate the infiltration capacity of the basin. This was not the purpose of this test, notwithstanding, it is possible to have a rough estimate of the infiltration capacity of the basin, based on the water level decrease since the cease of the injection until the time the water column above the basin infiltrates. Therefore, the maximum water level achieved was 0.26 m above the soil (at 18:10) when the injection ceased and it took until 23:00 for the water column above the basin to infiltrate, resulting in an infiltration rate of 0.26 meters in 5 hours. This is equal to 0.052 m/h, which, considering the total area of the infiltration basin as 100 m^2 returns a total infiltration capacity of 10.4 m^3/h. Clogging effect was not assessed since the basin is new.

PT1_2: Natural recharge episodes

Between November 2015 and January 2016 strong rainfall episodes have occurred in the DEMO site area, which have produced visible effects in the infiltration basins and, therefore, at monitoring wells (Figure 53). Daily rainfall data was collected from *Direção Regional de Agricultura e Pesca do Algarve* (DRAP) Meteorological station in Faro.

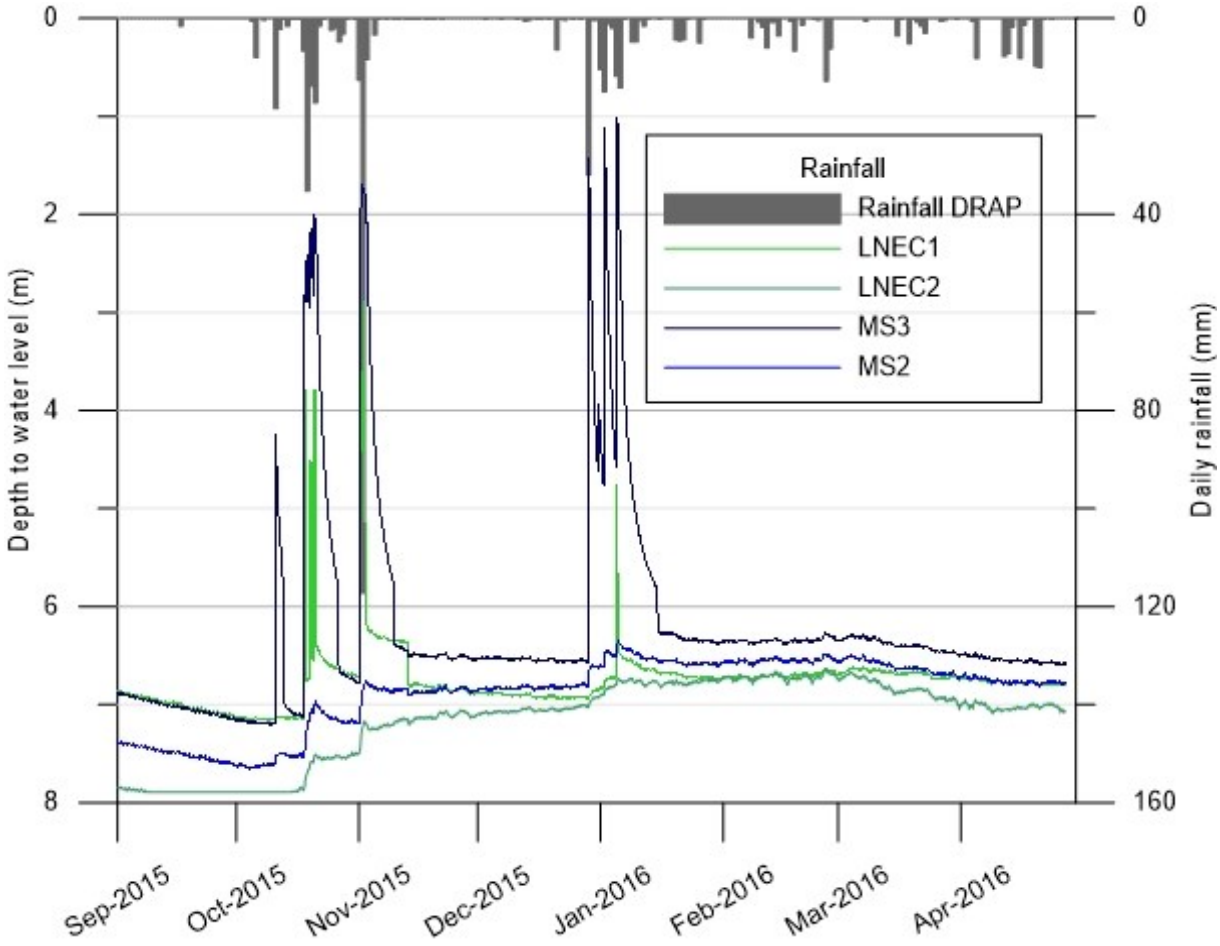

Figure 53 – Rainfall influence on monitoring wells around infiltration basins at Rio Seco, between September 2015 and April 2016.

As can be seen in the Figure 53, all of the monitoring wells respond to the major rainfall events, though the monitoring well MS3, the one located immediately after MARSOL basin is the one with the highest response to the rainfall events. Increases of groundwater level in the order of 4 to 6 meters can be seen at monitoring well MS3. Monitoring well LNEC1, located downstream the GABARDINE infiltration basins also presents significant increases in the groundwater level, but not as frequently as it happened with MS3 and also with a lower increase. The remaining monitoring wells, LNEC2 and MS2 showed only minor increases when compared with the previous.

In fact, focusing on the rainfall event in early January 2016, during which a 30 mm rainfall episode occurred, groundwater level at MS3 increased about 5 meters. In the same period, groundwater levels were measured manually twice a day at the infiltration basin and during which, a maximum increase of 4.33 m inside the infiltration basin was recorded (Figure 54). It is possible that higher

increases of groundwater level could have been achieved, but for security reasons, it was not possible to install a diver at the infiltration basin, so only manual measurements were performed.

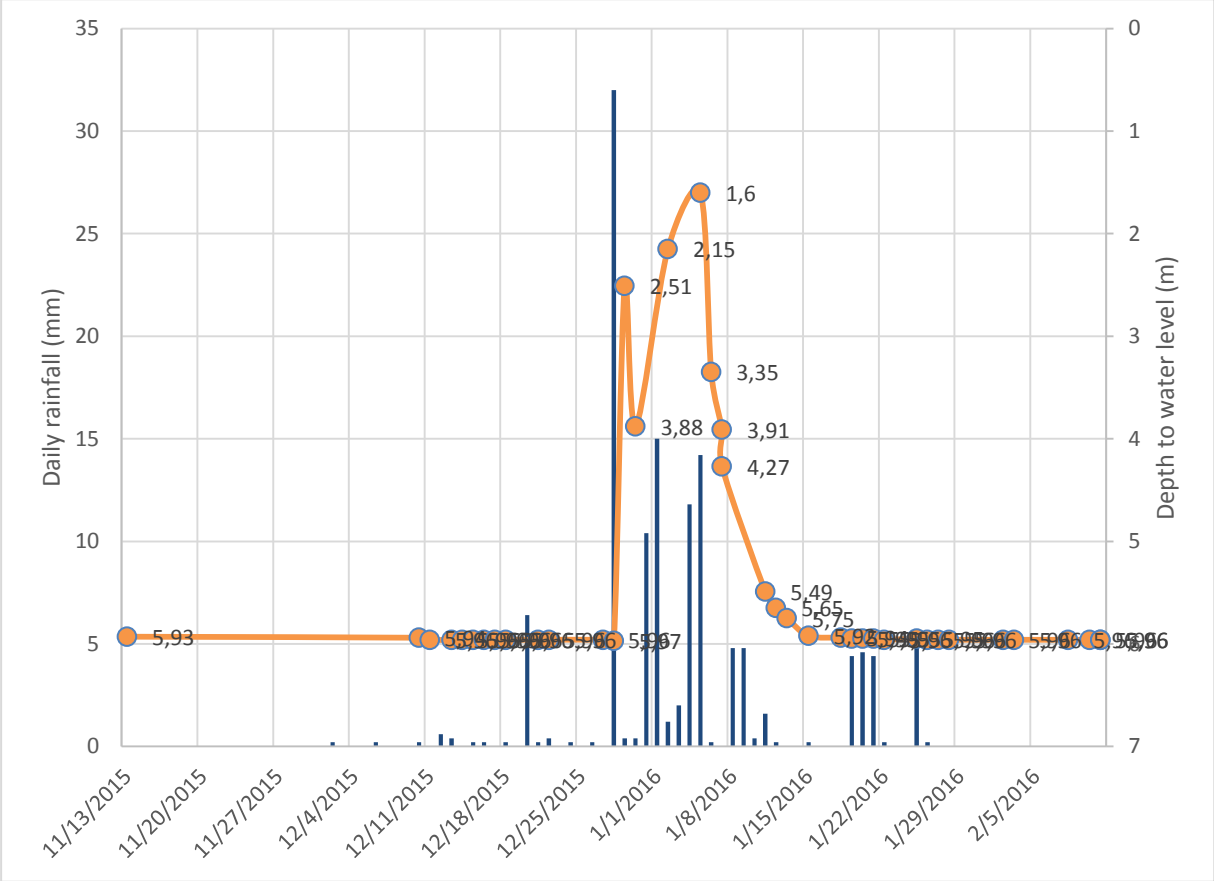

Figure 54 – Groundwater level measured manually at MARSOL basin

The facts that LNEC1 and MS3 are located immediately downstream the infiltration basins, and have relatively higher increase in groundwater level with rainfall events when compared with the remaining monitoring wells, evidences the impact of the natural recharge episodes in the infiltration basins, and their local/regional effect.

An overview of the conductivity at the monitoring wells also shows the effect of the rainfall events on the decrease of conductivity values (Figure 55). Again, the monitoring wells immediately downstream the infiltration basins (LNEC1 and MS3) show in general a higher influence by the rainfall events.

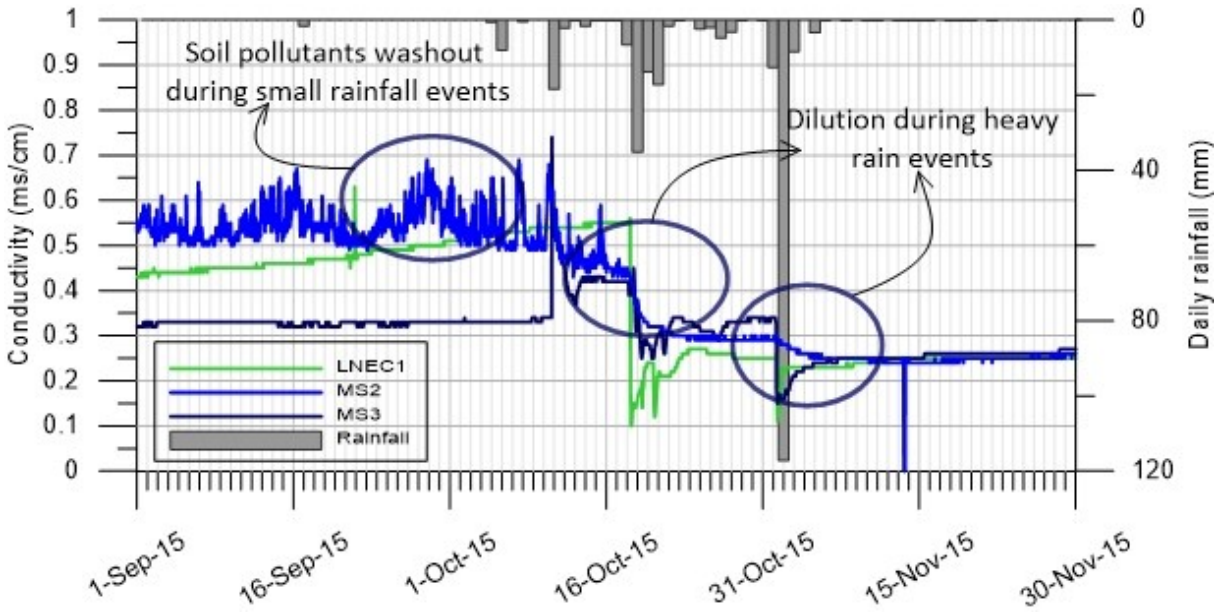

Figure 55 – Evolution of conductivity values at MS2

From Figure 55 it is possible to identify two distinct processes of groundwater remediation as a result of the infiltration basins activity. During small rainfall episodes, soil pollutants are washout from the groundwater. As opposed, during heavy rainfall events, a process of dilutions is instead more dominant. This data shows that the infiltration basins can have a significant impact in the remediation in Campina de Faro groundwater contamination, playing an important role at a local scale. On top of that, this is a passive system, which basically relies on natural recharge episodes in order to contribute to local groundwater contaminants removal or dilution such as Nitrates.

PT1_3: Infiltration in large wells, 1st October 2014

Test description

At Campina de Faro Demo Site PT1, one of the goals of the project consists in assessing the infiltration capacity of large diameter wells.

In this context, an injection test in a large diameter well, located near the infiltration basins from DEMO site PT1_1 and PT1_2 (Figure 56) was performed on October 1st 2014. The injected water was pumped from a well located 15 m next to the large diameter well. The pumping well is abstracting from the lower confined aquifer, while the injection large well is only in contact with the upper unconfined aquifer, hence, no interferences between the injection and pumping are expected.

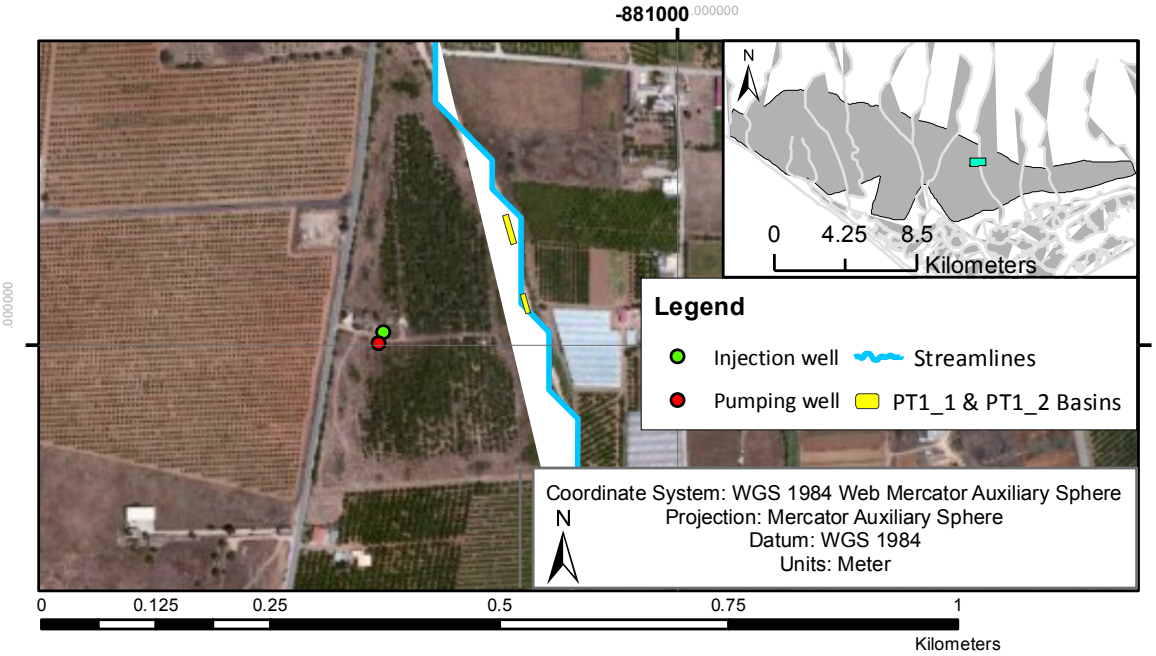

Figure 56 – Location of the injection and pumping well, as well as the infiltration, PT1

The well used for injection, shown in Figure 57, consists of a large diameter well with a diameter of 4.5 m and a total depth of 19 m. Depth to water level at the beginning of the test is 10.28 m. The well's characteristics are synthetized in Table 7.

Table 7 – Campina de Faro well characteristics

Total depth (m)	19
Diameter (m)	4.5
Radius (m)	2.25
Well surface area (m^2)	15.90
Depth to water level before the infiltration test (m)	10.28

Figure 57 – Infiltration test at DEMO site PT1_3, injection test at a large diameter well. The pumping well can be seen on the bottom of the left picture

The injection test consisted of a step test with three different flow rates as follows:

- Step 1: 7.5 and 6.5 m^3/h;
- Step 2: 16 m^3/h;
- Step 3: 35 m^3/h.

For each injection step, water flow rate was measured with a 200 l container. Water displacement (Δh), i.e. changes in the water level relative to a specific time, was recorded both manually and with an automatic CTD-Diver (with 1 minute interval between records). Besides the three injection steps, water displacement was also recorded for the recovery period, i.e. the period after the injection of water has ceased. The CTD-Diver was removed on October 7th 2014 (approx. 6 days after the injection test started).

For all three steps, injection lasted until water level stabilization was achieved. This can be considered a steady head injection, i.e. water level is stabilized, meaning that all water injected in the well is being infiltrated by the system. The injection test characteristics are synthetized in Table 8 . In this table, the value Water displacement (rise of water level) $\Delta \boldsymbol{h}$ (m) stands for the observed water displacement with reference to the beginning of each step, and Total (Accumulated) water displacement $\Delta \boldsymbol{h_{total}}$ (m) stands for the observed water displacement at the end of each step with reference to the initial depth to the water level (hydrostatic level=10.28m) of the injection test. The injected volume was calculated at each step by multiplying the injection rate by the step duration.

Table 8 – Injection test characteristics

	Step 1	Step 2	Step 3
Injection flow rate (m^3/h)	7.6 and 6.5	16	35
Water displacement (rise of water level) $\Delta \boldsymbol{h}$ (m)	0.46	0.73	1.13
Total (Accumulated) water displacement $\Delta \boldsymbol{h_{total}}$ (m)	0.46	1.18	2.31
Time to reach stable water level (min)	263	262	238
Step duration (min)	322	299	249
Injected volume (m^3)	37.47	79.73	145.25

After the injection period, recovery was monitored during 7934 min (about 6 days) and a residual recovery of 0.02 m was determined.

In fact, injection flow rate for step 1 was originally measured at 7.6 m^3/h, but at 142 minutes there was a decrease in the flow rate from 7.6 to 6.5 m^3/h. Hence, total injected volume for step 1 is equal to 7.6 X (141/60) + 6.5 X (181/60) = 37.47 m^3.

The observed water displacement for each step was 0.46 m for step 1, 0.73 m for step 2 and 1.13 m during step 3. During recovery period, observed water displacement was 2.29 (after approximately 6 days, when the CTD diver was removed) resulting in a residual recovery of 0.02 m.

Calculation of injected and infiltration volumes and rates

The estimation of the infiltration rates in the well was divided in three sections:

- Transient state injection period for each step – i.e., water level was not stabilized;

- Steady state injection period for each state – i.e. a water level stabilization was found;
- Transient state recovery period.

Transient state injection period

During the transient state of the injection period, the infiltration rate was estimated based on the observed water displacement and a theoretical water displacement, assuming the well as an impervious recipient. In this case, the theoretical water level rise for a given period of time (hc_t) is calculated according with the equation (1):

$$\textbf{(1)}\quad hc_t = \frac{Va_t}{A}$$

Where:

- hc_t stands for a theoretical water level displacement considering the well as an impervious recipient for a given time period (L);
- Va_t stands for the injected volume of water in the well for a given time period;
- A stands for the well's surface area (L^2).

Based on the observed water displacement (Δh_t) for a given time period and the well's area, the injected volume of water which didn't infiltrate and is stored in the well (Vs_t) is calculated, as in equation (2).

$$\textbf{(2)}\quad Vs_t = \frac{\Delta h_t}{A}$$

Where:

- Vs_t stands for the non-infiltrated injected volume producing a water displacement in the well for a given period of time (L^3);
- Δh_t stands for the observed water displacement in the well for a given period of time (L).

From this, infiltrated volume at a given period of time (Vi_t) is calculated by subtracting stored volume (Vs_t) from the injected volume (Va_t) for the same period of time. Hence, infiltration rate for a given time period is estimated by dividing infiltrated volume with the given time period and the well's area (equation (3)):

$$\textbf{(3)}\quad I_t = \frac{Vi_t}{\Delta t \times A}$$

Where:

- I_t stands for the infiltration rate at a given time period ($L \cdot T^{-1}$);
- Δt stands for the time interval of a given time period (T);
- Vi_t stands for the infiltrated volume of water for a given period of time (L^3).

Steady state injection period

During steady state, once no water level change is observed, it is assumed that all injected water is infiltrated by the system so Vs = 0 and infiltrated volume (Vi_t) is equal to injected volume (Va_t). For

a given time period, the injected volume in the well is calculated by multiplying the injection flow rate by the time interval.

As for the infiltration rate, it is calculated by dividing the injection flow rate by the well's surface area. Alternatively, infiltration rate can be calculated likewise in transient state, by dividing the infiltrated volume by a given time period and area. In both cases, the calculated infiltration rate should be the same.

Recovery period

For the recovery period, no water is injected in the system ($Va_t = 0$), therefore, infiltrated volume and rate are calculated based on the observed water level decrease for a given period of time, after injection has ceased. So being, infiltrated volume is calculated by multiplying the observed water displacement by the well's area (Equation (4)):

$$\textbf{(4)}\quad Vi_t = \Delta h_t \times A$$

Where:

- Vi_t stands for the infiltrated volume of water for a given time period (L^3);
- Δh_t stands for the observed water displacement in the well for a given period of time (L);
- A stands for the well's surface area (L^2).

Infiltration rate is then calculated by dividing the infiltrated volume of water in a given time period, by the interval of time for the same time period and the well's surface area (equation (5)):

$$\textbf{(5)}\quad I_t = \frac{Vi_t}{\Delta t \times A}$$

where:

- I_t stands infiltration rate for a given time interval Δt in the recovery period (L/T);
- Δt stands for the time interval for which infiltration is to be calculated (T).

Alternatively, infiltration rate can also be calculated by dividing water level displacement (Δh_{total}) with the time interval (Δt) for a given time period. The area considered for the test was the surface well area (Table 7) which is 15.90 m^2.

Results

Infiltration rates were estimated for the steady state and transient state of the injection period and for the recovery period (transient state). As mentioned before, transient state is a period during which water level in the well is not stable, as opposed, steady state happens when the water level in the well is stable, meaning that all injected water is being infiltrated by the system (or, when there is no injection, no infiltration is occurring). Therefore, water level displacement is the base on which infiltration was estimated. Figure 58 shows the manual and automatic records of the water displacement in the well in function of time and the injection flow rate to the well.

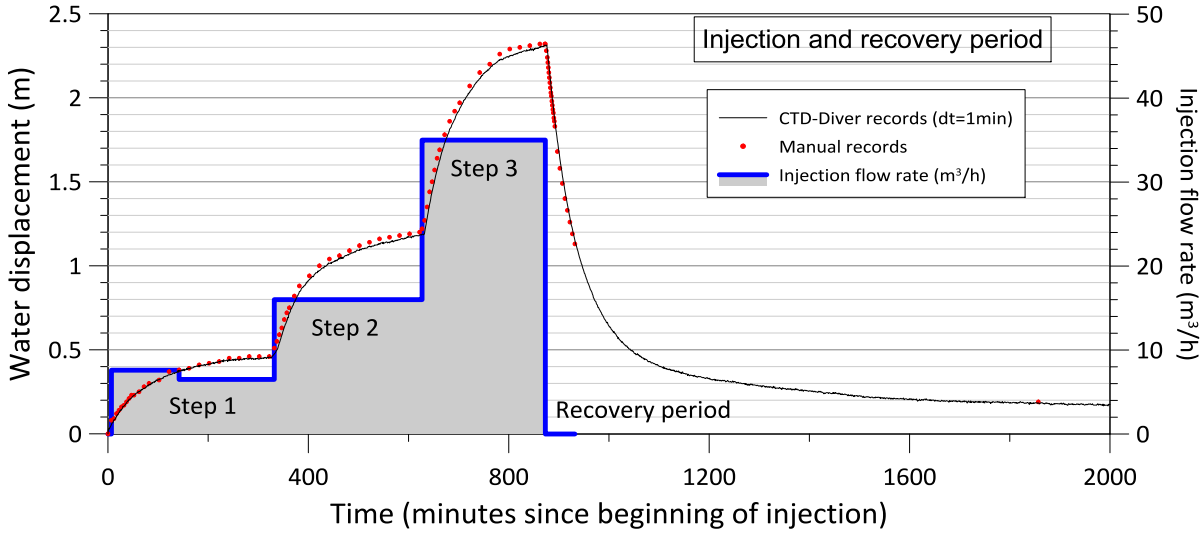

Figure 58 – Injection flow rate (right axis), manual and CTD records (left axis) for water displacement in the well as a function of time, for all the injection steps and recovery period

In Figure 59 a higher detail of the water displacement produced at each step of the injection and the recovery period is shown. Water displacements produced at each step were 0.46, 1.19 and 2.32 m respectively (Figure 58). These values are referenced with water level at the beginning of the test. The water level displacement produced at each step, with reference to the water level at the beginning of each step, were 0.46 , 0.73 and 1.13 m respectively for steps 1, 2 and 3 (Figure 59).

From Figure 58 and Figure 59 it is clear that higher injection flow rate produce a higher water displacement (check Table 8 for injection step times and characteristics).

Based in the equations mentioned before, infiltration rates were estimated for several time periods:

- a1) Step 1 transient state injection flow period (flow varying from 7.5 to 6.5 m^3/h);
- a2) Step 1 steady state injection flow period (flow at 6.5 m^3/h);
- b1) Step 2 transient state injection flow period (flow at 16 m^3/h);
- b2) Step 2 steady state injection flow period (flow at 16 m^3/h);
- c1) Step 3 transient state injection flow period (flow at 35 m^3/h);
- c2) Step 3 steady state injection flow period (flow at 35 m^3/h);
- d1) Transient state recovery period (no flow);
- d2) Transient state recovery period decomposed over 1 hour increment for the first 24 hours (no flow);
- d3) Transient state recovery period decomposed over 1 day increment for the first 5 days (no flow).

The results of the above mentioned time periods are synthetized in Table 9.

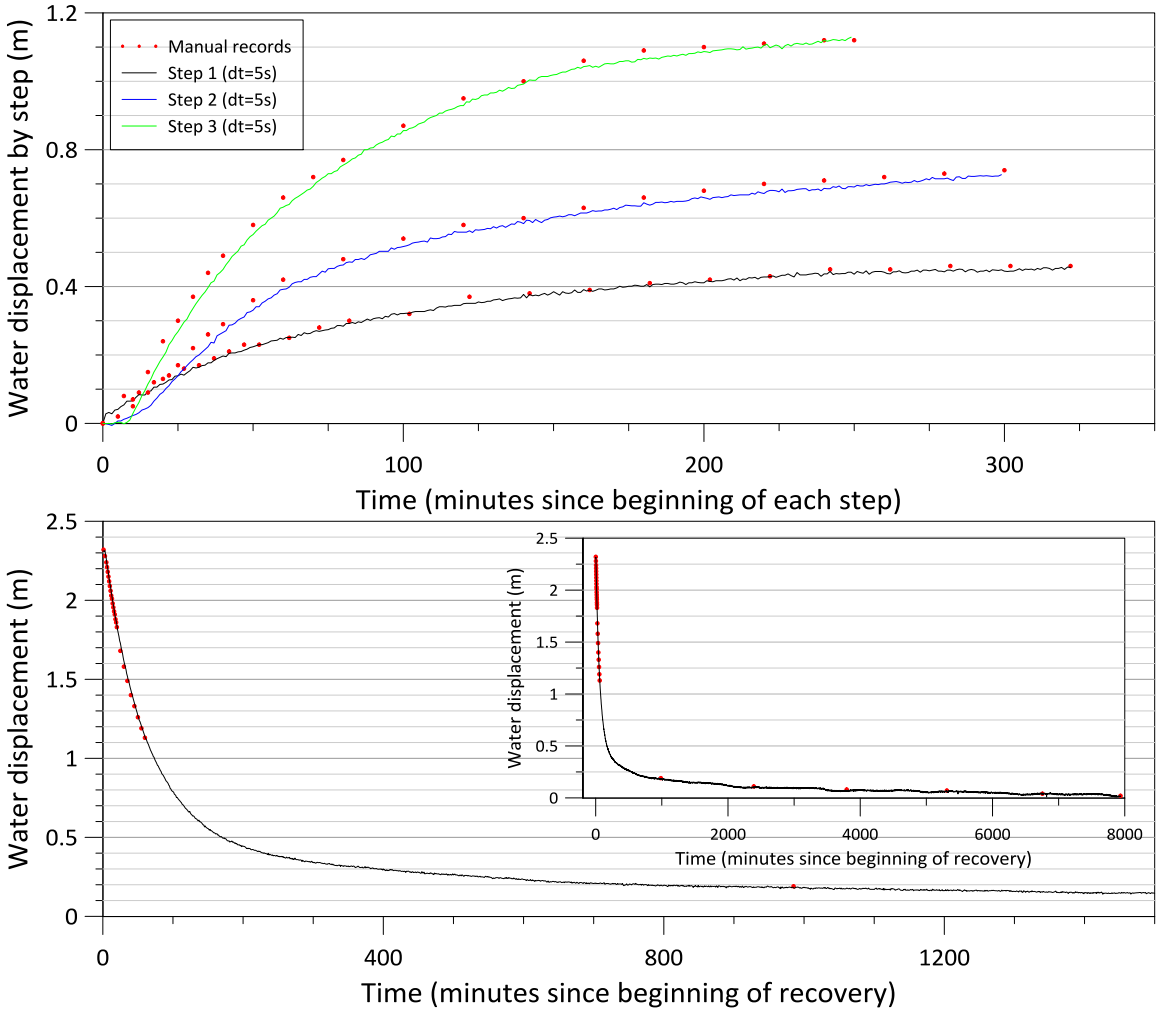

Figure 59 – Top: Water displacement in detail for each of the injection steps with the reference to the initial water level at the beginning of each step. Bottom: Water displacement in detail for the recovery period with reference to the initial head in the well at the beginning of the injection

Table 9 – Synthetized measured parameters during the injection and recovery period. Calculated infiltration volumes and rates from the infiltration test

Test step	State	t_0 (min)	h0 (m)	hf (m)	Δh (m)	Δt (min)	Q - Injection flow rate(m^3/h)	Va -Injected volume (m^3)	Vs- Injected non-infiltrated volume (m^3)	Vi - infiltrated volume (m3)	I - Infiltration rate (m/day)
a1) Injection	**Transient**	0	0.00	0.46	0.46	263	7.6 to 6.5	30.97	7.32	23.65	8.14
a2) Injection	**Steady**	263	0.46	0.46	0.00	59	6.5	6.39	0	6.39	9.81
b1) Injection	**Transient**	323	0.46	1.19	0.73	262	16	69.87	11.61	58.26	20.13
b2) Injection	**Steady**	585	1.19	1.19	0.00	37	16	9.87	0	9.87	24.14
c1) Injection	**Transient**	623	1.19	2.32	1.13	238	35	138.83	17.97	120.86	45.98
c2) Injection	**Steady**	861	2.32	2.32	0.00	11	35	6.42	0	6.42	52.82
d1) Recovery	**Transient**	873	2.32	0.03	2.29	7934	0	0.00	0	36.45	0.42
d2) Recovery decomposed over 1 hour increment for the first 24 hours	**Transient**	873	2.31	1.14	1.18	60	0	0.00	0.00	18.70	28.22
		933	1.14	0.67	0.46	60	0	0.00	0.00	7.33	11.06
		993	0.67	0.48	0.20	60	0	0.00	0.00	3.13	4.73
		1053	0.48	0.39	0.09	60	0	0.00	0.00	1.43	2.16
		1113	0.39	0.34	0.05	60	0	0.00	0.00	0.73	1.10
		1173	0.34	0.31	0.03	60	0	0.00	0.00	0.52	0.79
		1233	0.31	0.29	0.02	60	0	0.00	0.00	0.32	0.48
		1293	0.29	0.27	0.02	60	0	0.00	0.00	0.37	0.55
		1353	0.27	0.25	0.02	60	0	0.00	0.00	0.25	0.38
		1413	0.25	0.23	0.02	60	0	0.00	0.00	0.27	0.41
		1473	0.23	0.22	0.02	60	0	0.00	0.00	0.25	0.38
		1533	0.22	0.21	0.01	60	0	0.00	0.00	0.14	0.22
		1593	0.21	0.20	0.01	60	0	0.00	0.00	0.17	0.26
		1653	0.20	0.19	0.00	60	0	0.00	0.00	0.05	0.07
		1713	0.19	0.19	0.01	60	0	0.00	0.00	0.08	0.12
		1773	0.19	0.18	0.01	60	0	0.00	0.00	0.11	0.17
		1833	0.18	0.18	0.00	60	0	0.00	0.00	0.03	0.05
		1893	0.18	0.17	0.01	60	0	0.00	0.00	0.08	0.12
		1953	0.17	0.16	0.01	60	0	0.00	0.00	0.17	0.26
		2013	0.16	0.16	0.00	60	0	0.00	0.00	0.02	0.02
		2073	0.16	0.16	0.00	60	0	0.00	0.00	0.02	0.02
		2133	0.16	0.15	0.01	60	0	0.00	0.00	0.11	0.17
		2193	0.15	0.15	0.00	60	0	0.00	0.00	0.03	0.05
		2253	0.15	0.14	0.01	60	0	0.00	0.00	0.13	0.19
d3) Recovery decomposed over 1 day increments for 5 days	**Transient**	873	2.31	0.14	2.17	1440	0	0.00	0.00	34.46	2.17
		2313	0.14	0.10	0.05	1440	0	0.00	0.00	0.75	0.05
		3753	0.10	0.07	0.03	1440	0	0.00	0.00	0.46	0.03
		5193	0.07	0.06	0.01	1440	0	0.00	0.00	0.21	0.01
		6633	0.06	0.04	0.02	1440	0	0.00	0.00	0.33	0.02

- t_0 (min) – Initial time for a given time period;
- h_0 and h_f (m) – initial and final water level displacement respectively for a given time period;
- Δh (m) – Difference between initial and final water level displacement for a given time period;
- Δt (min) – time interval for a given period;
- Q (m^3/h) – injected flow rate manually measured.
- Va (m^3) – Injected volume of water in the well for a given time period;
- Vs (m^3) – injected volume of water in the well non-infiltrated, which is stored at the well for a given time period;
- Vi (m^3) – Infiltrated volume of water that has infiltrated for a given time period (Vi = Va – Vs);
- I – Infiltration rate calculated for a given time period;

Estimated infiltration rate for step 1 were 8.14 m/d during transient state (a1) and 9.81 m/d in steady state conditions (a2). For step 2, transient (b1) and steady state (b2) infiltration rates were calculated as 20.13 and 24.14 m/d respectively. Infiltration rates during step 3 were estimated as 45.98 m/d for transient state (c1) and 52.82 m/d for steady state conditions (c2).

For all the records of the recovery period (approx. 6 days), total infiltration rate was estimated as 0.42 m/d (d1). Nonetheless, the decomposed data by 1 hour increments (d2) indicates a maximum of 28.22 m/d and a minimum of 0.19 m/d which coincide with the first and last of the 24 hour time period of the recovery period respectively. The data decomposition by 1 day increments of the recovery period (d3) indicates a maximum infiltration rate of 2.17 m/d for the first day and 0.02 m/d for the last day of the recovery period.

In Figure 60 it can be seen that infiltration rate increases positively until stabilizing as the injected flow rate increases and decreases exponentially with time in the recovery period (after injection has ceased). These data suggests a clear relation and dependency between the infiltration rate and the hydraulic load in the well, i.e. the water level elevation in relation with the hydrostatic water level at the beginning of the injection test (10.28 m).

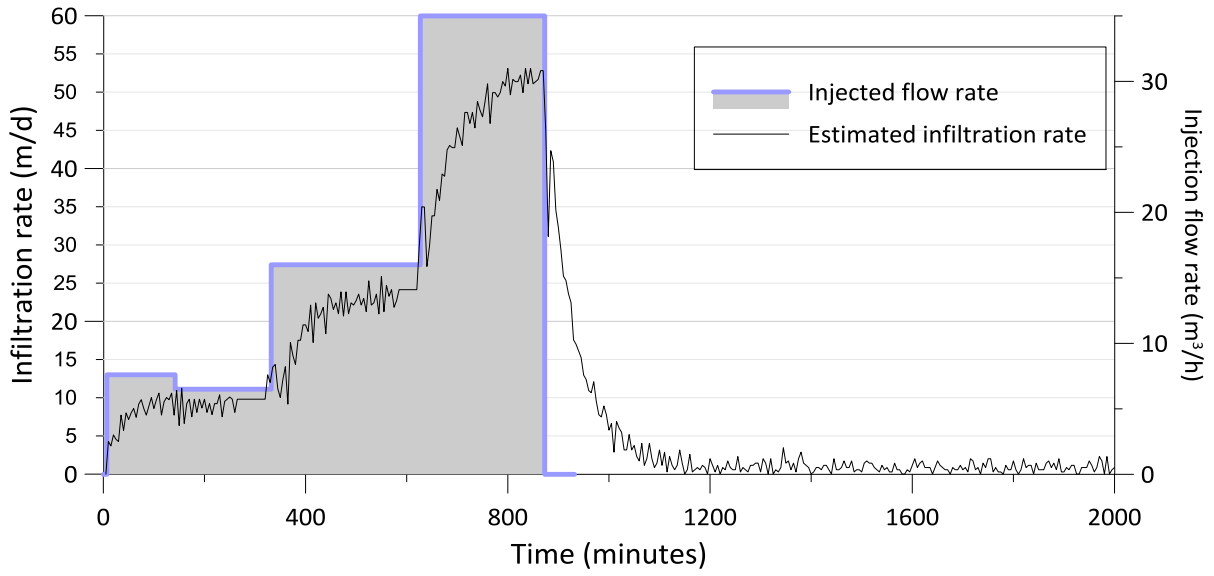

Figure 60 – Estimated infiltration rate for the three steps of injection period and recovery period for a 5-minute increment time

The scatter plot between the hydraulic head and the infiltration rate shown in Figure 61 indicates the positive correlation between the hydraulic load and injection rate for the three steps of the injection period and the recovery period, as mentioned before. For the injection period (Figure 61 A), a linear fit was found with a squared R (or coefficient of determination) of 0.9812, with the equation y = 22.236x + 0.1162. It can be seen that for the highest hydraulic load found, 2.30 m, the infiltration rate was 52.82 m/d (which was achieved during the 3rd step steady state period).

For the recovery period (Figure 61B), a 3rd degree polynomial function fit was found with a squared R value of 0.9366, which, for the observed hydraulic load presents an acceptable fit with the estimated infiltration rate. 3 distinct sections can be identified in this fit. The first section consists of hydraulic

loads varying from 0 to 0.5 m, for which infiltration rate is almost irrelevant. The second section includes hydraulic load values between 0.5 and 1.75 m, for which infiltration rate apparently increases linearly as hydraulic load increases. The third section consists of hydraulic load values higher than 1.75 at which infiltration rate appears to stabilize near 40 m/d, although there is not enough data available to verify this assumption. This stabilization can also be related with the time lag between the ceasing of pumping and injection and the wellbore water storage in the well.

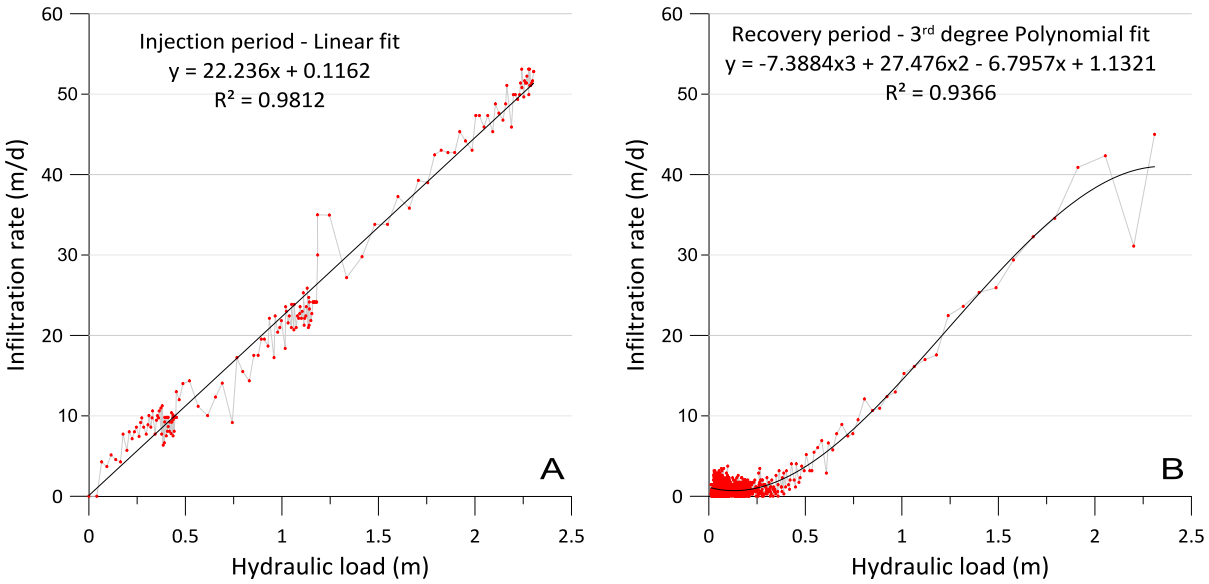

Figure 61 – Scatter plot between the hydraulic load and infiltration rate. A: injection period (with a linear function fit). B: Recovery period (with 3rd degree polynomial function fit)

The presented fits can be used to estimate infiltration rates as a function of the hydraulic load in the well for upcoming injection tests in the same conditions as the one presented in this report and assuming no clogging effect is occurring.

PT1: Variation of regional groundwater content in nitrates, May 2014, 2015 and 2016

To determine the variation in the water quality of Campina de Faro aquifer before starting the MAR in the PT1 DEMO site, a campaign was held in May 2014. Nitrate samples were analysed for two more years, May 2015 and May 2016. 72 wells were monitored, using the same wells monitored in 2008, during GABARDINE project (Figure 62).

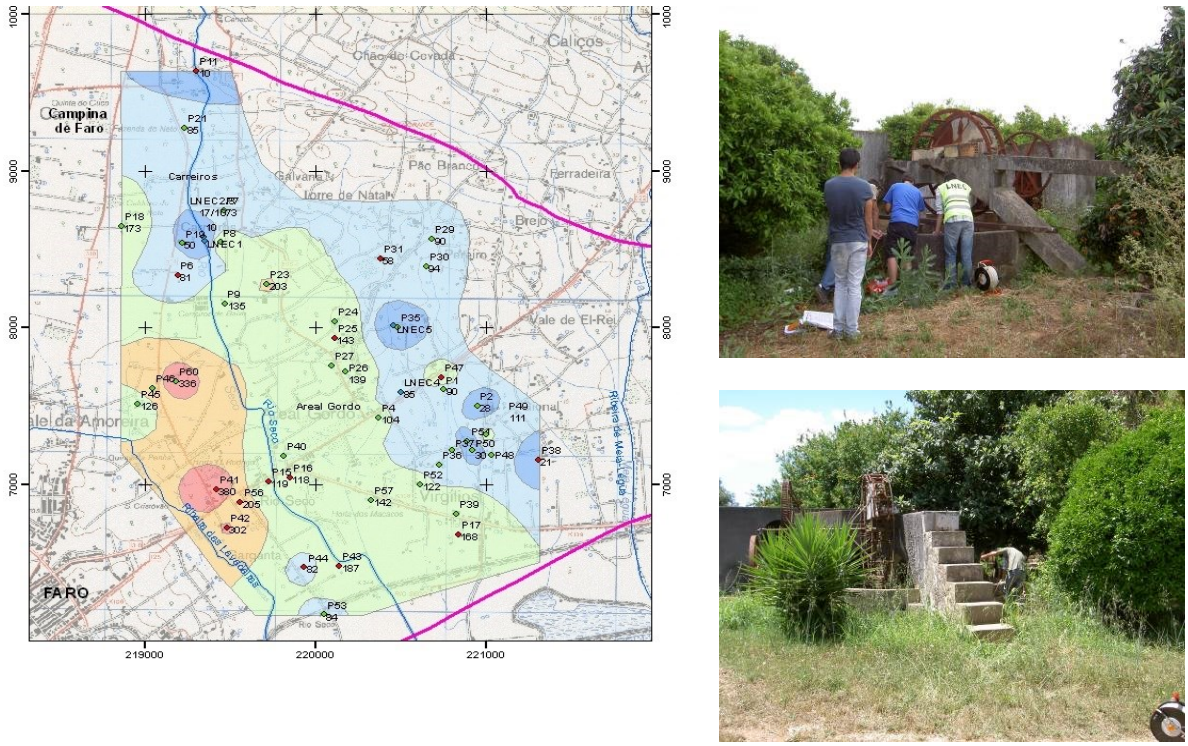

Figure 62 – Nitrate concentration in the groundwater of Campina de Faro aquifer (PT1_3 Campina de Faro) in April 2008

The results for 2014, 2015 and 2016 are shown in Figure 63, for the same locations shown in Figure 62. The comparison of these results allowed identifying the influence of the MAR experiments developed at Campina de Faro aquifer. The data was interpolated using Inverse Distance Weighted with 12 points.

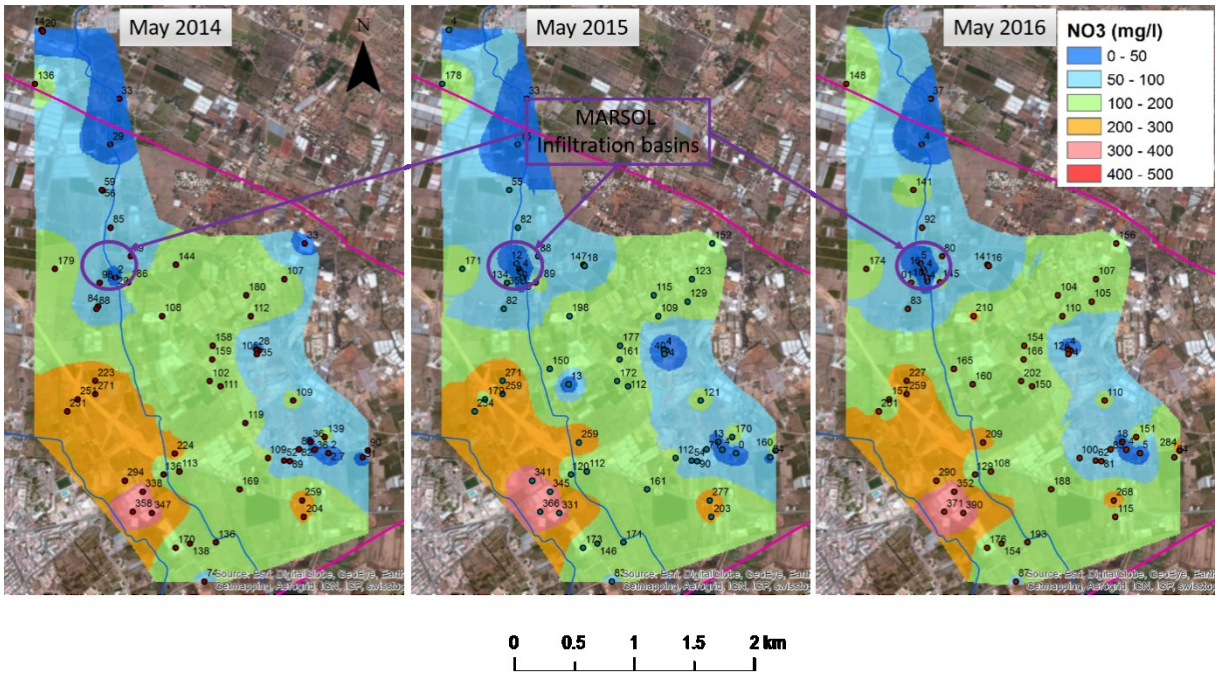

Figure 63 – Evolution of nitrate concentration in groundwater. Interpolated values from sampling points

In general, nitrate concentration does not appear to have relevant changes, though at a local scale, the quality seems to have been improving since 2014 close to the location of the infiltration basins.

In order to have a better perception of the groundwater content in nitrate evolution, a raster operation was performed, subtracting the interpolated values in May 2014 and May 2015 with the values interpolated in May 2016, which is shown in Figure 64.

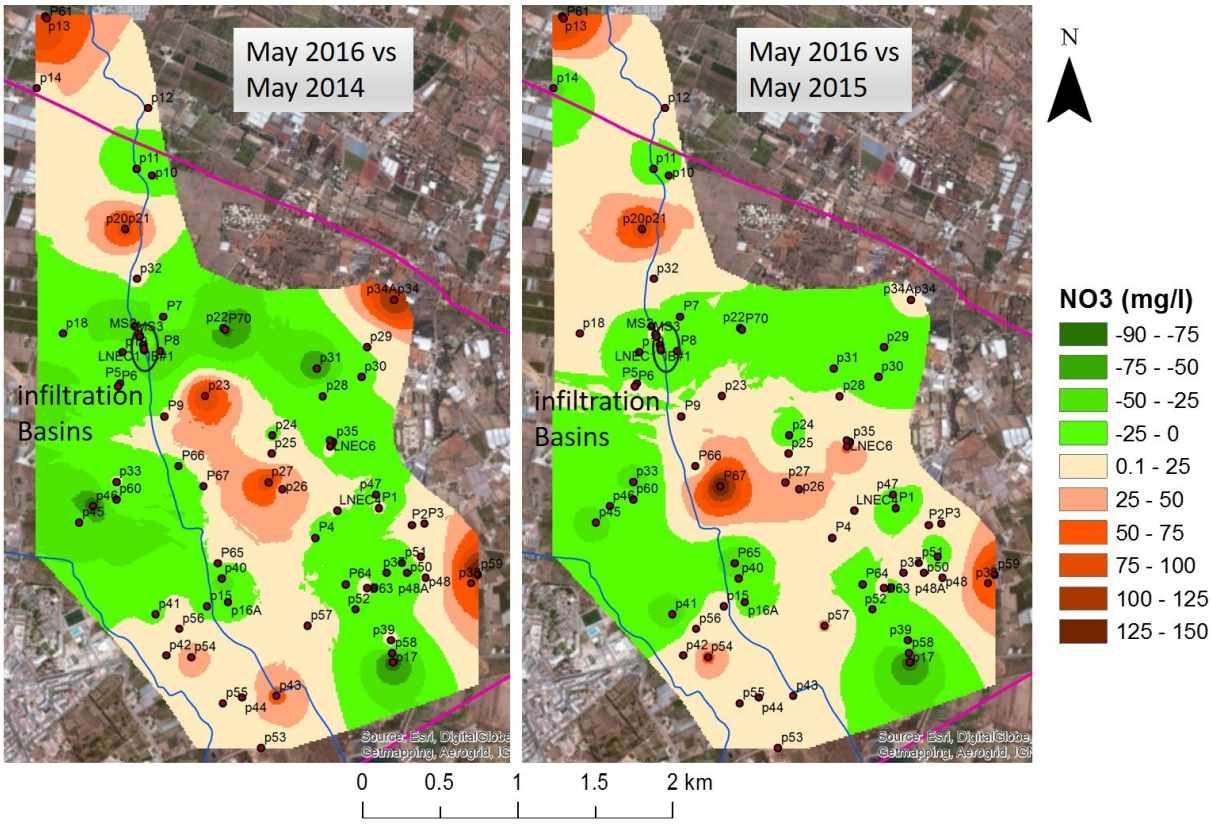

Figure 64 – Raster operation between interpolated values showing, in green, the areas were groundwater quality improved and, in red, the areas that have worsen quality. Left: difference between May 2014 and May 2016. Right: difference between May 2015 and May 2016

From Figure 64 in can be easily seen that the groundwater content in nitrate has been improving significantly around the area of the infiltration basins. This improvement can be associated with the increased groundwater infiltration produced by the infiltration basins.

The evolution of nitrate concentration at the monitoring points since the GABARDINE project Nitrate campaigns is presented at Table 10.

Table 10 – Nitrate concentration evolution at monitoring points

			GABARDINE Project NO_3 (mg/l)				MARSOL Project NO_3 (mg/l)		
Point	**Coord X**	**Coord y**	**Oct-06**	**Apr-07**	**Oct-07**	**Apr-08**	**May-14**	**May-15**	**May-16**
P1	220756	7604	94	115	108	90	109	121	110
P2	220953	7502	24	37	30	28	-	-	-
P3	221030	7510	136	-	-	-	-	-	-
P4	220375	7427	102	140	102	104	119	-	-
P5	219204	8350	106	102	119	95	84	-	-
P6	219193	8332	107	106	98	81	88	82	83
P7	219463	8748	87	95	84	73	79	88	80
P8	219447	8544	191	265	227	179	186	189	145
P9	219470	8153	135	116	128	135	-	-	-
p10	219397	9593	-	-	-	-	-	-	-
p11	219302	9634	24	28	0	10	29	16	4
p12	219373	9996	24	-	-	-	33	33	37
p13	218754	10546	-	-	-	-	14	4	527
p14	218705	10115	189	-	-	-	136	178	148
p15	219725	7017	190	167	0	119	136	120	129
p16A	219851	7041	133	138	147	118	113	112	108
p17	220839	6682	135	172	165	163	204	203	115
p18	218862	8648	191	211	153	173	179	171	174
p19	219218	8537	69	77	70	50	98	134	101
p20	219238	9271	12	-	99	66	56	-	-
p21	219234	9274	126	112	101	85	59	55	141
p22	219824	8682	143	-	146	111	144	147	141
p23	219714	8275	278	283	232	203	108	198	210
p24	220117	8040	144	132	156	139	158	177	154
p25	220112	7930	76	164	165	143	159	161	166
p26	220178	7717	216	196	147	139	111	112	150
p27	220093	7758	186	134	180	147	102	172	202
p28	220420	8274	113	104	109	95	112	109	110
p29	220686	8566	112	100	104	90	107	123	107
p30	220651	8389	109	91	111	94	-	129	105
p31	220384	8440	56	62	63	58	180	115	104
p32	219305	8976	55	-	-	-	85	82	92
p33	219183	7761	240	-	-	-	223	271	227
p34	220848	8851	130	-	140	91	33	152	156
p34A	220848	8851	32	-	-	-	-	-	-
p35	220483	8000	15	53	4	10	35	4	4
p36	220728	7123	47	44	52	50	89	90	81
p37	220802	7217	69	74	-	82	82	-	-
p37A	220802	7217	75	75	71	-	86	71	85
p38	221310	7154	18	21	8	21	31	24	84
p39	220828	6813	185	234	223	192	259	277	268
p40	219813	7183	264	246	237	188	224	-	-

			GABARDINE Project NO_3 (mg/l)				MARSOL Project NO_3 (mg/l)		
Point	**Coord X**	**Coord y**	**Oct-06**	**Apr-07**	**Oct-07**	**Apr-08**	**May-14**	**May-15**	**May-16**
p41	219417	6969	440	421	330	380	294	341	290
p42	219481	6723	330	361	348	302	358	366	371
p43	220141	6480	15	13	15	187	136	171	193
p44	219936	6471	88	89	76	82	138	146	154
p45	218960	7518	208	-	171	126	231	234	201
p46	219043	7615	292	309	231	284	251	179	157
p47	220739	7683	-	137	127	119	-	-	-
p48	221037	7187	-	70	107	53	2	3	5
p48A	221037	7187	-	-	-	-	3	-	-
p49	221007	7315	-	124	99	111	139	170	151
p50	220925	7216	-	33	21	30	36	4	4
p51	220894	7277	-	20	9	22	36	13	18
p52	220616	6997	-	145	123	122	-	-	-
p53	220050	6170	-	75	78	84	74	83	87
p54	219632	6711	-	-	-	-	347	331	390
p55	219820	6436	-	-	-	-	170	173	176
p56	219560	6881	-	232	203	205	338	345	352
p57	220330	6900	-	185	154	142	169	161	188
p58	220834	6737	-	-	-	-	-	-	-
p59	221349	7207	-	-	-	-	90	160	284
p60	219182	7656	-	280	205	336	271	259	259
P61	218764	10532	-	-	-	-	20	-	-
P63	220685	7127	-	-	-	-	52	54	62
P64	220558	7148	-	-	-	-	109	112	100
LNEC1	219348	8549	36	11	15	10	-	5	4
LNEC2	219343	8579	23	25	54	17	20	35	10
LNEC3	219342	8579	16	3	5	10	2	4	-
LNEC4	220506	7589	-	90	81	85	-	-	-
LNEC5	220462	8010	-	39	139	33	28	4	4
LNEC6	220465	7972	-	-	-	-	-	40	126
MS1	219292	8691	-	-	-	-	-	5	16
MS2	219315	8646	-	-	-	-	-	12	5
MS3	219322	8626	-	-	-	-	-	4	4
P65	219789	7273	-	-	-	-	-	259	209
P66	219556	7855	-	-	-	-	-	150	165
P67	219705	7734	-	-	-	-	-	13	160
P70	219834	8672	-	-	-	-	-	18	16

2.2 PT2: QUERENÇA-SILVES LIMESTONE KARSTIC AQUIFER SYSTEM (ALGARVE)

2.2.1 Introduction and objective

PT2 Querença-Silves limestone karstic aquifer system (Algarve) has two main DEMO sites (Figure 1), each one with a different goal:

- PT2_4 – SB Messines two SAT basins. The two basins have been constructed under MARSOL project. Their aim is to improve the waste water treatment plant (WWTP) effluent quality, prior to its discharge into Ribeiro Meirinho (PT2_5), a stream which naturally recharges the karstic aquifer in part of its river bed.
- PT2_6 – Cerro do Bardo MAR area. In this area, a set of infrastructures were rebuilt aiming to facilitate and increase the overall infiltration capacity of this karstic area. The aim is to enhance the groundwater availability using wet year's surface water surplus to augment the groundwater storage through MAR techniques. This will contribute to increase the water availability in dry years, possibly enhancing the downgradient water supply wells productivity (Águas do Algarve, AdA, water supply wells in Figure 1).

2.2.2 Motivation for the site selection

The Querença-Silves aquifer is the largest and most important groundwater body in the Algarve region. Protecting its water quality and ensuring the water availability are crucial steps for a good regional water management.

PT2_4 SB Messines area was selected for the construction of SAT basins based on the following background considerations and advantages:

1. This area was studied under PROWATERMAN project where an interpretation of the possible interconnections between pollutant sources, their pathways and local surface-groundwater connections was made, based on data obtained from field campaigns using water quality and quantity data, and electrical resistivity tomography methods (Leitão *et al*., 2014).
2. SB Messines WWTP, belonging to a MARSOL project actor Águas do Algarve (AdA), was discharging its secondary treated effluent in Ribeiro Meirinho, and was identified as possibly affecting the surface water quality of this stream and, indirectly, Querença-Silves karst aquifer through infiltration from the karsified river bed.
3. A SAT facility has been proposed and accepted by AdA to minimise the environmental impact created by the discharges. Besides, emerging contaminants that were not accounted for could also be treated prior to the discharge.

PT2_6 Cerro do Bardo MAR area was selected based on the following background considerations and advantages:

1. This is an area with a relevant water availability problem (severe droughts are recurrent in this Mediterranean climate area, although followed by wet years). The drought that occurred during 2004 and 2005 had an estimated water supply deficit of about 50 hm^3.
2. As in most Mediterranean climate area, on the other hand, wet years do occur, with surplus of the same order of magnitude, e.g. during the hydrologic 2000-2001 year, with an

estimated surplus of 52 hm^3, discharged directly to the Arade estuary area sea as Funcho and Arade dam were at maximum capacity.

3. Besides, the new Odelouca dam is now in full operation, allowing a connection by tunnel directly towards Funcho dam downstream and from there by cannel to Alcantarilha Water Treatment Plan (WTP). An estimated extra capacity of 70 hm^3 is now available in wet years that could be injected upstream of the groundwater pumping wells of Alcantarilha WTP.
4. A relevant amount of MAR knowledge and groundwater data is available, having been gathered on another EU sponsored project, the ASEMWaterNet Multi-Stakeholder Platform for ASEM S&T Cooperation on Sustainable Water Use (FP6 INCO-CT2005-510897, cf. http://www.asemwaternet.org.pt/).
5. A relevant amount of surface and groundwater data, including climate change, water budget and groundwater recharge estimations is available, having been gathered on the Portuguese FCT sponsored PROWATERMAN project (http://www.lnec.pt/hidraulica-ambiente/pt/projectos/detalhe/prowaterman-agua-ecossistemas-aquaticos-e-atividade-humana-uma-abordagem-integrada-e-participativa-na-definicao-de-estrategias-inovadoras-e-prospetivas-de-gestao-integrada-de-recursos-hidricos-no-s/).
6. A MAR/groundwater thematic MSc, Thesis was developed at MARSOL partner institution LNEC, i.e. OLIVEIRA (2007, cf. http://repositorio.lnec.pt:8080/xmlui/handle/123456789/12424).
7. Very useful MAR infiltration facilities (large well and potential river bed experimental area) have been made available by MARSOL project actor APA Ambiente at Cerro do Bardo.
8. Very useful and not yet in use new groundwater pumping well have been made available by MARSOL project actor Águas do Algarve near Cerro do Bardo case study site.
9. A regional groundwater flow model has been developed, allowing simulating real time aquifer responses, by MARSOL partner Universidade do Algarve, for Querença-Silves aquifer.

2.2.3 Geological/hydrogeological setting

PT2, Querença-Silves DEMO site, is located northeast of Silves, Algarve region, Portugal.

The Querença-Silves aquifer system (Figure 65) is the largest aquifer in Algarve, located in the center of the Algarve region, in south Portugal, a region characterized by a Mediterranean climate with dry and warm summers and cool wet winters. It is considered a karst aquifer formed by Jurassic (Lias-Dogger) carbonate sedimentary rocks covering an irregular area of 324 km^2 from the Arade River (at the west) to the village of Querença (at the East) (Monteiro *et al.*, 2006 and Monteiro *et al.*, 2007). The system is delimited south by the Algibre thrust, which is the main onshore thrust in the Algarve Basin, separating the Lower/Early and the Upper/Late Jurassic and to the north by the Triassic-Hettangian rocks (Terrinha, 1998) (Figure 66). The main outlets of the aquifer are springs located at the aquifer boundaries, particularly the Estômbar springs, in the west, where the aquifer borders the Arade River, which forms an estuary (Hugman *et al.*, 2013) and supports several important groundwater dependent ecosystems.

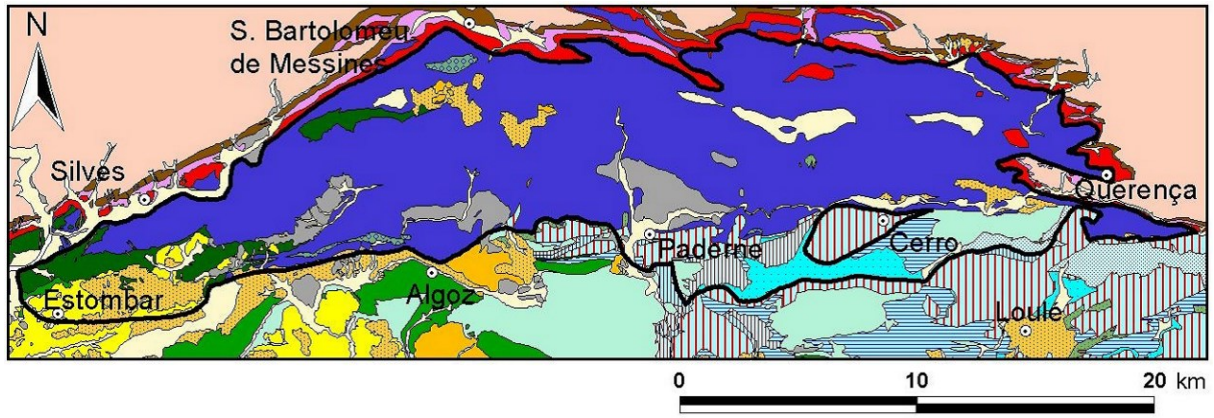

Adapted from Almeida *et al*. (2000)

Figure 65 – Detailed lithostratigraphic map (with locally known names) of the Querença-Silves aquifer and its surrounding. The underlined formations in the legend consist of the main formations of the QS Aquifer

Querença-Silves aquifer system lies in a region strongly affected by tectonic activities. As stated before, Algibre thrust, which constitutes the south limit of the QS, is a boundary that divides the Algarve Basin in two distinct morphological domains: the northern domain with large outcrops of lower Jurassic rocks and the south domain with highly fractured upper and middle Jurassic formations. Another important fault in this system visible in the geologic map (Manuppella, 1992) is the NW-SE S. Marcos da Serra – Quarteira fault, which crosses the QS system diagonally from SB Messines to the village of Paderne. This fault divides de QS aquifer system in two domains, the eastern domain, with a steep piezometric gradient, and the western domain, with smoother piezometric gradient.

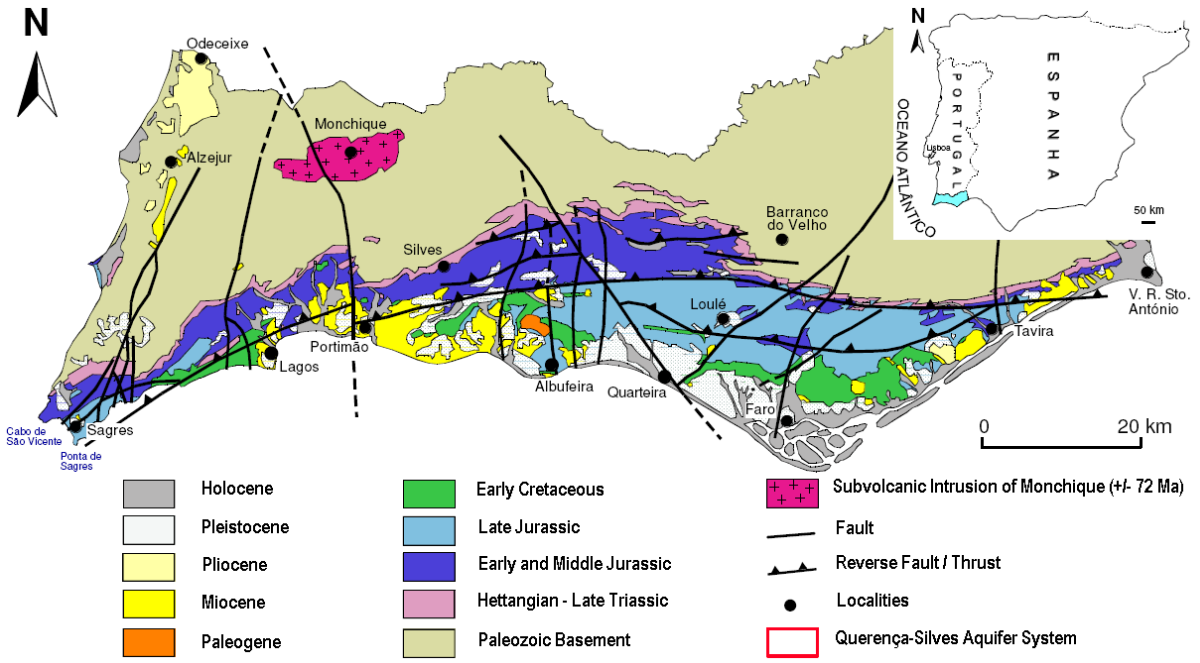

Adapted from Lopes (2006); Manuppella (1992) and Terrinha (1998)

Figure 66 - Simplified geologic map of the Algarve

Manuppella *et al.* (1993) present a cross-section of the central Algarve region (Figure 67). This cross-section allows a synthetized visualization of the geometric relations of the Early/Lower Jurassic lithology which support the Querença-Silves aquifer system Identified in blue, in Figure 67.

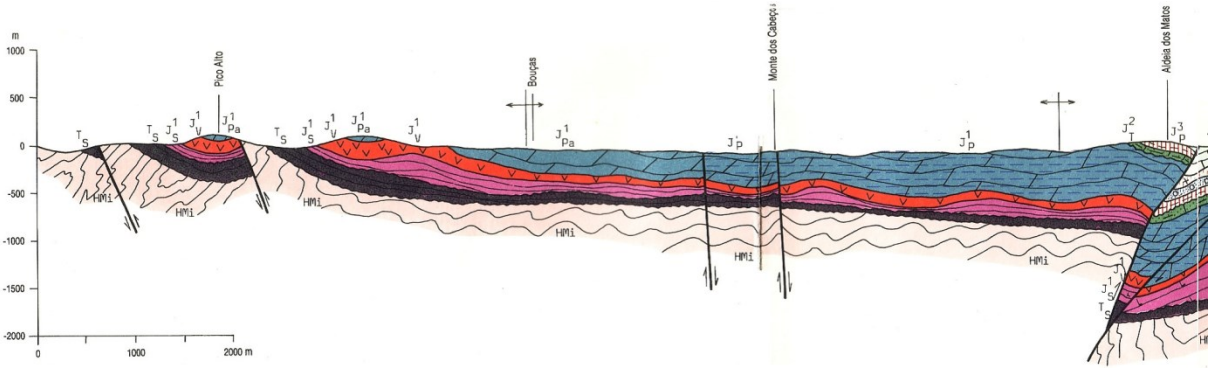

Adapted from Manuppella *et al*. (1993)

Figure 67 – Geometry of the carbonated rocks of early Jurassic which constitute the most important support of the aquifer system Querença-Silves (dark blue colour, to the left of the Algibre thrust)

According to previous studies, the hydrogeological setting of the Querença-Silves karstic aquifer has a complex compartmented structure, with, as stated before, two distinct domains separated by a fault: a western domain and an eastern domain. Its western domain has a well-developed karst, westward flow direction, with the main discharge areas along the Arade River, with particular relevance to Estômbar springs (westernmost point). Its eastern domain has more random flow directions, less regular piezometric surfaces (Figure 68) and a lower karst development. The tectonic

activity of this region results in its widespread fracturing, defining a significant number of semi-independent aquifer blocks, with more or less constrained and restricted hydraulic links between them. Such hydraulic restrictions are more expressive in the eastern domain, because in the western domain the pervasive karstic network largely obliterates such tectonic setting (Mendonça and Almeida, 2003; Monteiro *et al.*, 2006).

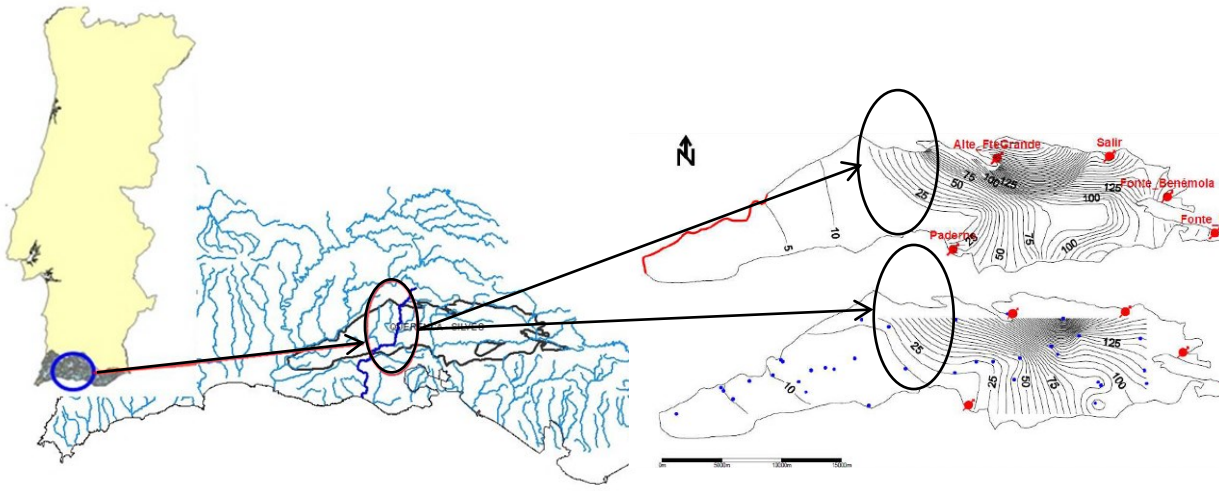

Adapted from Monteiro *et al.*, 2006

Figure 68 – Site location along Ribeiro Meirinho stream and central-western area of Querença-Silves aquifer, and its piezometry (upper right: modelled; lower right: measured) (Leitão *et al.*, 2014)

The Ribeiro Meirinho stream is located in the central-western area of Querença-Silves aquifer and its upper reaches are located outside the aquifer, in Serra Algarvia. The latter are Palaeozoic terrains, composed mainly of schist and graywakes, essentially impervious lithologies, being, therefore, the main source of water for this stream until it reaches the Jurassic limestones, dolomites, dolomitic limestones and other, less important, calcareous formations composing the karst aquifer of Querença-Silves.

An extensive literature review allowed the identification of "three generations" for the estimation of the water balance of the QS nowadays available as follows:

- Almeida (1985) and Almeida *et al.* (2000) estimated a total balance of 70 ± 17 hm^3/year, using the Kessler method (1965) in the areas where carbonated rocks outcrops are present (in which the average recharge varies between 40 and 60% of precipitation) and a sequential water balance in the soil in the areas where carbonate rocks are covered by soils or sedimentary deposits (in which recharge varies between 5 and 18% with an average of 10%).
- Vieira and Monteiro (2003) refined the previous balance with the infiltration values determined for the covered and outcropping areas of the carbonate rocks proposed by Almeida (1985) and Almeida *et al.* (2000). However, in this case, it was possible to use a new generation of geological maps in which the percentage of covered and uncovered areas of the aquifer were much more reliable. This information allowed to estimate a value in the range of the highest values proposed in the previously mentioned balance. In that case, a total annual average recharge of 93.4 hm^3/year was estimated.
- Oliveira *et al.* (2008) estimated a 100 hm^3/year balance with a sequential daily water balance model, later updated by Oliveira *et al.* (2011) to 94 hm^3/year.

Due to its karstic properties, there is a strong relationship between the aquifer and the streams with some influent sections that can significantly contribute to its recharge (Monteiro *et al.*, 2006; Reis *et al.*, 2007, Salvador *et al.,* 2012). This is the case of Ribeiro Meirinho, which undergoes a sharp reduction of the flow rate when it reaches the calcareous formations, having several sinks in its bed. It is estimated that besides direct recharge, an extra amount of 62 x hm^3/year, originating from surface flow produced on the drainage area outside the aquifer, infiltrates when the rivers reach the aquifer system (Oliveira and Oliveira, 2012).

Regarding aquifer abstractions, Nunes *et al.* (2006) estimated a mean annual withdrawal for irrigation of 31 hm^3, and Stigter *et al.* (2009) estimated a 10% of mean aquifer recharge was abstracted for urban water supply. These values are expected to drop, now that the surface reservoir of Odelouca is operational.

Almeida *et al.* (2000) and Andrade (1989) present transmissivity values calculated from pumping tests. Estimated values were 1006 m^2/day to South of Silves city, 727 and 83 m^2/day to North of Paderne village, 155 m^2/day to West of Querença and values of 1200 and 1700 m^2/day to North of Purgatório. According to Almeida *et al.* (2000), storage coefficient values vary between $5x10^{-3}$ and $3x10^{-2}$.

2.2.4 Developing the infrastructures

PT2_4: S. Bartolomeu de Messines SAT basins

Laboratory soil-column apparatus

Before building the SAT basin infrastructures at S. Bartolomeu de Messines, a laboratory soil-column facility was designed at LNEC (Figure 69) to simulate the performance of different soil mixtures in SAT conditions, in terms of the soil infiltration properties and soil retention capacity through adsorption and biodegradation (see also WP14).

The laboratory setup consisted of a PEAD column with 50 cm height and 5 cm diameter. During the experiments the tested soil occupied 30 cm of the column height, and the empty space above allowed the existence of a controlled height of water on the top of the soil, simulating the SAT basin real conditions. The soil-column was attached to a compaction system composed of a standardized weight disk for soil compaction and a ruler for dropping height determination (Figure 69, left). The soil-column has a tight lid base with an outlet port which is connected to a sample tube where the outflow water is collected. An inert Teflon membrane filter is added to the soil-column bottom for fine particles retention.

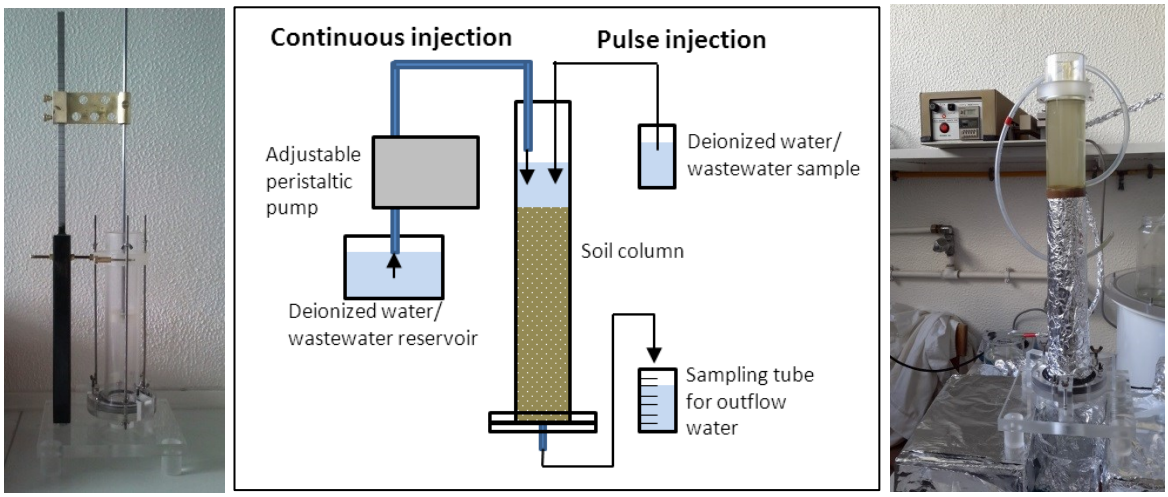

Figure 69 – Soil-column apparatus and diagram of operation

For continuous water injection, a volumetric peristaltic pump was used. For pulse injection, the water was directly poured from a container to the column. Outflow samples were collected at defined periods.

S. Bartolomeu de Messines SAT Basins

The SAT system built at S. Bartolomeu de Messines waste water treatment plant (WWTP) aims to improve the water quality of the treated effluent coming from the WWTP, prior to its discharge into Ribeiro Meirinho. This river recharges Querença-Silves karstic aquifer, lying below, since a part of its riverbed is influent to the aquifer (Figure 1).

The design of S. Bartolomeu de Messines SAT Basins was carried out in a joint collaboration between LNEC and TARH in order to assure the system optimal operation capacity and versatility. The SAT system design, built in June 2016, consists of two SAT basins 15 m x 7 m designed to work continuously with gravitational water flow, without any pumping requirements and to work either in parallel (simultaneously) or in series, in case a second round in the treatment is proved to be necessary.

Figure 70 shows a schematic design of the SAT basins system.

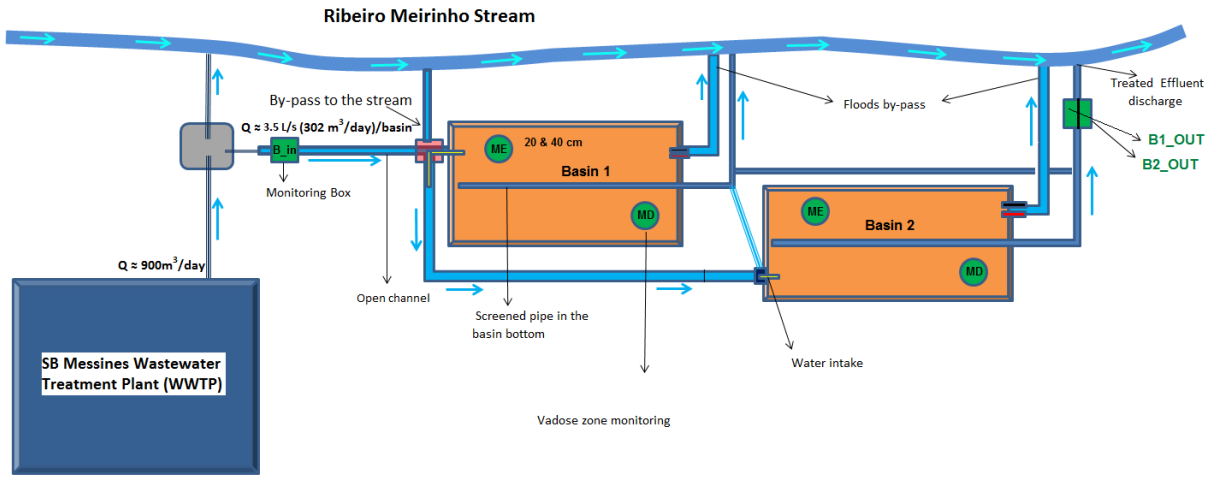

Legend - B_in: Basin inflow; B1_OUT: Basin 1 outflow; B2_OUT: Basin 2 outflow; ME: Left margin; MD: right margin

Figure 70 – Schematic design of S. Bartolomeu de Messines MARSOL SAT basins

Figure 71 presents the actual layout of the SAT scheme.

Figure 71 – MARSOL SAT basins at S. Bartolomeu de Messines waste water treatment plant

Considering the soil-column experiment results, using wastewater and soil from the DEMO site, it was estimated that, for both basins with the referred dimensions, the flow would round 3.5 L/s, i.e. 1/3 of the daily effluent. All hydraulic and monitoring structures necessary for the SAT system operation were dimensioned based on this figure. However, this flow rate might be reduced in the future due to clogging. To avoid this, the following preventing measures were conducted:

- Construction of a large derivation box for sedimentation with an release valve;
- Construction of a connection channel between the derivation box and the first basin;
- The basins are prepared to allow digging several small furrows in the soil top.

Furthermore, the channel and the two basins were designed to be equipped with a flood control discharger (flood by-pass) that will divert any extra flow to Ribeiro Meirinho.

The basins and the connection between them were designed to receive the WWTP effluent that will percolate through a strata sequence (composed of 40% local soil, 40% coarse sand and 20% vegetal compost) with about 60 cm thick. This composed soil was specially designed and proved to optimize the remaining contaminants' retention while still ensuring the infiltration of appreciable flows (see section 2.2.5). The SAT treated effluent is drained through a PVC screened pipe to the river, where the WWTP conventional treatment is usually discharged. Furthermore, the basins allow a complete drainage of the soil, in order to improve the treatment with aerobic/anaerobic cycles.

Figure 72 shows the details of the longitudinal profile of the SAT basins.

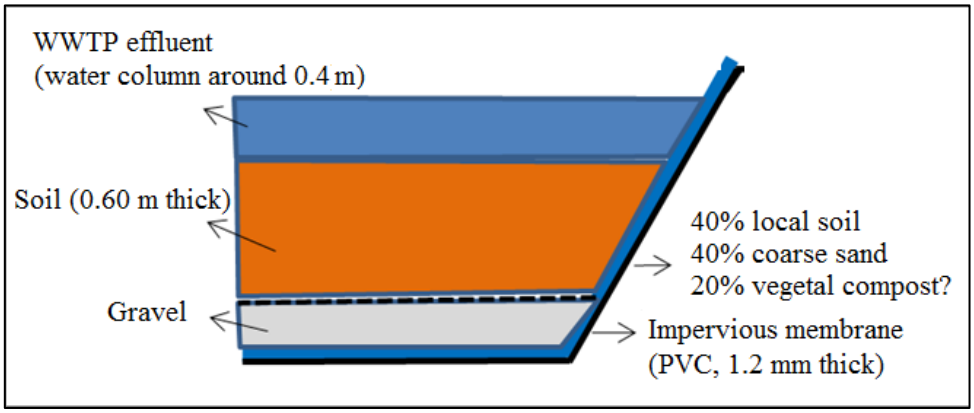

Figure 72 – Detail of the longitudinal profile of MARSOL SAT basins

Flow control is manually operated through a system of six valves. As for the water quality control, three monitoring boxes were installed, one after the derivation box outlet (Figure 70) and two after each SAT basin (B1_OUT and B2_OUT in Figure 70). The monitoring boxes were built to allow installing the sensors and to collect water samples, before and after the treatment (Figure 73). The soil-water is monitored thanks to two suction capsule structures (Figure 74) placed in two points at each basin, in a total of four capsules per basin (Figure 70).

In the three monitoring boxes, three Smart Water network wireless sensors were used to perform remote water quality monitoring (electrical conductivity, temperature, pH and redox potential) and communication in real time, for water inflow (B_IN) and water outflow in both basins (B1_OUT and B2_OUT). Besides, water was sampled weekly, during 3 months, and analysed for 24 pharmaceutical

compounds, organic matter, NH_4^+, NO_2^-, NO_3^-, PO_4^{3-}, HCO_3^-, Cl^-, SO_4^{2-}, Ca^{2+}, Mg^{2+}, Na^+, K^+, B, Zn, Cu. The same parameters, except for the pharmaceutical compounds, were analysed in the water collected from the suction capsules placed in two points and two depths (20 cm and 40 cm) at each basin.

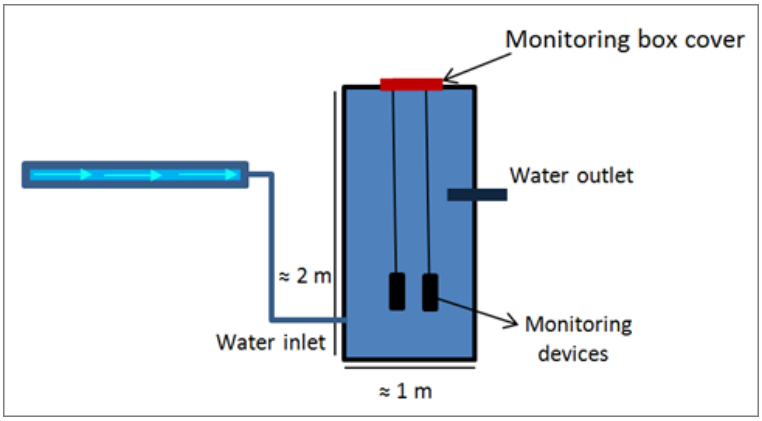

Figure 73 - Detail of monitoring box cross section

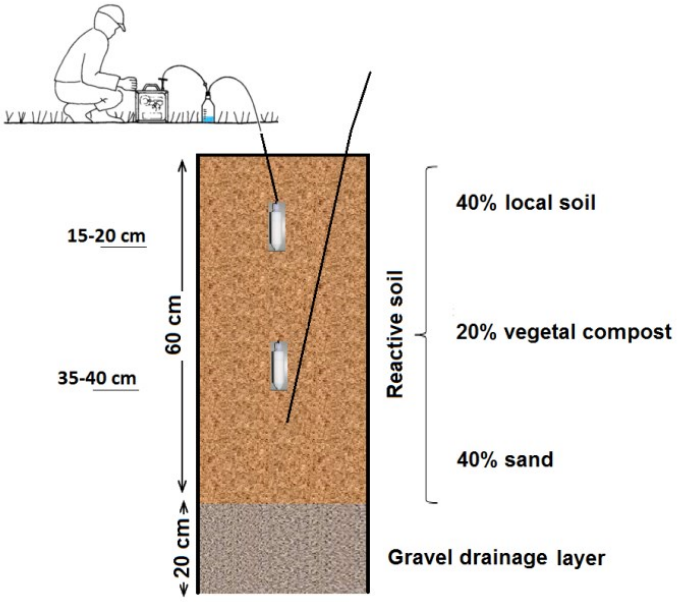

Figure 74 – Detail of the composed soil and sampling devices, at the MARSOL SAT basins

PT2_6: Cerro do Bardo MAR area

Cerro do Bardo karstic area (Figure 1) main goal is to increase groundwater storage using wet years surface water surplus (from three dams, cf. Figure 75) to augment the water availability in dry years and facilitate downstream water supply.

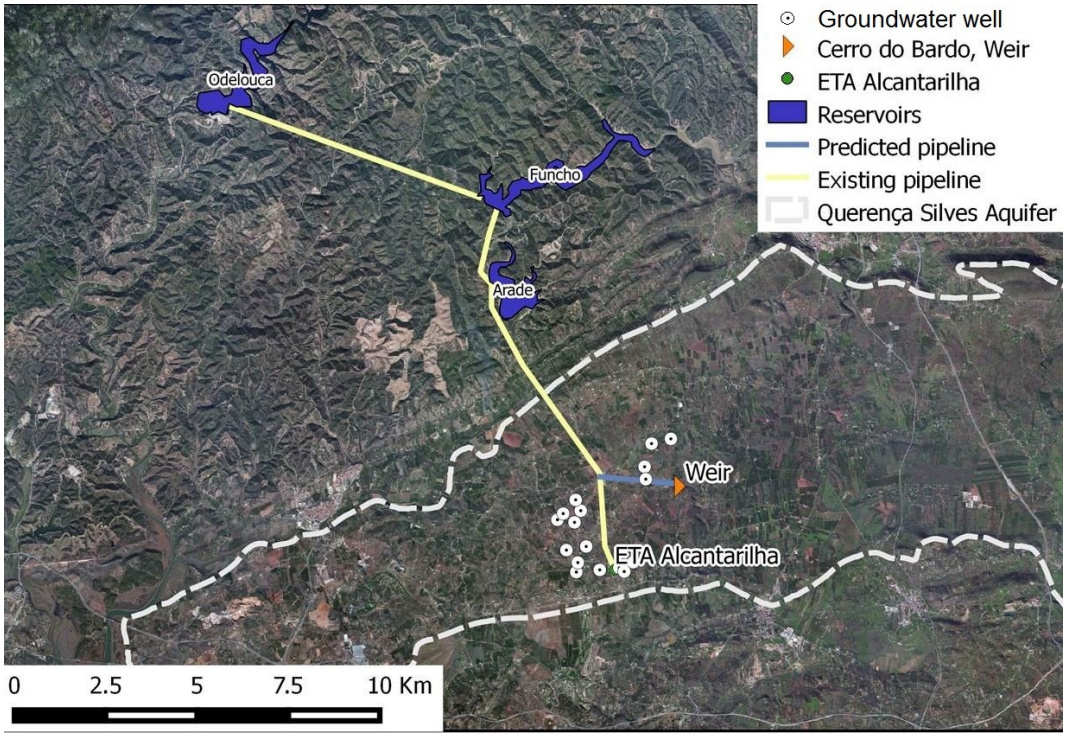

Figure 75 – Location of Cerro do Bardo area and infrastructures with interest to the DEMO site PT2_6. ETA stands for Water Treatment Plant

For this purpose, an area close to the existing pipeline, which connects the three dams to the water treatment plant, has been studied in several previous works (Oliveira, 2007; Leitão et al., 2014). Previous data shows that this was probably an adequate site for infiltration, but tests were needed to assess the infiltration capacity and the main flow direction.

The infrastructures and monitoring facilities developed at Cerro do Bardo are: (1) a 2 m diameter and 34 m depth infiltration dug well (Cerro do Bardo well, CB), (2) a weir (or Aivados small dam) with approximately 26 m long, graved 70 cm deep in the soil and 40 cm thick, and (3) two piezometers constructed in February 2016 (CB1 and CB2). The well and the weir already existed before MARSOL and were rehabilitated during this project, in November 2014 (Figure 76). A more detailed description of the construction works done can be encountered in deliverable D4.2.

Figure 76 – Cerro do Bardo large well and weir (Aivados dam) rehabilitation

CB well's characteristics are synthetized in Table 11.

Table 11 – Cerro do Bardo well characteristics

Parameter	Value
Total depth before works (m)	32
Total depth after works (m), considering a 1 m mouth	33
Diameter (m)	2
Depth to water level at beginning of injection test (m)	29.6
Well's surface area (m^2)	3.14
Well's total floodable volume (Area x depth to water level)[1] (m^3)	93

[1] Considering the current water level and that no infiltration would occur, this would be the total amount of water needed for the water level to reach the well's top casing

The piezometers were drilled in January/February 2016. The first piezometer (CB1) was drilled 15 meters E-SE away from CB well (Figure 77), and was designed with the following objectives: i) collecting local stratigraphic information and therefore reduce the uncertainty related to CB's behaviour during infiltration; ii) water level monitoring; iii) water quality monitoring; and iv) infiltration and tracer test observation well. This piezometer was screened just below the water level, at the depth of the first observed flow during drilling.

As for CB2, it was drilled immediately upstream the weir (Figure 77), 160 m E-SE from CB dug well with the main objective of: i) water level monitoring in the limit of CB MAR system; ii) assess the hydraulic characteristics of the local upper section of Querença-Silves Aquifer System through the realization of a pumping test; iii) assess and outline the water flow direction and storage time during a trace and infiltration test. Due to the need to perform a pumping test (predicted flow of 35 m^3/h) this piezometer was designed for a diameter of 180 mm. The screens were placed at the most productive depths observed during the drilling.

Figure 77 – New piezometers at Cerro do Bardo. CB1 in the left and CB2 in the right

The lithological formations intercepted by both piezometers were, especially in the presence of water (found typically at depths of 38 meters, but with a hydrostatic level of 30 m), unstable and forced the use of a steel casing in CB1, instead of the designed PVC.

Table 12 summarizes the main characteristics of both piezometers.

Table 12 – Main characteristics of Cerro do Bardo MARSOL piezometers

Characteristics	CB1	CB2
Drilling depth (m)	52	72
Cased depth (m)	46	70
Casing (type)	Steel	PVC
Casing diameter (mm)	152.4	180
Screens (type)	Slotted pipe, 2 mm aperture	Hand-made slotted pipe
Screening position (m)	36 - 41	57 - 68
Main geological formations	Limestone, partially weathered and karstified	Limestone, partially weathered and karstified

In both piezometers the lithologic observation of the drilled cuttings allowed the identification of a first formation, of about 15 to 20 meters thick, composed of yellow limestone, clay, silt and sand filling dissolution cavities and open fractures. Deeper, the yellow limestone becomes a grey limestone, being dominant at least up to 70 meters depth. The occurrence of clay, silt and sand associated to the grey limestone weathering was also observed. In both piezometers formations revealed to be fractured and karstified with the occurrence of dissolution cavities spotted during the drilling.

Figure 78 illustrates the hydrogeological conceptual model possible to outline from the drilling data.

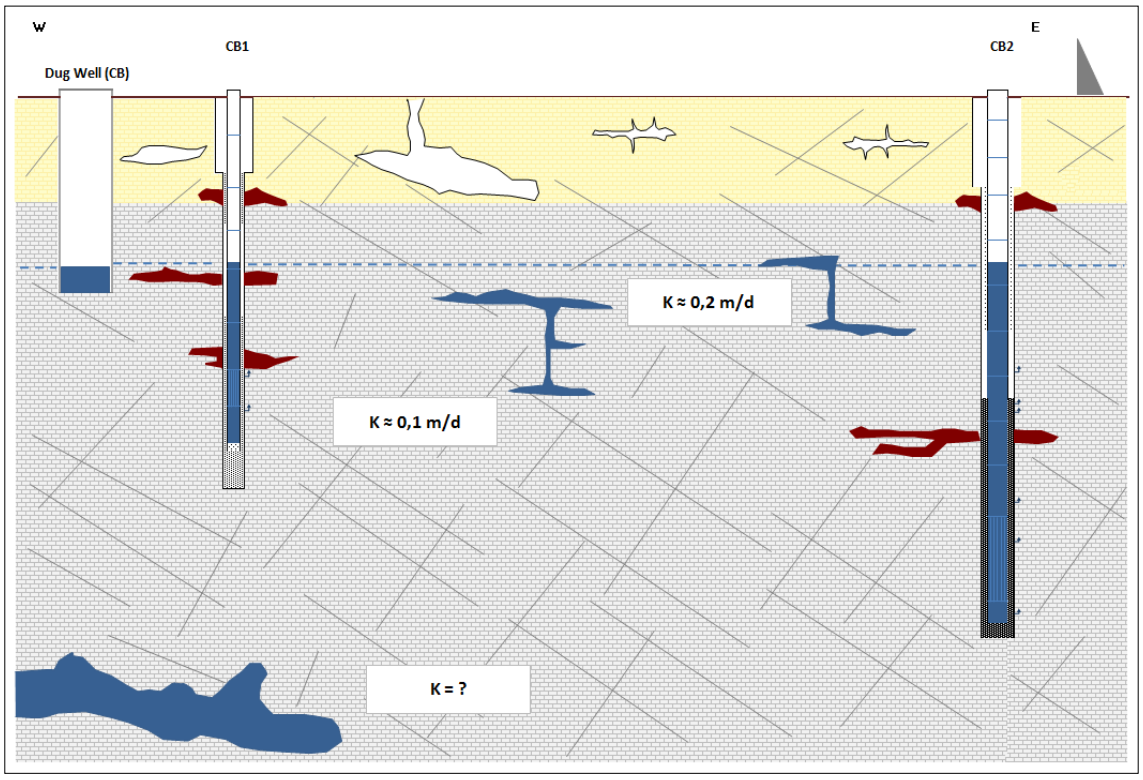

Figure 78 – Hydrogeological conceptual model at Cerro do Bardo

Besides the constructed piezometers, the monitoring network was increased by carrying out a hydrogeological inventory, where several wells, suitable for monitoring purposes, were identified in the surrounding area. Information about its constructive aspects is limited but total depth varies between 70 - 120 m. Most of them are equipped with a pump and used for irrigation purposes, mostly during the dry season. Most of the wells presented closed wellheads and therefore it was not possible to measure the water level.

A total of four private wells (Figure 79) were selected for monitoring purposes which proved to be very useful for regional water quality control. During the construction of CB1 and CB2 no significant interference was noticed in any of these neighbour boreholes. As for the infiltration and trace test results they will be discussed later in the test interpretation.

Figure 79 – Monitoring network and location of SJS2 well, as well as the approximate tracing of the pipeline installed to derive water up to CB well

The characteristics of the monitored wells are shown in Table 13 and their location in Figure 79.

Table 13 – Main characteristics of the wells in Cerro do Bardo area

	Well owner			
	Mr. Caetano	**Mr. Fernando**	**Mr. Luís**	**Mr. Lídio**
M	182801	183176	183216	182200
P	25697	25506	25469	25513
Level	~63	~65	-	~50
Total Depth (m)	124	100	120	70
Pump depth (m)	80	60	65	50
Q (L/s)	4.5	5	5	4.5
Screened zone	-	60-70	-	30-50
Water level (m)	50	47	-	36.6

Figure 80 presents the measurements of the depth to the water table taken in the wells located in the area. The only clear interference is observed in CB well during the development of the piezometer CB1, located 15 meters E-SE away from CB well (Figure 77).

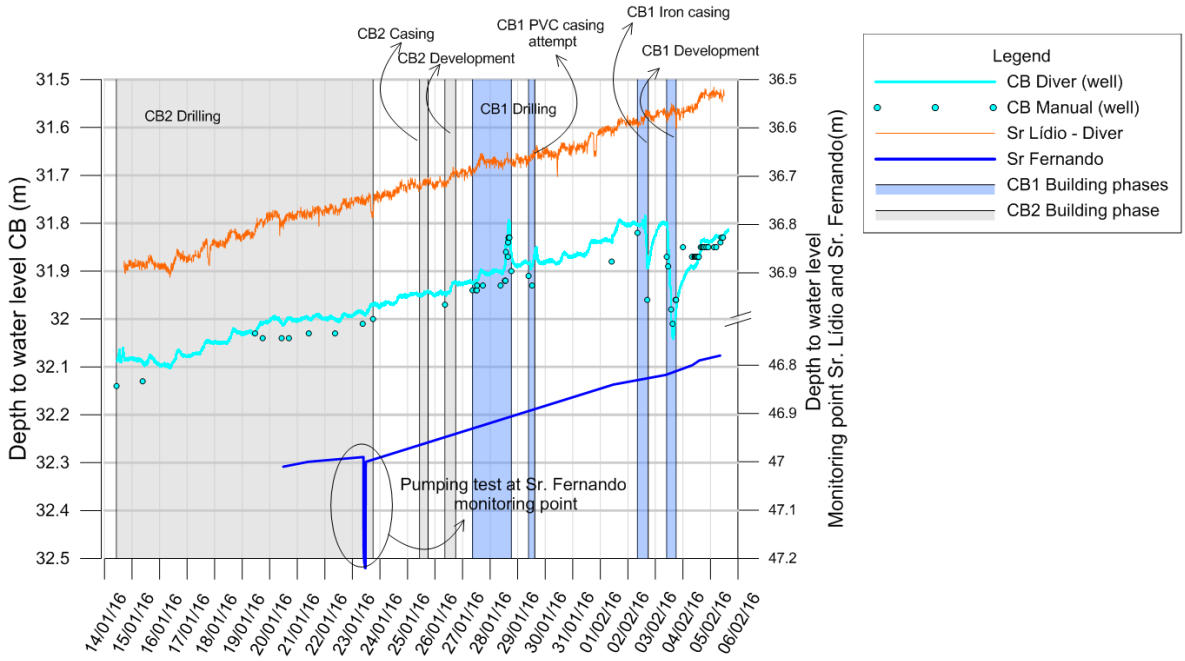

Figure 80 – Depth to the water table measured during the new piezometer drilling and development at Cerro do Bardo

The extent of the monitoring network is adapted to the test regime that is presently being followed in the MARSOL project. As the Cerro do Bardo MAR field can develop towards a situation of continuous operations the monitoring network might have to be enlarged and densified, depending on the infiltration flows and potential influenced area.

2.2.5 Investigation experiments and monitoring results

PT2_4: S. Bartolomeu de Messines SAT basins

Preliminary assessment of the WWTP quality

The treated effluent from São Bartolomeu de Messines WWTP was sampled and analysed by LNEC (May 2014). This water corresponds to the recharge water intended to be used in the SAT basins as well as in the soil-column previous tests. This wastewater originates from a semi-urban area with an elderly population, where consumption of pharmaceuticals is relatively high. Thus, the concentration of a predefined set of drugs typically consumed was measured. Furthermore, three component markers where chosen: boron, copper and zinc. These markers correspond to some of the higher concentrations in heavy metals found in the wastewater (Cu and Zn) and boron is a typical tracer for these waters. In Table 14 a list of the parameters analysed as well as the results obtained are

presented. Furthermore, for this type of water at least monthly data of the chemical composition (i.e. pH, TSS, COD, BOD5, N total, P total, N-NH4, N-NO3, faecal coliforms, EC, all N forms, phosphates and sulphates) has been acquired by Águas do Algarve water supply and waste water company.

Figure 81 – Sampling the WWTP for water collection WP14 at PT2_4 – WWTP at SB Messines

Later in September 2014, IWW has made new analysis at the entrance (raw wastewater) and outflow (treated wastewater) of the SB Messines WWTP, to analyse other pharmaceutical compounds. Table 14 presents a summary of the results, only for the cases where the concentrations were above the quantification limit, at least in one analysis. The water was filtered prior to analysis.

Later in 2016, during the experimental SAT basins period, several other water samples were collected and analysed. This will be presented later in this report.

Table 14 – Results of the raw (WW in) and treated wastewater (WW out) quality of SB Messines WWTP in different campaigns

Parameter		LNEC (AmbiPar Control)	IWW analysis	
		WW out	WW in	WW out
Date	**Unit**	23-05-2014	26-09-2014	26-09-2014
Ammonium	mg/L	17.3	26	23
Arsenic	mg/L	-	<0.0010	<0.0010
Biological Oxygen Demand (BOD5)	mg/L	-	100	36
Boron	mg/L	0.059	-	-
Cadmium	mg/L	-	<0.0020	<0.0020
Calcium	mg/L	-	24	31
Chemical Oxygen Demand	mg/L	-	320	150
Chloride	mg/L	-	113	99.8
Copper	mg/L	0.0072	<0.010	<0.010
Dissolved Organic Carbon	mg/L	-	49	19
Electrical conductiviy	µS/cm	-	969	979
Iron	mg/L	-	0.12	<0.100
Lead	mg/L	-	<0.001	<0.001
Magnesium	mg/L	-	17	18
Manganese	mg/L	-	0.03	0.04
Nickel	mg/L	-	<0.020	<0.020
Nitrate (NO_3^-)	mg/L	<0.27	<1.00	<1.00
Nitrite (NO_2^-)	mg/L	0.0269	0.2	0.16
Potassium	mg/L	-	15	17
Sodium	mg/L	-	75	86
Sulfate	mg/L	35.4	63	11.3
Total suspended solids	mg/L	-	148	58
Total alkaline earths	mmol/L	-	1.3	1.51
Total hardness	°dH	-	7.28	8.49
Total phosphates	mg/L	-	15	10
Total phosphorous	mg/L	-	4.8	3.3
Zinc	mg/L	0.055	-	-
Pharmaceuticals*				
4-tert-Octylphenol	µg/L	-	-	0.04
Acesulfame	µg/L	-	44	18.3
Amidotrizoate	µg/L	-	-	0.52
Atenolol	µg/L	-	0.17	0.09
Beta-Sitosterol	µg/L	-	-	10.6
Bisoprolol	µg/L	-	0.3	0.04
Bisphenol A	µg/L	-	-	0.09
Carbamazepine	µg/L	0.33	0.19	0.51
Caffein	µg/L	0.14	-	0.1
DEET	µg/L	-	-	0.08
Diclofenac	µg/L	-	2.9	0.24
EDTA	µg/L	-	-	6.6
Iomeprol acid	µg/L	-	0.3	0.07
Iopromide	µg/L	-	0.16	7
Ioxithalamin acid	µg/L	-	-	0.06
Metoprolol	µg/L	<0.06	0.19	0.04
Naproxen	µg/L	-	6.2	0.4
Propanolol	µg/L	<0.01	0.018	0.03
Sotalol	µg/L	-	-	0.07
Sulfamethoxazole	µg/L	-	0.047	0.02
Trimethoprim	µg/L	<0.02	-	0.01
Tris(1,3-dichlor-2-propyl)phosphat	µg/L	-	-	0.5
Tris(1-chlor-2-propyl)phosphat	µg/L	-	-	1.5
Tris(2-chloroethyl)phosphat	µg/L	-	3.1	0.52

*Only those with concentrations above the detection limit

- Not analysed

Besides, soil samples were collected at the site from a depth of 5 to 20 cm. These samples allowed classifying SB Messines soil has a clay-rich soil with a large fraction of pebbles.

Laboratory soil-column experiments and results

A set of soil-column experiments were conducted to analyse the natural soil ability to retain contaminants, as well as its hydraulic behaviour under different conditions. Results were compared to those obtained in soil-column experiments conducted with a soil mixture that aimed to increase the natural soil capabilities as a reactive layer to be installed in SAT basins. The removal of contaminants in the wastewater of SB Messines was analysed aiming at understanding the best conditions for improving the water quality for the following main group of contaminants: metals, nitrogen, major ions and pharmaceuticals. Both natural soil and different soil mixtures were studied using cycles of saturation and non-saturation, the latter allowing the oxygenation of the soil column.

The natural soil of the DEMO area used in experiments is a loamy sand (81.91% sand, 15.95% silt and 2.14% clay), having quartz, calcite, montmorillonite and anorthite as major mineral constituents and traces of dolomite, illite, kaolinite and hematite. It has 24.02% of carbonate percentage, low organic matter (OM) content (2.66%), average bulk density of 1.44 g/cm^3 and average porosity of 43.6%. Soil samples were collected at the approximate location of the infiltration site in the outskirts of SB Messines WWTP, from a depth of 5 to 20 cm.

For the soil mixture different components were considered. An increment of OM percentage, particularly in this natural soil which has low OM content, can greatly contribute to the increase of biological activity and therefore the chances of biodegradation processes to occur, as it represents a supply of organic carbon. A commercial organic soil was acquired to be used in the mixture. Another factor to be taken into account is the reactive layer hydraulic behaviour. In fact, although time of contact is essential for contaminant retention, it is also important that this reactive layer does not behave as a cap layer. This would result in long ponding periods in the area of infiltration. To increase the soil mixture permeability, an “artificial sand” was selected. This component results from the industrial extraction of inert materials, more specifically limestone, common in Algarve, which is crushed into specified particle sizes. The crushing process allowed for a larger reactive surface to be available, which facilitates surface retention and cationic exchange processes. Also, the increment of calcium (Ca^{2+}) and magnesium (Mg^{2+}) concentration can enhance cationic exchange and retention processes by the displacement in rock matrix, which ultimately can result in fixation of other elements such as heavy metals. The soil mixture was previously tested in soil-column pre-experiments, and a final composition for the reactive layer was selected: 40 % (w/w) of natural soil, 40 % (w/w) of artificial sand and 20 % (w/w) of organic matter. Other soil mixture compositions tested, with larger percentages of OM, resulted in macropores and compaction due to fine particle washing out.

Table 15 synthetises the procedures adopted in the main soil-column experiments conducted, from different experiment time to the type of injection method. This is the result of a continuous learning process to achieve the more representative methodology of the real scale infrastructures. Initially water injection was continuous (C3 and C4), but throughout the experiments it was decided that the conditions should replicate those in the real scale basins. This was achieved by saturation/non-saturation cycles, where water is inserted in controlled volumes on the top section of the column.

This created a 20 cm pond above the soil which slowly infiltrated. Experiment time varied and in some cases (C4 and C5) the experiment was stopped as result of clogging which blocked water passage in the column.

Table 15 – Synthesis of the operating details of the soil-column experiments conducted

Soil-column experiment	C3	C4	C5	C8
Soil thickness (cm)	20	30	30	30
Type of soil	Natural	Natural	Natural	Mixture
Saturation conditions	Always saturated	Unsat./ saturated cycles	Unsat./ saturated cycles	Unsat./saturated cycles
Injection method	Continuous	Continuous/ pulse	Pulse	Pulse
Water matrix	Deionized/Waste water	Wastewater	Deionized/Waste water	Wastewater
Experiment time length (days)	5	33	16	46

Although special attention was given to inflow/outflow contaminant concentration comparison, the soil hydraulic behaviour was carefully observed as it is fundamental to define the real scale basins functioning schedules. Considering hydraulic behaviour for natural soil, and taking as reference the first day of experiment, C5 showed highest flow rate (1.504 cm^3/min) and permeability (2.536 m/d) while C4 showed the worst results (0.363 cm^3/min and 0.589 m/d). For soil mixture behaviour, C8 had higher flow rate and permeability (3.340 cm^3/min, 3.278 m/d) when compared to the natural soil behaviour.

Concerning inflow water quality, from 32 parameters analysed, C3 had 17 values above the limit of recovery (LOR), C4 and C5 had 17 and C8 had 26. Comparing the outflow in terms of quality, and more precisely average concentration of metals, from 11 parameters considered, C3 had 7 parameters where outflow concentration is higher than inflow, while C4 had 6 and C5 had 9. C8 had only 3 parameters in which outflow average concentration surpasses the inflow, although inflow sample presents a slight enrichment in certain metals when compared to other columns inflow water. Phosphorus shows the highest concentration reduction in all columns. Results are synthetized in Table 16.

Table 16 – Metals and metalloids results comparison (mg/L)

	Parameter	C3		C4		C5		C8	
		IN	OUT	IN	OUT	IN	OUT	IN	OUT
Metals	Aluminium	0.0140	0.0287	0.0110	0.0110	0.0110	0.0149	0.0570	0.0179
	Antimony	-	-	-	-	-	-	0.0830	0.0194
	Barium	0.0673	0.2431	0.0523	0.4855	0.0523	0.4420	0.1800	0.3753
	Boron	0.2360	0.2802	0.2350	0.7805	0.2350	0.7579	0.7230	0.4392
	Chromium	-	-	-	-	-	-	0.0022	0.0014
	Copper	0.0055	0.0075	0.0020	0.0034	0.0020	0.0108	0.0033	0.0022
	Iron	0.0362	0.0241	0.0408	0.0034	0.0408	0.0066	0.0634	0.0559
	Lithium	-	-	-	-	-	-	0.0167	0.0152
	Manganese	0.0627	0.0578	0.0387	0.4285	0.0387	0.0547	0.0572	0.5567
	Molybdenum	0.0020	0.0025	-	-	0.0020	0.0048	0.0024	0.0054
	Nickel	0.0020	0.0052	0.0021	0.0094	0.0021	0.0081	0.0069	0.0036
	Phosphorus	4.7300	0.4173	2.7900	0.0555	2.7900	0.1023	5.5200	1.2654
	Selenium	-	-	-	-	-	-	0.0270	0.0166
	Thallium	-	-	-	-	-	-	0.0740	0.0145
	Vanadium	0.0010	0.0070	0.0010	0.0025	0.0010	0.0048	0.0055	0.0011
	Zinc	0.0350	0.0031	0.0027	0.0021	0.0027	0.0060	0.0049	0.0039

Note: red values represent higher outflow concentrations compared to inflow

For nitrogen cycle components, ammonia showed high concentration at inflow and a reduction at outflow for all columns, while nitrites present low concentration at inflow and high concentration at outflow. C3, C5 and C8 show higher average concentration of nitrates at outflow when compared to inflow. Concentration at outflow in C8 reaches 140.46 mg/L, a very high value when compared to C3 (0.86 mg/L) and C5 (6.51 mg/L) - Table 17. This is probably due to the existence of N in the organic soil added.

Table 17 – Nitrogen components results comparison (mg/L)

	Parameter	C3		C4		C5		C8	
		IN	OUT	IN	OUT	IN	OUT	IN	OUT
Nitrogen cycle	Ammonia	32.80	1.36	34.20	1.45	34.20	0.65	48.90	1.99
	Nitrites	0.02	1.10	0.005	5.08	0.005	3.51	0.01	2.10
	Nitrates	0.27	0.86	2.00	2.00	2.00	6.51	2.00	140.45*

Note: red values represent higher outflow concentrations compared to inflow

*This very high value probably comes from the organic compost used, but no analysis was performed

Concerning major ions, for the 7 parameters considered, 4 were above inflow concentration C4, C5 and C8. C8 experiment shows a worse overall behaviour for these parameters than that with higher average concentrations - Table 18.

Table 18 – Major ions results comparison (mg/L)

	Parameter	C3		C4		C5		C8	
		IN	OUT	IN	OUT	IN	OUT	IN	OUT
Major ions	Calcium	29.4	76.5	43.6	95.30	43.6	103.39	37.8	132.2
	Chloride	-	97.7	91.1	111.85	91.1	97.99	118	116.5
	Magnesium	17.4	31.0	29	47.80	29	45.80	28.4	40.6
	Phosphate	6.3	0.2	7.68	0.10	7.68	0.09	15.2	4.0
	Potassium	16.7	10.6	14.8	7.11	14.8	15.84	23.6	29.9
	Sodium	58.0	39.0	71.6	56.80	71.6	22.53	92.5	83.3
	Sulphate	88.0	8.9	64.7	82.45	64.7	52.63	70.9	77.3

Note: red values represent higher outflow concentrations compared to inflow

Saturation and non-saturation cycles showed that after a long non-saturation period some contaminants concentration at outflow show an increasing trend. This was detected in C8 and may have resulted in a significant alteration in the column conditions, where pH values show a temporary decrease (Figure 82) which ultimately resulted in the temporary release of some previously retained metals (Figure 83 and Figure 84) and major ions (Figure 85).

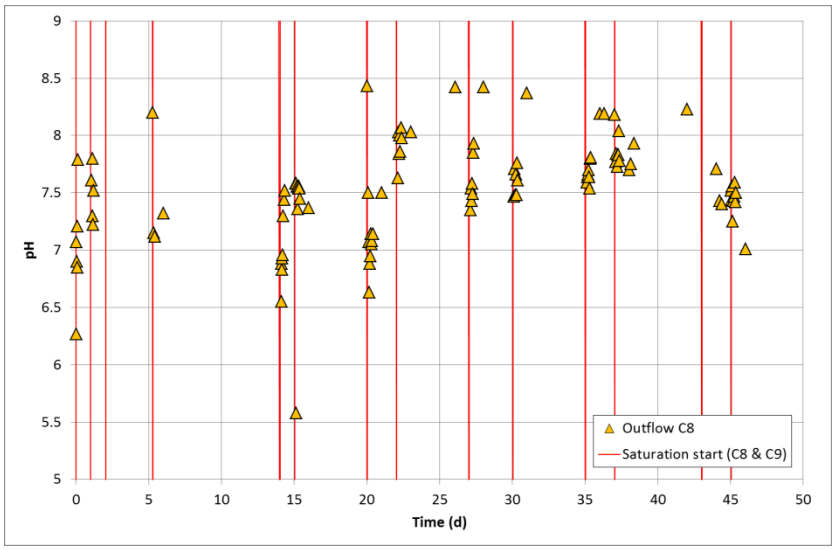

Figure 82 – pH vs time

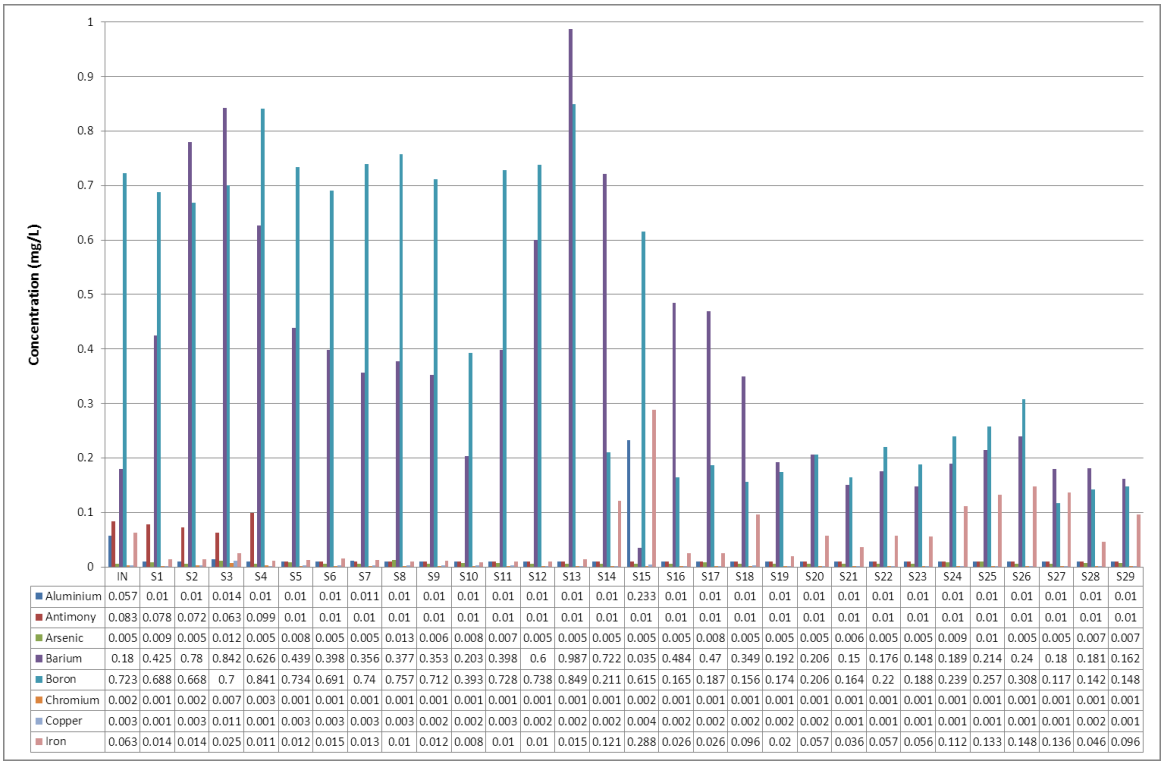

	IN	S1	S2	S3	S4	S5	S6	S7	S8	S9	S10	S11	S12	S13	S14	S15	S16	S17	S18	S19	S20	S21	S22	S23	S24	S25	S26	S27	S28	S29
Aluminium	0.057	0.01	0.01	0.014	0.01	0.01	0.01	0.011	0.01	0.01	0.01	0.01	0.01	0.01	0.01	0.233	0.01	0.01	0.01	0.01	0.01	0.01	0.01	0.01	0.01	0.01	0.01	0.01	0.01	0.01
Antimony	0.083	0.078	0.072	0.063	0.099	0.01	0.01	0.01	0.01	0.01	0.01	0.01	0.01	0.01	0.01	0.01	0.01	0.01	0.01	0.01	0.01	0.01	0.01	0.01	0.01	0.01	0.01	0.01	0.01	0.01
Arsenic	0.005	0.009	0.005	0.012	0.005	0.008	0.005	0.005	0.013	0.006	0.008	0.007	0.005	0.005	0.005	0.005	0.005	0.008	0.005	0.005	0.005	0.006	0.005	0.005	0.009	0.01	0.005	0.005	0.007	0.007
Barium	0.18	0.425	0.78	0.842	0.626	0.439	0.398	0.356	0.377	0.353	0.203	0.398	0.6	0.987	0.722	0.035	0.484	0.47	0.349	0.192	0.206	0.15	0.176	0.148	0.189	0.214	0.24	0.18	0.181	0.162
Boron	0.723	0.688	0.668	0.7	0.841	0.734	0.691	0.74	0.757	0.712	0.393	0.728	0.738	0.849	0.211	0.615	0.165	0.187	0.156	0.174	0.206	0.164	0.22	0.188	0.239	0.257	0.308	0.117	0.142	0.148
Chromium	0.002	0.001	0.002	0.007	0.003	0.001	0.001	0.001	0.001	0.001	0.001	0.001	0.001	0.001	0.001	0.002	0.001	0.001	0.001	0.001	0.001	0.001	0.001	0.001	0.001	0.001	0.001	0.001	0.001	0.001
Copper	0.003	0.001	0.003	0.011	0.001	0.003	0.003	0.003	0.003	0.002	0.002	0.003	0.002	0.002	0.002	0.004	0.002	0.002	0.002	0.002	0.002	0.001	0.001	0.001	0.001	0.001	0.001	0.001	0.002	0.001
Iron	0.063	0.014	0.014	0.025	0.011	0.012	0.015	0.013	0.01	0.012	0.008	0.01	0.01	0.015	0.121	0.288	0.026	0.026	0.096	0.02	0.057	0.036	0.057	0.056	0.112	0.133	0.148	0.136	0.046	0.096

Figure 83 – Metals inflow/outflow concentration in Column 8 (1st set)

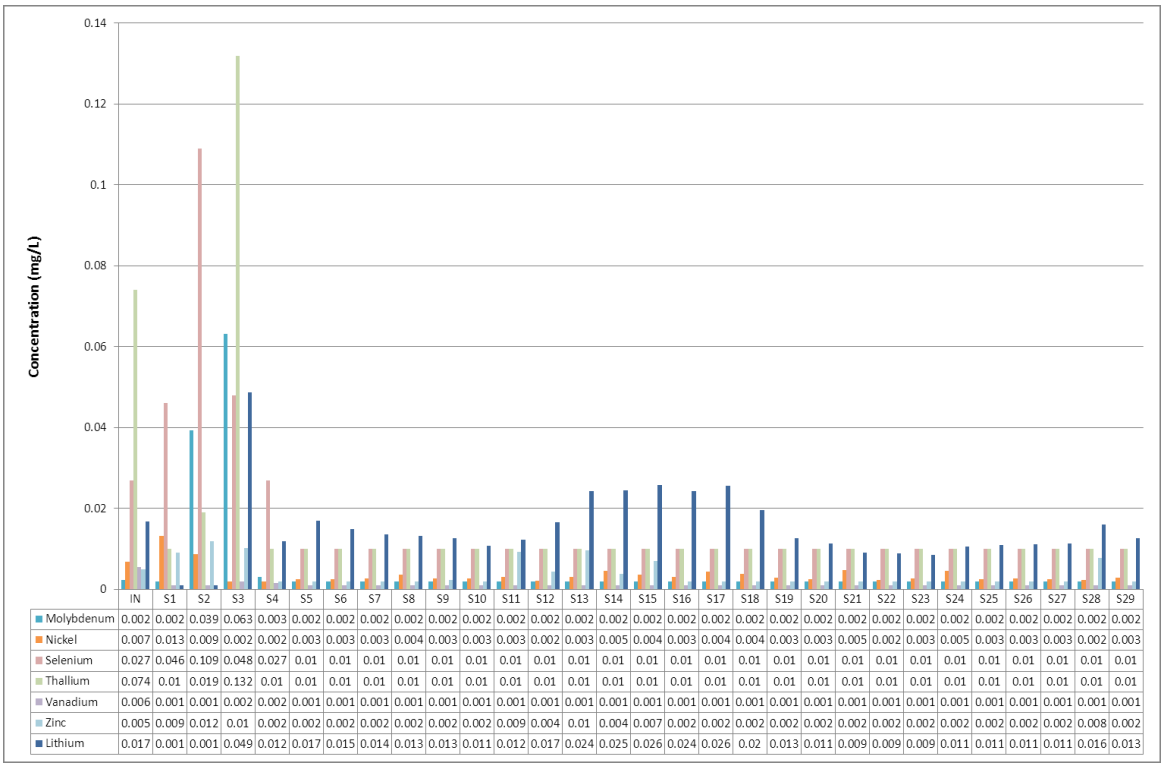

	IN	S1	S2	S3	S4	S5	S6	S7	S8	S9	S10	S11	S12	S13	S14	S15	S16	S17	S18	S19	S20	S21	S22	S23	S24	S25	S26	S27	S28	S29
Molybdenum	0.002	0.002	0.039	0.063	0.003	0.002	0.002	0.002	0.002	0.002	0.002	0.002	0.002	0.002	0.002	0.002	0.002	0.002	0.002	0.002	0.002	0.002	0.002	0.002	0.002	0.002	0.002	0.002	0.002	0.002
Nickel	0.007	0.013	0.009	0.002	0.002	0.003	0.003	0.003	0.004	0.003	0.003	0.003	0.002	0.003	0.005	0.004	0.003	0.004	0.004	0.003	0.003	0.005	0.002	0.003	0.005	0.003	0.003	0.003	0.002	0.003
Selenium	0.027	0.046	0.109	0.048	0.027	0.01	0.01	0.01	0.01	0.01	0.01	0.01	0.01	0.01	0.01	0.01	0.01	0.01	0.01	0.01	0.01	0.01	0.01	0.01	0.01	0.01	0.01	0.01	0.01	0.01
Thallium	0.074	0.01	0.019	0.132	0.01	0.01	0.01	0.01	0.01	0.01	0.01	0.01	0.01	0.01	0.01	0.01	0.01	0.01	0.01	0.01	0.01	0.01	0.01	0.01	0.01	0.01	0.01	0.01	0.01	0.01
Vanadium	0.006	0.001	0.001	0.002	0.002	0.001	0.001	0.001	0.001	0.001	0.001	0.001	0.001	0.001	0.001	0.001	0.001	0.001	0.001	0.001	0.001	0.001	0.001	0.001	0.001	0.001	0.001	0.001	0.001	0.001
Zinc	0.005	0.009	0.012	0.01	0.002	0.002	0.002	0.002	0.002	0.002	0.002	0.009	0.004	0.01	0.004	0.007	0.002	0.002	0.002	0.002	0.002	0.002	0.002	0.002	0.002	0.002	0.002	0.002	0.008	0.002
Lithium	0.017	0.001	0.001	0.049	0.012	0.017	0.015	0.014	0.013	0.013	0.011	0.012	0.017	0.024	0.025	0.026	0.024	0.026	0.02	0.013	0.011	0.009	0.009	0.009	0.011	0.011	0.011	0.011	0.016	0.013

Figure 84 – Metals inflow/outflow concentration in Column 8 (2nd set)

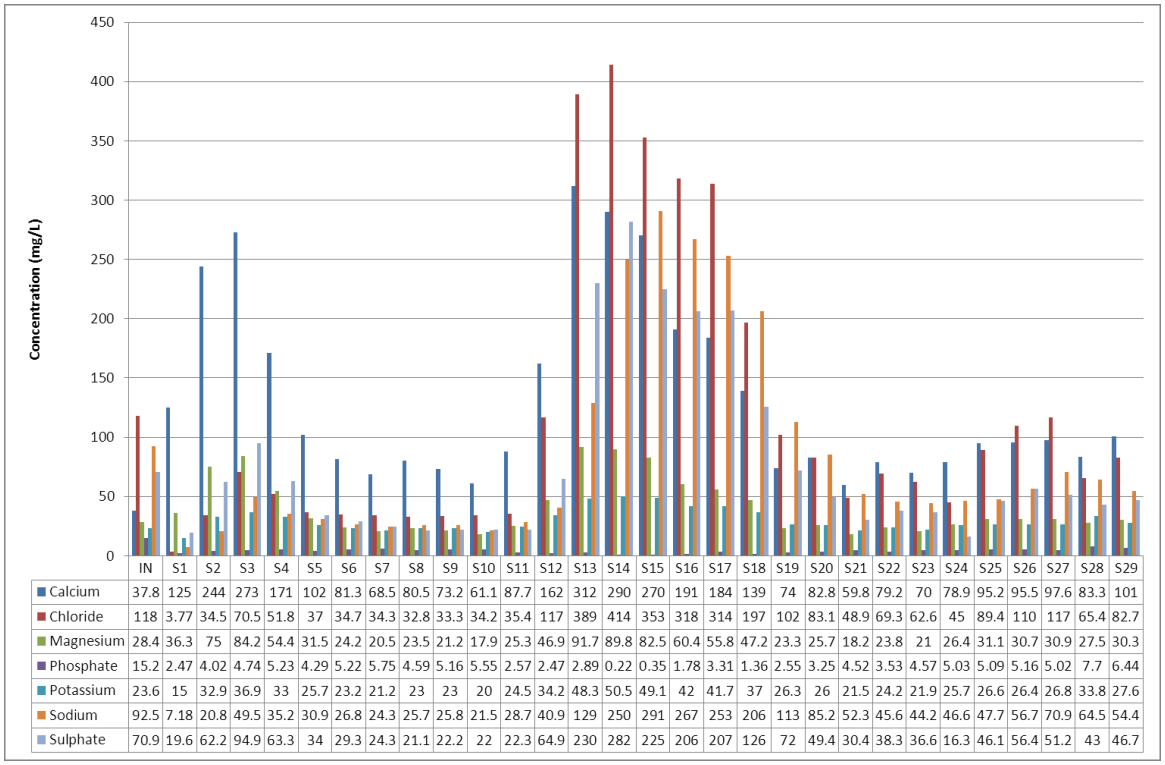

	IN	S1	S2	S3	S4	S5	S6	S7	S8	S9	S10	S11	S12	S13	S14	S15	S16	S17	S18	S19	S20	S21	S22	S23	S24	S25	S26	S27	S28	S29
Calcium	37.8	125	244	273	171	102	81.3	68.5	80.5	73.2	61.1	87.7	162	312	290	270	191	184	139	74	82.8	59.8	79.2	70	78.9	95.2	95.5	97.6	83.3	101
Chloride	118	3.77	34.5	70.5	51.8	37	34.7	34.3	32.8	33.3	34.2	35.4	117	389	414	353	318	314	197	102	83.1	48.9	69.3	62.6	45	89.4	110	117	65.4	82.7
Magnesium	28.4	36.3	75	84.2	54.4	31.5	24.2	20.5	23.5	21.2	17.9	25.3	46.9	91.7	89.8	82.5	60.4	55.8	47.2	23.3	25.7	18.2	23.8	21	26.4	31.1	30.7	30.9	27.5	30.3
Phosphate	15.2	2.47	4.02	4.74	5.23	4.29	5.22	5.75	4.59	5.16	5.55	2.57	2.47	2.89	0.22	0.35	1.78	3.31	1.36	2.55	3.25	4.52	3.53	4.57	5.03	5.09	5.16	5.02	7.7	6.44
Potassium	23.6	15	32.9	36.9	33	25.7	23.2	21.2	23	23	20	24.5	34.2	48.3	50.5	49.1	42	41.7	37	26.3	26	21.5	24.2	21.9	25.7	26.6	26.4	26.8	33.8	27.6
Sodium	92.5	7.18	20.8	49.5	35.2	30.9	26.8	24.3	25.7	25.8	21.5	28.7	40.9	129	250	291	267	253	206	113	85.2	52.3	45.6	44.2	46.6	47.7	56.7	70.9	64.5	54.4
Sulphate	70.9	19.6	62.2	94.9	63.3	34	29.3	24.3	21.1	22.2	22	22.3	64.9	230	282	225	206	207	126	72	49.4	30.4	38.3	36.6	16.3	46.1	56.4	51.2	43	46.7

Figure 85 – Column 8 major ions inflow/outflow concentrations

Regarding the pharmaceutical compounds, C8 showed the best results, i.e. none of the commonly persistent compounds were found in the outflow, although atenolol, bisoprolol, metoprolol, propranolol, sotalol, diclofenac, gemfibrozil, naproxen and carbamazepine were detected in the inflow. In C3, outflow analysis showed carbamazepine, diclofenac, gemfibrozil, hydrochlorothiazide, ibuprofen, levetiracetam, naproxen and primidone above LOR. C4 showed benzafibrate, carbamazepine, diclofenac, gemfibrozil and naproxen concentrations above LOR at outflow, while in C5 presented concentration above LOR of benzafibrate, carbamazepine, diclofenac, gemfibrozil, ibuprofen and naproxen.

To also understand how concentrations of possible retained contaminants vary along column, soil samples were collected and analysed after C3 and C5 experiments stopped. C3 shows almost equal concentration of boron, copper and zinc in top and bottom sections, but boron concentrations were lower. Ammonia showed higher concentrations when compared with nitrates and nitrites, being heavily retained in the soil top section, while nitrates where not detected in both sections and nitrites showed very small concentration. Phosphorous and phosphates showed higher concentrations in the soil top section. For C5, boron and copper showed slightly lower concentrations to those detected in C3, and ammonia shows a high concentration on the top section. Nitrates and nitrites were also detected in higher concentration on column top section. Phosphorous and phosphates showed lower concentrations in both sections when compared to C3 and sulphates where not detected in both sections.

Batch experiments were also conducted in natural soil and soil mixture to understand the maximum contaminant retention capacity for the same parameters. Obtained results show similar results for soil-column experiments.

From the both batch experiments results comparison soil mixture shows better effects on supressing recalcitrant pharmaceuticals, where one out of 14 above LOR[1] in inflow was detected in outflow, namely carbamazepine. This element also occurs in the outflow of the batch conducted in natural soil, where seven out of 14 above LOR show persistent behaviour.

Other parameters also show better results for the soil mixture where the average removal percentage is 64% vs 57% of natural soil. Also, the number of compounds that showed concentration increase at outflow is higher in natural soil than in soil mixture.

The main conclusions that can be drawn are: (1) the presence of a soil mixture with OM layer favours the retention/degradation, mainly through sorption and biotransformation processes, primarily for metals (retained both in clay fraction and OM); (2) the sequence of oxic/anoxic conditions is the best approach to ensure maximum attenuation efficiency, since some elements degrade better in oxic conditions (such as the biological oxidation of ammonia into nitrite and nitrate), while others are degraded under anaerobic conditions; and (3) the existence of high pH favours the retention of heavy metals attached to soils.

Given the results obtained, concerning both hydraulic and quality aspects, a set of recommendations can be made.

The increase in the organic matter content in the soil used for SAT-MAR has shown general improvement of the outflow water quality when compared with the inflow. Thus, if the natural soil to be used as reactive layer has low concentration of organic matter (which is the case of the DEMO site natural soil), it should be artificially integrated in a soil mixture.

The increase of organic matter can result in lowering the soil resistance, due to the increase in porosity resultant from the washing out process; the latter creates preferential flow paths, cavities and air pockets that led to the thickness decrease of the reactive layer. Consequently, the addition of a skeleton component can be useful to avoid these phenomena. “Artificial sand”, which is an inexpensive material produced from limestone crushing, was a good example to increase permeability and also to give structure to the soil, without any relevant impact in terms of quality at outflows as the matrix of this component is the same as the natural soil (limestone).

Also, the implementation of saturation/unsaturation cycles to the soil allows it to oxygenate, enabling the degradation/retention of compounds under oxidation reactions, as well as periods of oxygen depleted environment that enhance anaerobic degradation. This will also reduce biological clogging effects, as the small turbulence of inflow water and air exposure can hinder biofilm production on the soil top. It is recommended that basins operate, if possible, in a regular schedule, as the implementation of large periods of non-saturation conditions can ultimately result in the

[1] LOR - Limit of recovery

remobilization of contaminants, and these periods should be avoided to prevent drastic changes in the reactive layer conditions.

Water influx should be relatively low. This allows avoiding turbulence and the creation of suspended solids as well as the remobilization of contaminants retained in the soil matrix.

It is also important to keep in mind that the experimental results obtained in laboratory, both for permeability and recharge water quality, are expected to be different from those obtained in basin scale experiments. This fact can result from scaling factors and natural soil heterogeneity, together with local differences resulting from changes in vegetation, topography or man activity. The different field conditions are not possible to control in the same manner as soil-column experiments. At infiltration basin scale other processes, such as root growth in the reactive layer, could benefit the long-time hydraulic behaviour by smoothing the clogging effects. On the other hand, uncontrolled effluent – with the natural variations that a wastewater can experience – can have adverse results in the basin operational status.

SB Messines SAT Basins

During 2.5 months, from September 15th to November 30th 2016, SB Messines WWTP effluent was partially diverged to the SAT basins (see Section 2.2.4) for further treatment (Figure 70) by the SAT Basins. The WWTP effluent has percolated the 60 cm strata sequence (composed of 40% local soil, 40% coarse sand and 20% vegetal compost) and was then drained to the river. Different aerobic/anaerobic cycles were tested in the SAT basins.

To monitor the experiment, three Smart Water network wireless sensors were used to perform remote water quality monitoring and communication in real time, for water inflow (B_IN) and water outflow in both basins (B1_OUT and B2_OUT) (Figure 70). The parameters measured were electrical conductivity (EC), temperature (T), pH and redox potential (ORP).

Besides the continuous measurements of those water quality parameters at the water inflow and the two water outflows, water was manually sampled every week, during 2.5 months, from September 15th to November 30th, 2016. The soil-water was also monitored using suction capsules placed in two points and two depths (20 and 40 cm) at each basin (Figure 70 and Figure 74), in a total of four capsules per basin.

Electrical conductivity, temperature, pH and redox potential

Figure 86 to Figure 88 show the results obtained for the continuous measurements in water inflow and two outflows. Basin 1 sensor had a problem during a 2-week period, during which no data was therefore obtained.

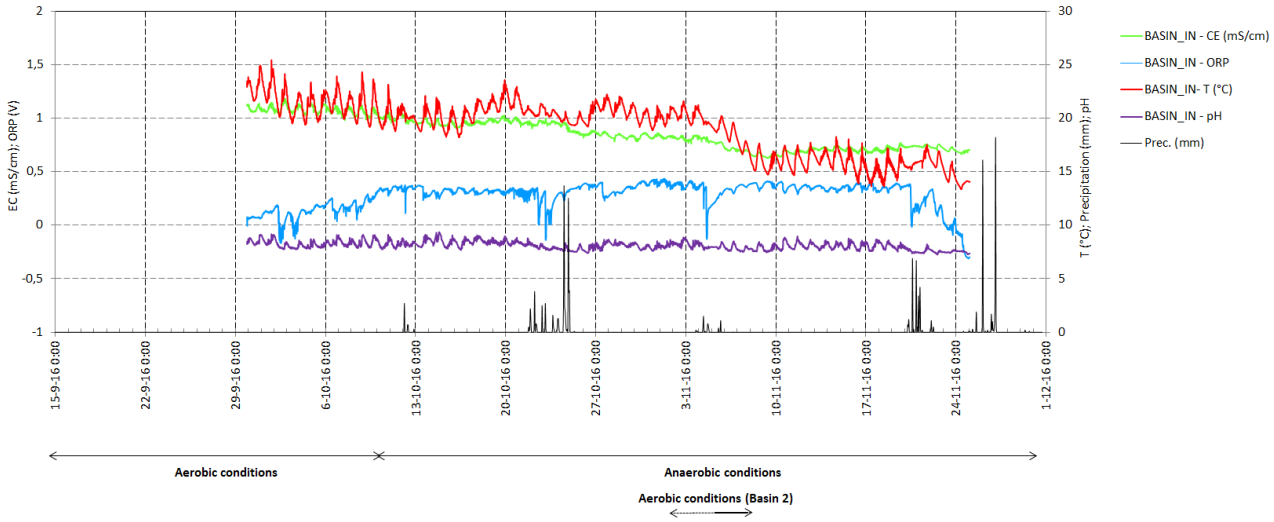

Figure 86 – Electrical conductivity, temperature, pH and redox values at the basin entrance (Basin_IN)

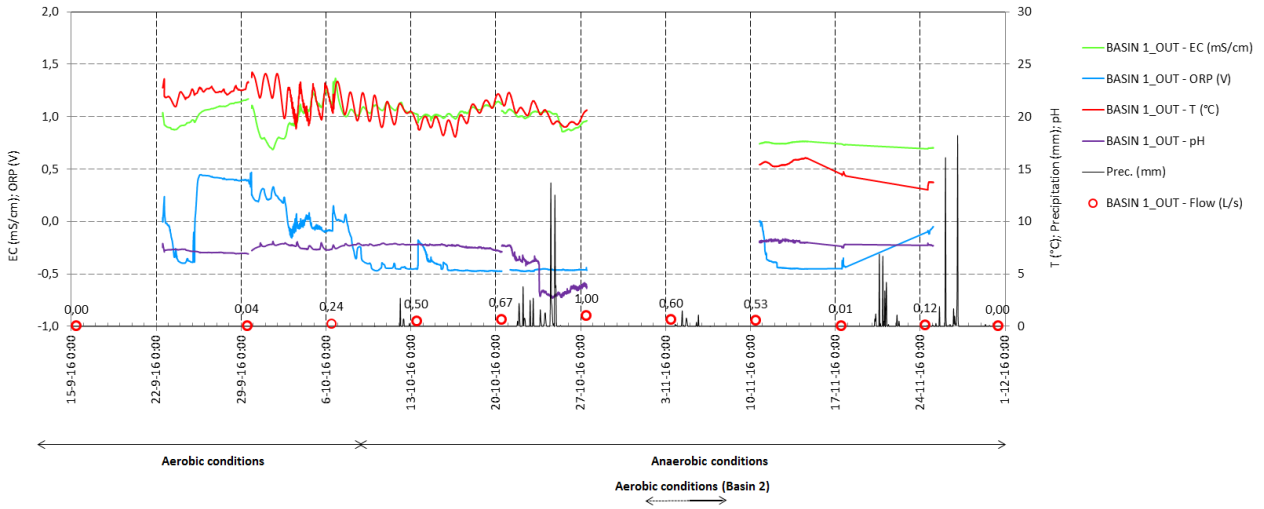

Figure 87 – Electrical conductivity, temperature, pH and redox values in Basin 1 outflow (Basin 1_OUT)

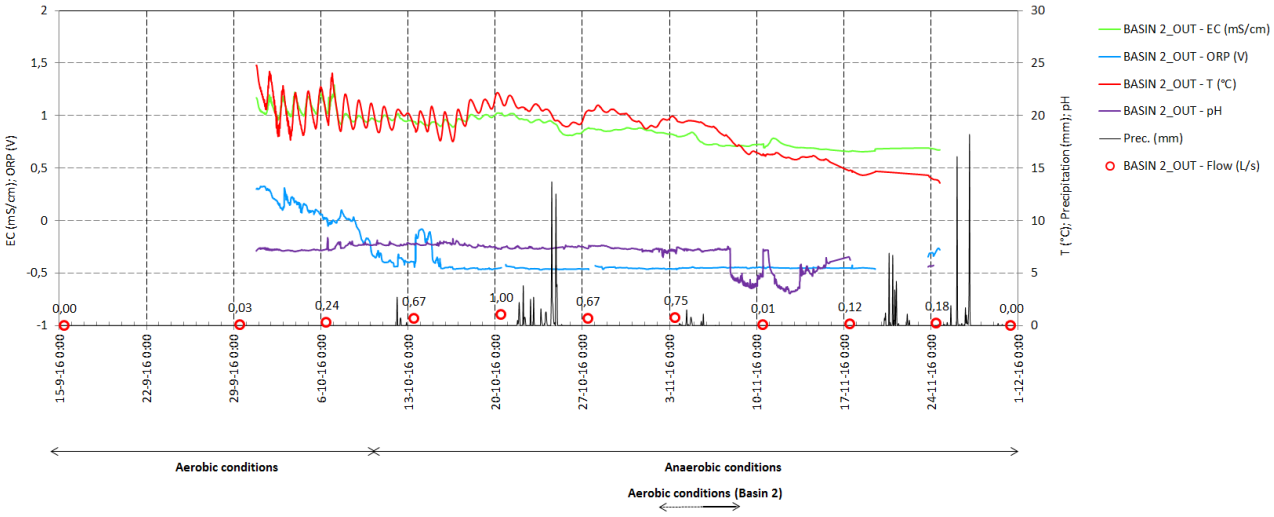

Figure 88 – Electrical conductivity, temperature, pH and redox values in Basin 2 outflow (Basin 2_OUT)

Concerning temperature, an expected general trend of decrease is observed towards the approach of the (late) autumn. It is also possible to see daily variations, which tend to diminish in the basins outflow (Figure 87 and Figure 88) for the period of lower temperatures, possibly due to smaller daily variations of temperature.

Electrical conductivity (EC) values show a quite stable pattern along the 2.5-month period of experiment, with a predictable decrease towards the period of higher precipitation. The values tend to decrease after rain events (e.g. week of 20-27 November 2016) due to dilution. It is also possible to recognize a linear relation between EC and temperature, where higher EC values correspond to higher temperatures. This is possible due to higher dissolution of salts when temperatures are higher. The values of EC at the basin outflow (Figure 87 and Figure 88) show no clear improvement (decrease) when compared to the basins entrance (Figure 86), as expected.

Redox potential (ORP or Eh) had positive values in the water at the basins entrance for almost all the experiment period, with values around 400 µS/cm. In several occasions lower values were observed after rain periods (Figure 86). At the basins outflow (Figure 87 and Figure 88) the ORP values characterize two periods: 1) first, where the basin was not saturated with water, creating aerobic conditions and therefore higher ORP values and 2) second, where the basin was saturated with a column of water, creating an anaerobic environment (with little or no available free oxygen) expressed by the obtained negative ORP values, typical of anoxic conditions. These changes in the redox conditions have a clear effect in the nitrogen cycle and on the pharmaceutical compounds removal.

Finally, pH values varied between 7 and 8 in all three situations, therefore slightly basic conditions with the daily patterns typical of the photosynthetic activity occurring in the WWTP lagoons. The drastic changes registered in the pH of both Basin 1 and 2, in different periods, were not confirmed by manual measurements. Possibly this was an error in the sensors reading. The pH basic values create favourable conditions for the precipitation of most heavy metals dissolved in the water.

Major ions

The following major ions were analysed: HCO_3^-, Cl^-, SO_4^{2-}, Ca^{2+}, Mg^{2+}, Na^+, K^+. The results obtained are presented in Figure 89 to Figure 95, where B1 and B2 stands for Basin 1 or 2; ME for left margin; MD for right margin; 20 and 40 for cm depth in the soil. So, for instance, B1_MD-20 is the water sample from Basin 1, right margin and 20 cm depth in the soil.

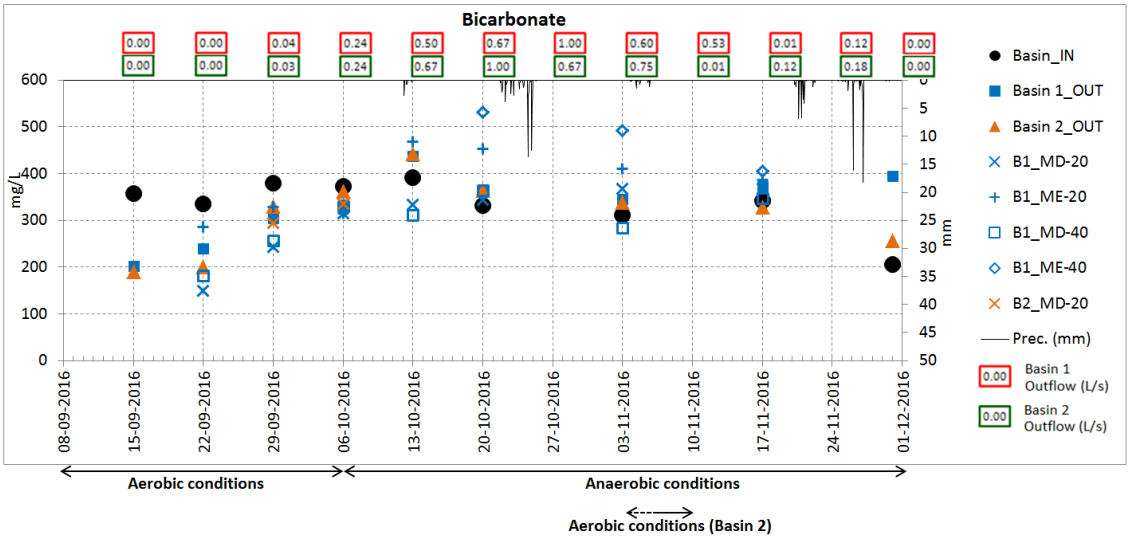

Figure 89 – Bicarbonate concentration in water samples obtained during SAT basin experiments

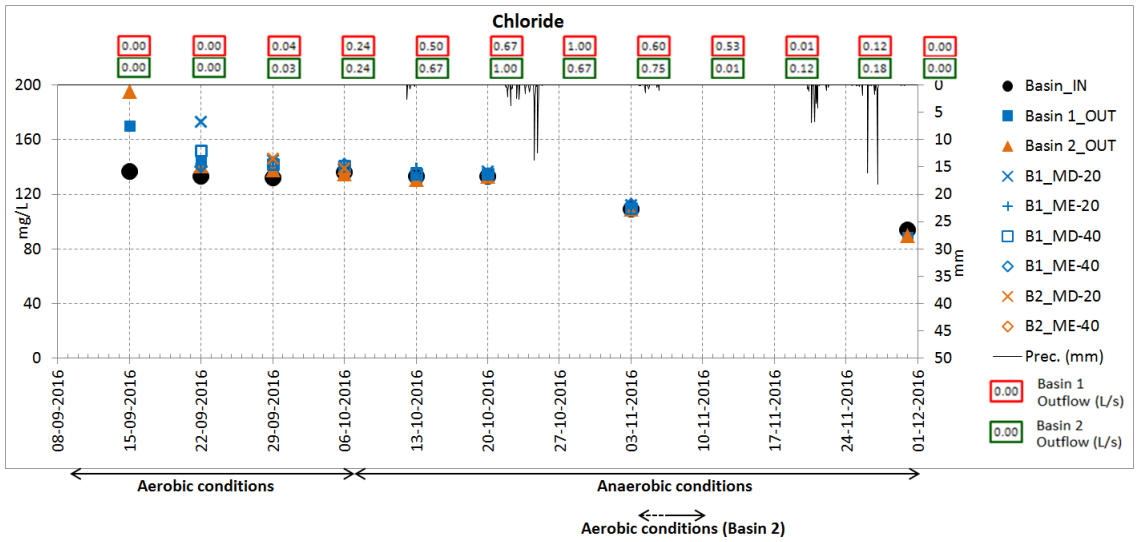

Figure 90 – Chloride concentration in water samples obtained during SAT basin experiments

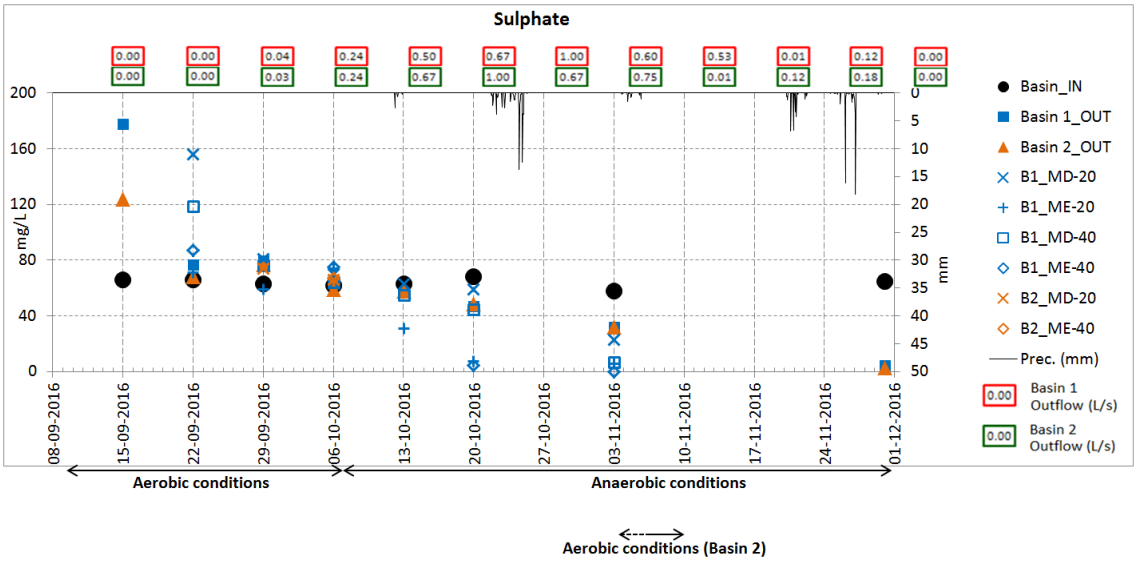

Figure 91 – Sulphate concentration in water samples obtained during SAT basin experiments

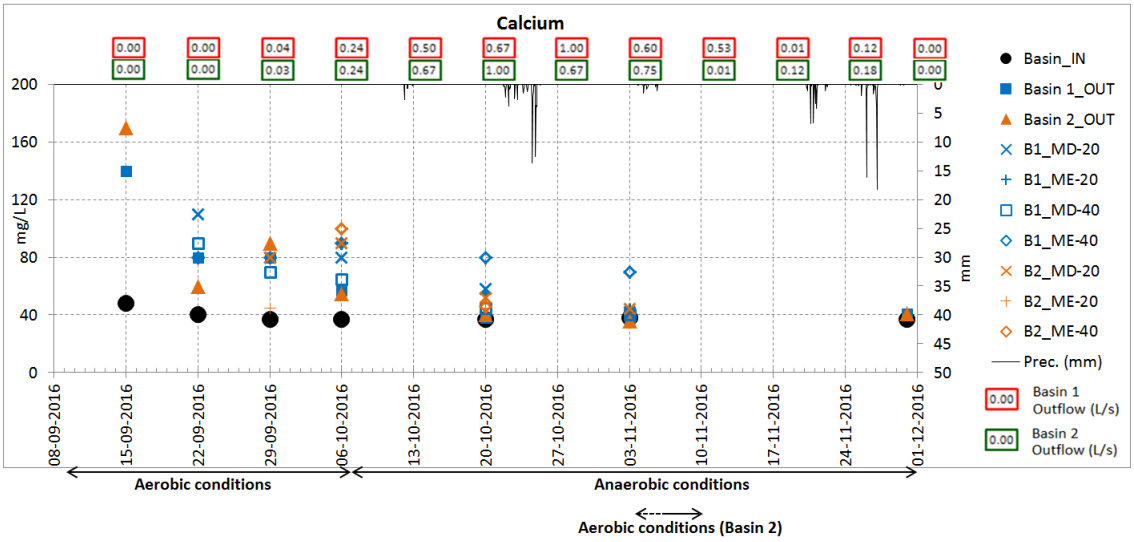

Figure 92 – Calcium concentration in water samples obtained during SAT basin experiments

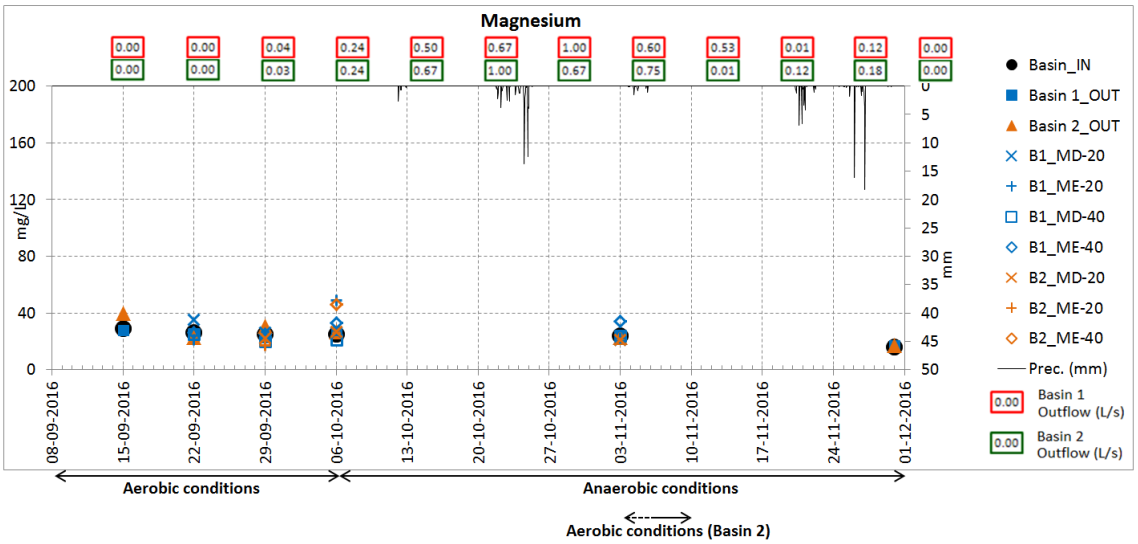

Figure 93 – Magnesium concentration in water samples obtained during SAT basin experiments

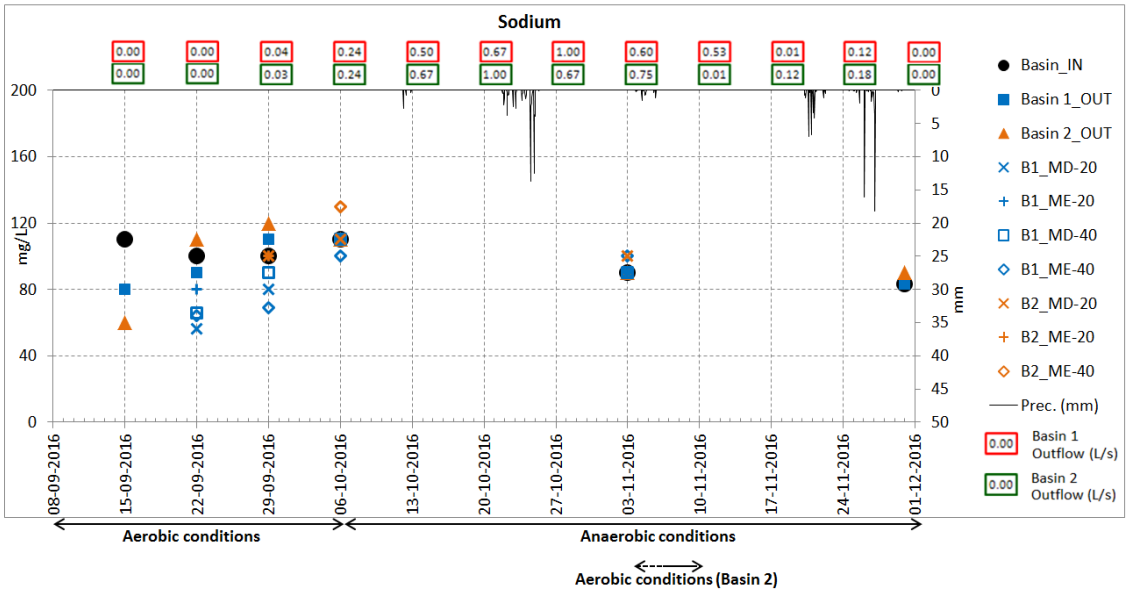

Figure 94 – Sodium concentration in water samples obtained during SAT basin experiments

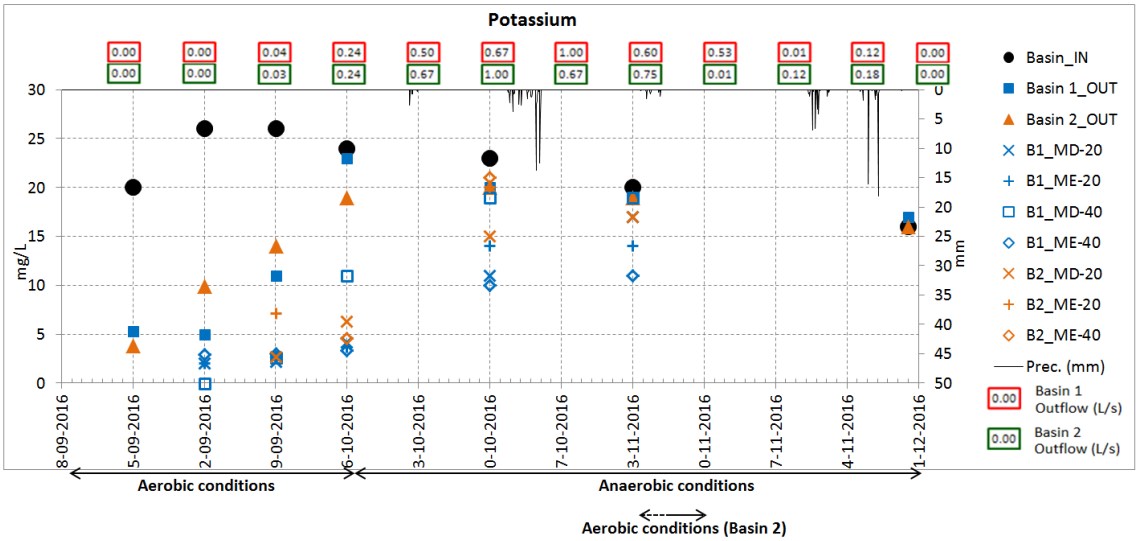

Figure 95 – Potassium concentration in water samples obtained during SAT basin experiments

From the figures, the following observations can be done as a result of the soil-water interactions along the experiment [note in the figures the precipitation and the two basin's outflow (which gives an idea about the relative contact time soil-water – the higher the outflow, the lower the contact time)]:

- For the anions, some dilution can be observed after rain events.
- Except for the first reading (15/9/2016), there is no relevant difference between the anions concentration in the outflow of the two basins.
- Bicarbonate (HCO_3^-) is the anion presenting higher concentrations followed by (Cl^-) and sulphate (SO_4^{2-}).
- Chloride behaves as a conservative ion, with very little interaction soil-water, and therefore no significant changes occurred throughout the experiment, when comparing water entering the SAT system (Basin_IN) and water flowing out of the system (Basin 1_OUT and Basin 2_OUT).
- Sulphate ions concentration has increased from inflow to the outflow (i.e. from Basin_IN to Basin 1_OUT/Basin 2_OUT) during the first stages with aerobic conditions and has decreased during the anaerobic stages. This could be due to SO_4^{2-}soil lixiviation since it happened only in the first sampling period. After October 6th, during anaerobic conditions, the action of sulphate-reducing bacteria should have been responsible for the reduction of sulphate possibly to hydrogen sulphide, thus diminishing SO_4^{2-} concentration in the outflow.
- Bicarbonate concentration decreased in the first stages, probably due to the photosynthetic activity (uptake of HCO_3^- as a CO_2 source) occurring in the SAT water column (to a higher extent during the longer daytime period season, September) until it reaches a chemical equilibrium throughout the experiment (during Autumn).
- For cations concentration, some small dilution can be observed after rain events.
- Basin 1 and Basin 2 outflows show different cations concentrations possibly due to heterogeneities in clay content.

- Sodium (Na^+) is the anion presenting higher concentrations followed by calcium (Ca^{2+}) and magnesium (Mg^{2+}) and, in a much lower concentration, potassium (K^+).
- Calcium concentration shows the expected initial increase after SAT system, due to its release from the calcium carbonate-rich soil matrix, until equilibrium.
- Magnesium is very stable throughout the experiment probably due to the presence of its competitive cation (Ca^{2+}) in much higher concentrations.
- Sodium and potassium show an initial decrease in the water concentration outflow when compared with the water entering the SAT system. This is probably due to cation exchange with soil matrix-Ca^{2+}, until chemical equilibrium is reached, 3 to 4 weeks after the experiment began.

Nutrients (N and P) and metals

The following nutrients, boron and metals were analysed in the water sampled weekly: ammonia (NH_4^+), nitrite (NO_2^-), nitrate (NO_3^-), phosphate (PO_4^{3-}), boron (B), zinc (Zn) and copper (Cu). Zn and Cu have been selected based on previous work (Leitão *et al*., 2014) and analyses (see page 86). However, the results obtained in this experiment were always below the quantification limit, which, due to the low water volume available in the soil-water, was one order of magnitude higher than the limit of recovery of the previous analyses.

The results obtained are presented in Figure 96 to Figure 100. From the figures, the following conclusion can be drawn:

- Nitrogen behaviour clearly shows the effects of the aerobic and anaerobic phases of the soil zone. In the first one, the presence of oxygen is responsible for transforming most NH_4^+ in NO_3^- through: $2\ NH_4^+ + 3O_2 \rightarrow 2NO_2^- + 2H_2O + 4H^+$ and $2NO_2^- + O_2 \rightarrow 2NO_3^-$. In the anaerobic phase, NH_4^+ stays stable and almost no nitrate or nitrite is detected. Between 3/11/2016 and 10/11/2016 oxygenated water has flown from Basin 2 through the gravel drain (cf. Figure 72) below the 60 cm soil of Basin 1 (in a period where pipes were being tested) causing nitrification in the 40 cm soil zone sampling closer to that water entrance (right margin, B1_MD-40), as can be seen in Figure 98.
- Phosphate concentration varies strongly in the inflow water along the experiment. Two behaviours can be observed. In the first period, almost all PO_4^{3-} is retained by the Ca-rich soil particles, probably as hydroxyapatite, a highly water insoluble compound. After 3/11/2016, the concentrations in the water entering the basins are equivalent to the outflows, consistent with the soil saturation, responsible for the above discussed variation of the other water quality parameters.
- Boron is a very stable element along the experiment, with values similar in the water at the SAT basins inflow and outflows. Only in the last sampling period a decrease in this element was observed, but a larger observation period is needed to follow this pattern.

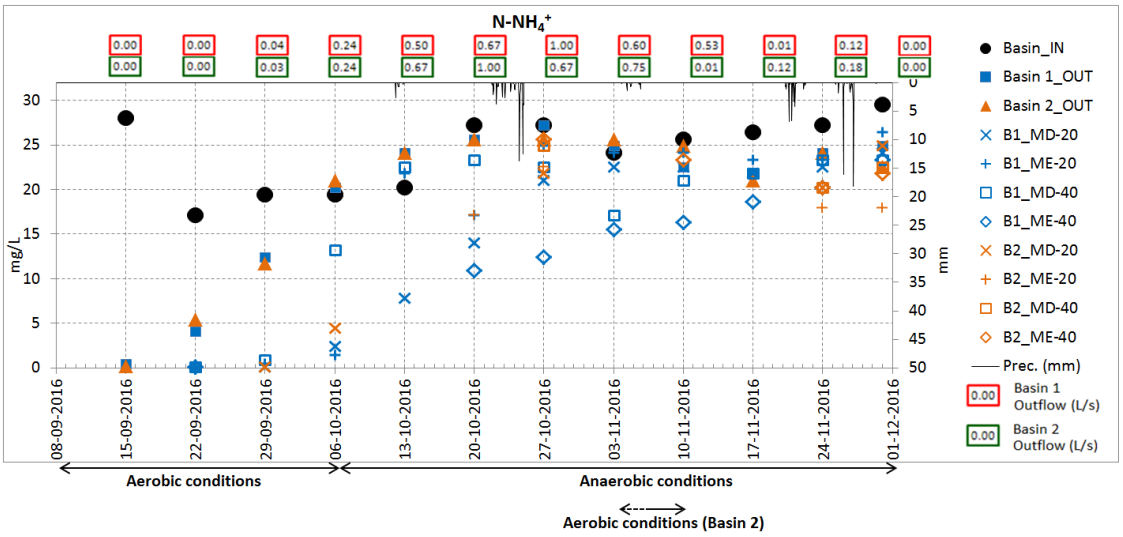

Figure 96 – Ammonia concentration in water samples obtained during SAT basin experiments

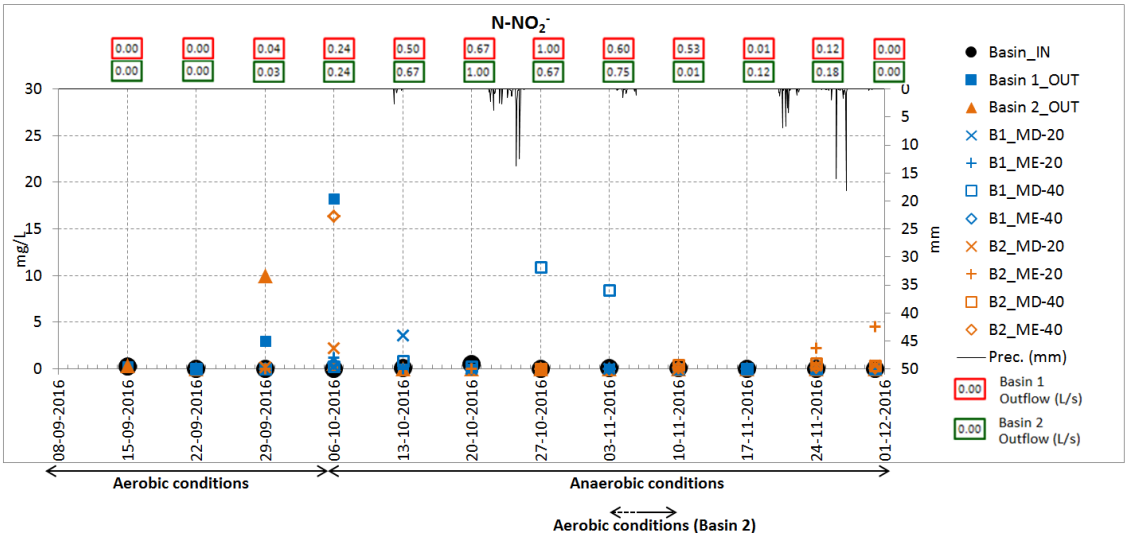

Figure 97 – Nitrite concentration in water samples obtained during SAT basin experiments

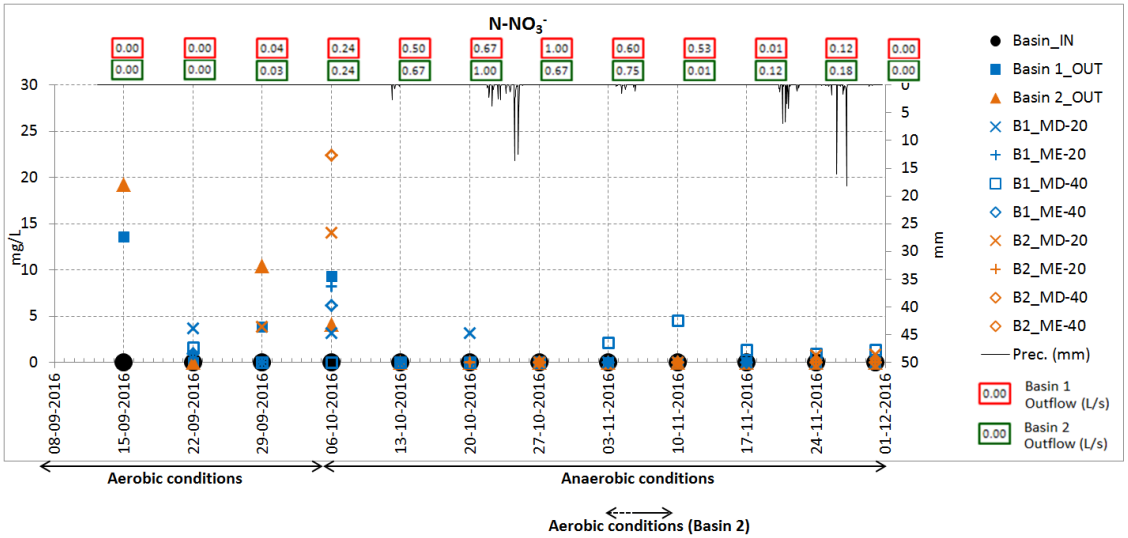

Figure 98 – Nitrate concentration in water samples obtained during SAT basin experiments

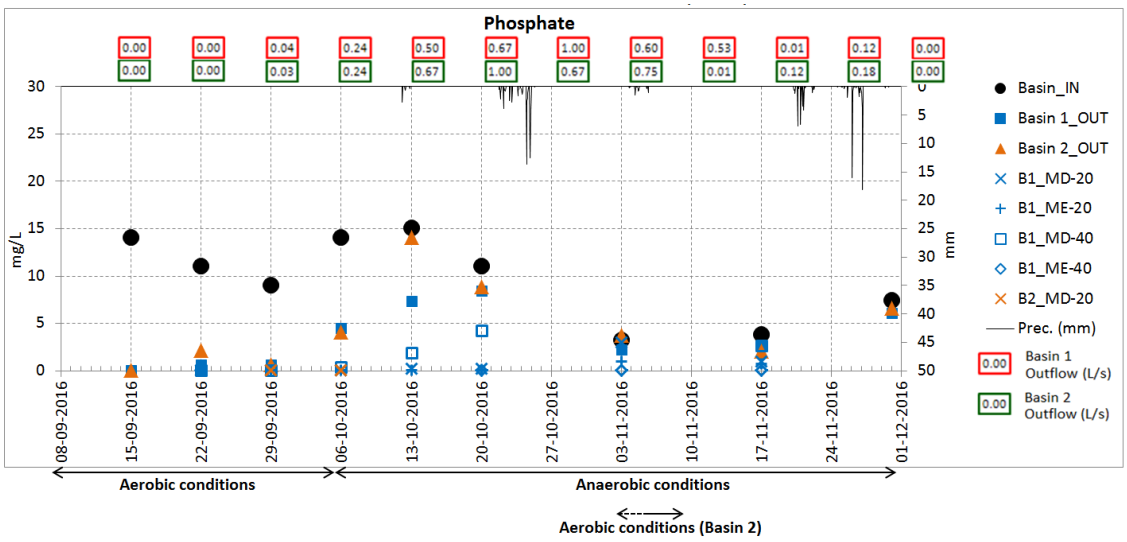

Figure 99 – Phosphate concentration in water samples obtained during SAT basin experiments

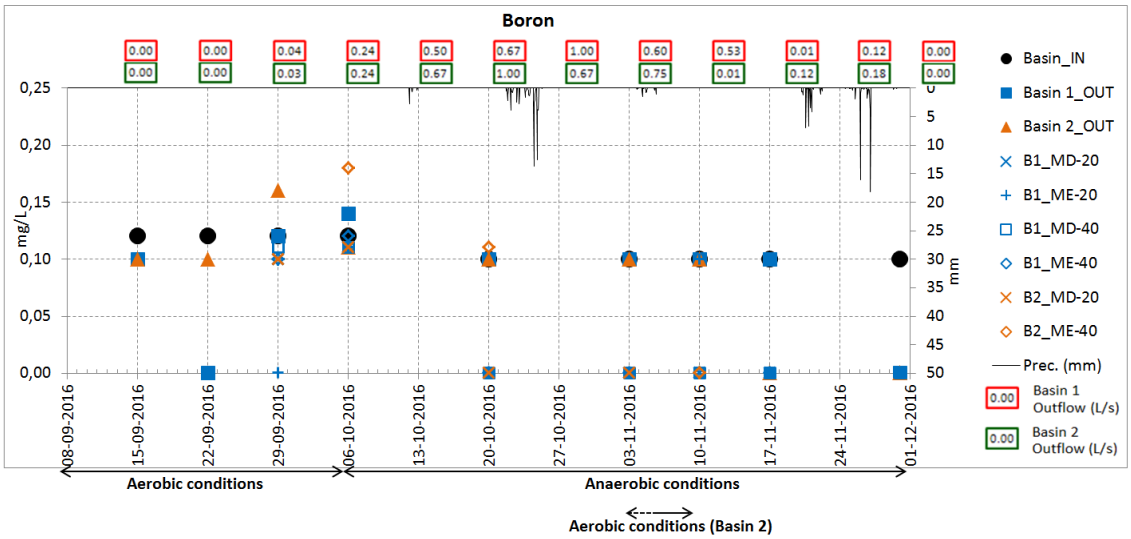

Figure 100 – Boron concentration in water samples obtained during SAT basin experiments

Pharmaceutical compounds and organic matter

During 2.5 months, from September 15th to November 30th, 2016, 24 pharmaceutical compounds (PhCs) were monitored in SAT inflow and outflow, once in the late phase of the aerobic phase, and twice (for Basin 1 outflow) or three times (for Basin 2 outflow) during the anaerobic phase. Turbidity and dissolved organic matter were also monitored on a weekly basis – Figure 101 for Basin 1 and Figure 102 for Basin 2. Both basins showed similar performance regarding the bulk parameters analysed.

Turbidity was measured to evaluate the SAT soil capacity to retain particles, including non settleable fines, which relates with soil compaction. The results showed that, after October 27th, the SAT soil compaction was enough to retain some particles, since basins outflow consistently presented lower turbidity values than the basin inflow (Figure 101 and Figure 102).

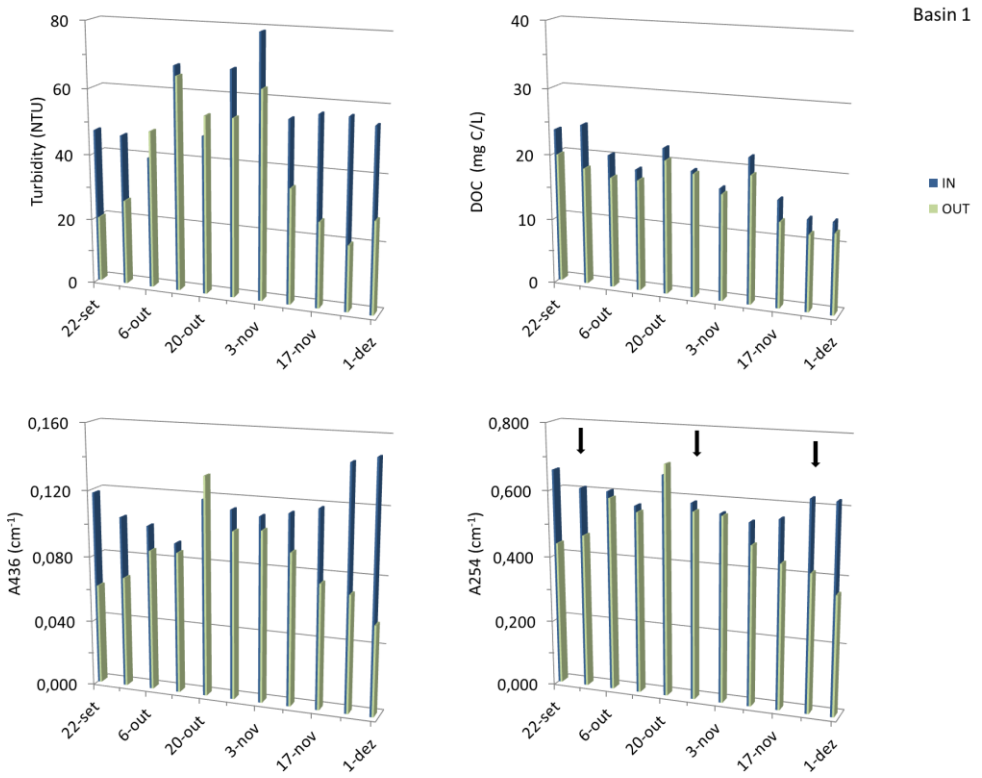

Figure 101 – Turbidity, DOC, A436 and A254 at the Basin 1 inflow (IN) and outflow (OUT)
(arrows in A245 chart indicate sampling days for PhCs; Oct. 6th transition from aerobic to anaerobic conditions)

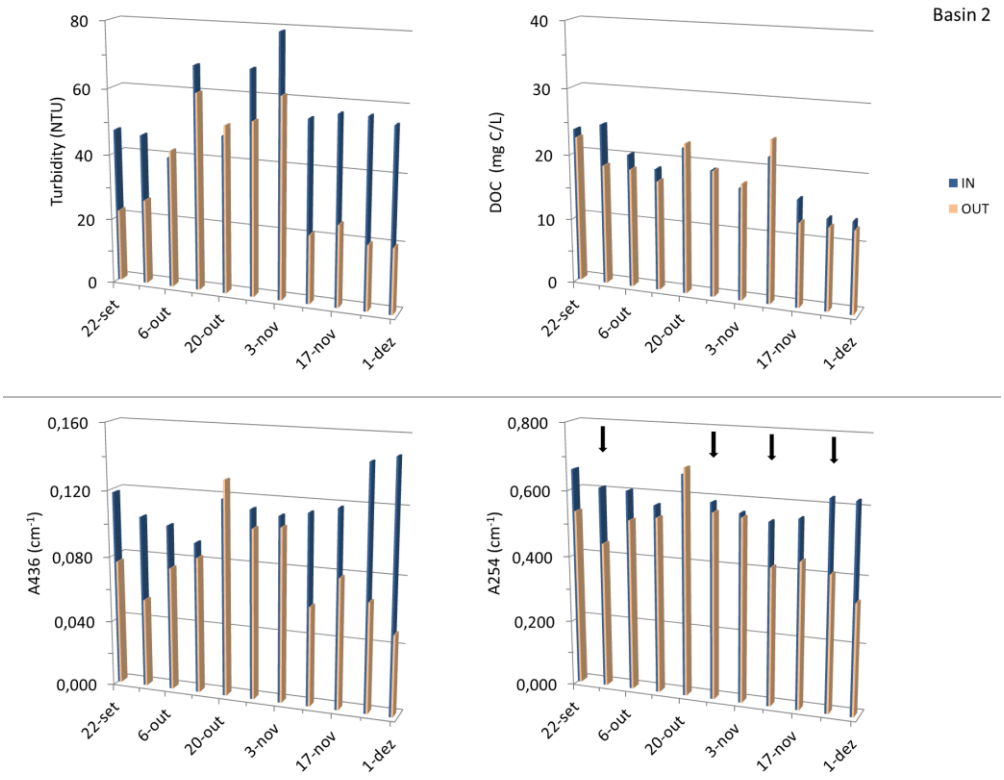

Figure 102 – Turbidity, DOC, A436 and A254 at the Basin 2 inflow (IN) and outflow (OUT)
(arrows in A245 chart indicate sampling days for PhCs; Oct. 6th transition from aerobic to anaerobic conditions)

The dissolved organic matter was analysed as dissolved organic carbon (DOC), absorbance at 254 nm (A254), representing organic matter with aromatic character and/or double C-C bonds, and as absorbance at 436 nm (A436) - representing colour.

DOC concentration at the basin inflow varied between 14 and 25 mg C/L and the basins outflow showed lower concentrations corresponding, however, to a not very expressive decrease (up to 23%). Nevertheless, removal rates of colour (A436) and organic matter (A254) were considerable (63%-67% for A436; up to 42%-46% for A254) – Figure 101 and Figure 102.

The removals (computable as 1-Cin/Cout) observed in the beginning of the test (first 3-4 weeks) are attributed mainly to sorption processes – the observed decrease over time is consistent with soil saturation. Aerobic biodegradation should have also occurred but to a lower extent compared with sorption. Organic matter removals were not expressive during the following four weeks (October 13th to November 3rd). This period corresponded to the soil microbiota adaptation to the existing anaerobic conditions, and hence with low biological activity. After November 1st, increasing removals of organic matter were observed. This was probably due to the biodegradation associated to the increased anaerobic microbial activity. Identical behaviour is foreseen for the pharmaceutical compounds removal.

Regarding the PhCs (Figure 103 to Figure 113), only eleven out of the 24 compounds analysed were quantified in the Basin_IN water samples (Table 19). Ten of these PhCs were at concentrations below 0.2 µg/L, whereas for carbamazepine the concentration was much higher (0.7-0.8 µg/L), which is consistent with its recalcitrant behaviour towards the conventional wastewater treatment.

Table 19 – Pharmaceutical compounds (PhCs) analysed and quantified (x) in the Basin_IN water samples

PhCs analysed	PhCs quantified	PhCs analysed	PhCs quantified
Atenolol	X	Gemfibrozil	X
Betaxolol		Ibuprofen	X
Bisoprolol	X	Indometacin	
Metoprolol	X	Ketoprofen	
Pindolol		Naproxen	X
Propanolol	X	Carbamazepine	X
Sotalol	X	Diazepam	
Acetylsalicylic acid		Etofibrate	
Bezafibrate		Fenofibrate	
Clofibric acid		Pentoxifylline	
Diclofenac	X	Phenacetin	
Fenoprofen		Phenazone	X

Almost all PhCs were attenuated by the SAT basins (Figure 103 to Figure 113; trend not observable for those in very low concentrations). The concentration of diclofenac, metoprolol, propranolol, sotalol, atenolol and ibuprofen at basins outflow were always lower than at the inflow, and the same occurred for carbamazepine, a particularly important results due to its higher content and

recalcitrance through WWTP. The observed PhC removals should have occurred mainly in the soil zone (not at SAT basin water column) by sorption and/or biodegradation processes. As discussed for the dissolved organic matter, in the first weeks of testing, the removal may have occurred mainly by sorption processes through the soil and afterwards by biodegradation under anaerobic conditions. For instance, diclofenac and phenazone have been described as biodegradable in oxic and anoxic conditions (Vilanova *et al.*, 2015). The PhC removal rates depend on their physic-chemical properties, namely their hydrophobic character and electric charge for sorption processes, and biodegradability for biodegradation processes.

In the soil samples collected in November 30th 2016, at 0 – 5 cm and 5 – 25 cm, no pharmaceutical compounds were found, confirming that biodegradation is the dominant process. Most limits of recovery were between 5 and 10 µg/L.

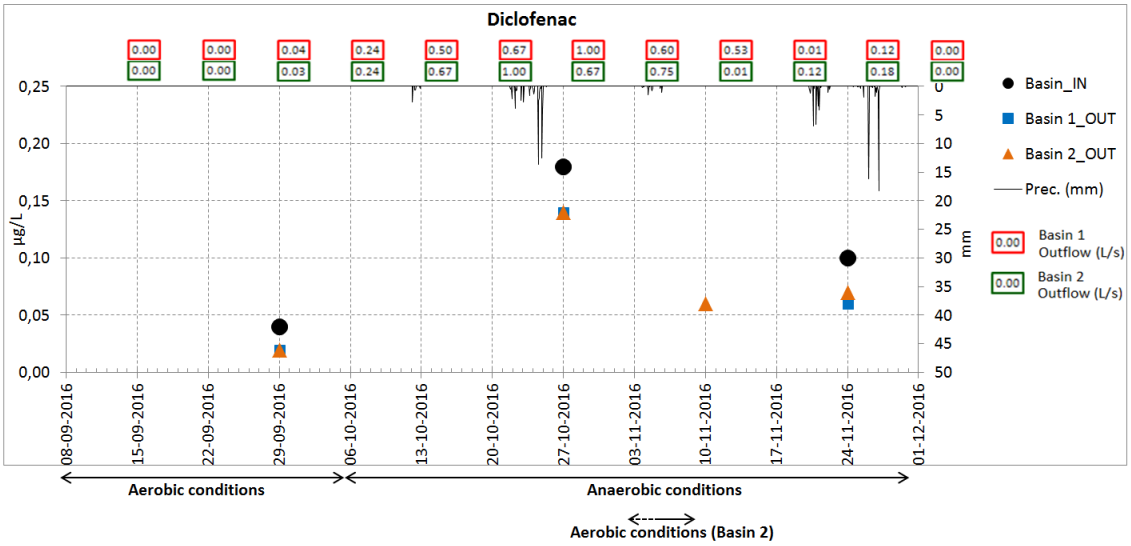

Figure 103 – Diclofenac concentration in water samples obtained during SAT basin experiments

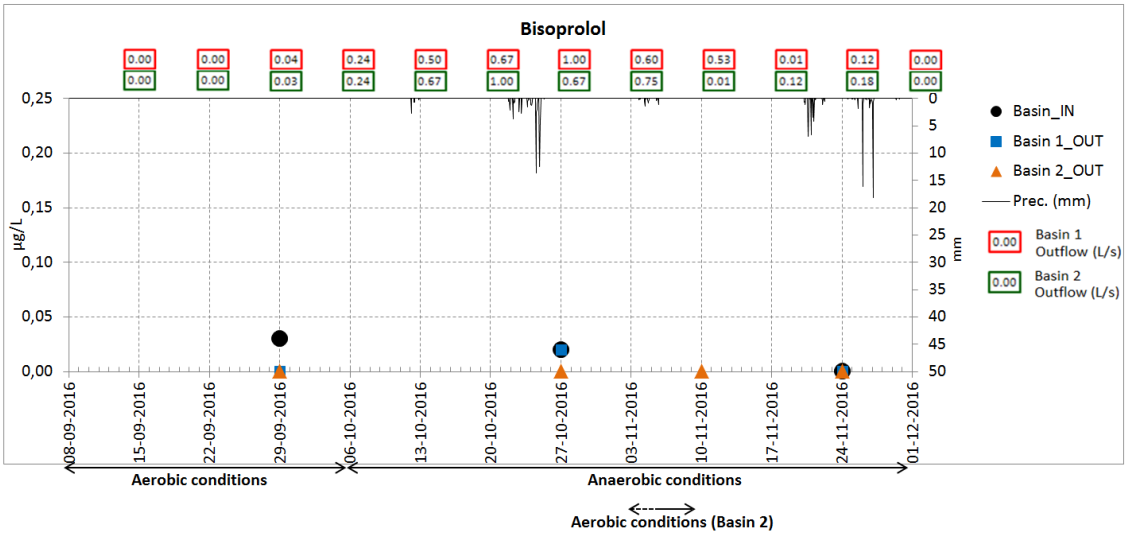

Figure 104 – Bisoprolol concentration in water samples obtained during SAT basin experiments

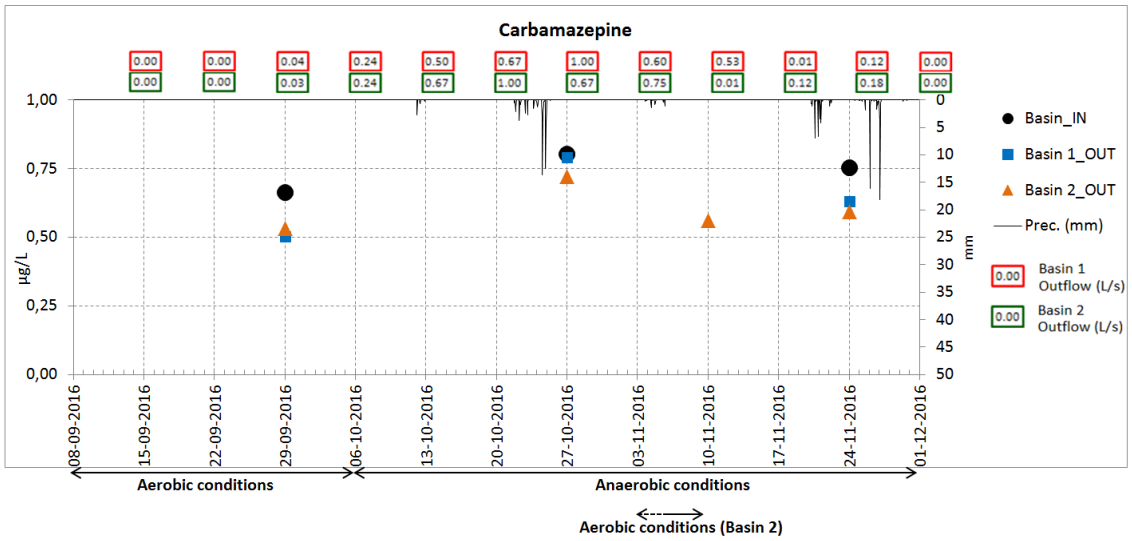

Figure 105 – Carbamazepine concentration in water samples obtained during SAT basin experiments

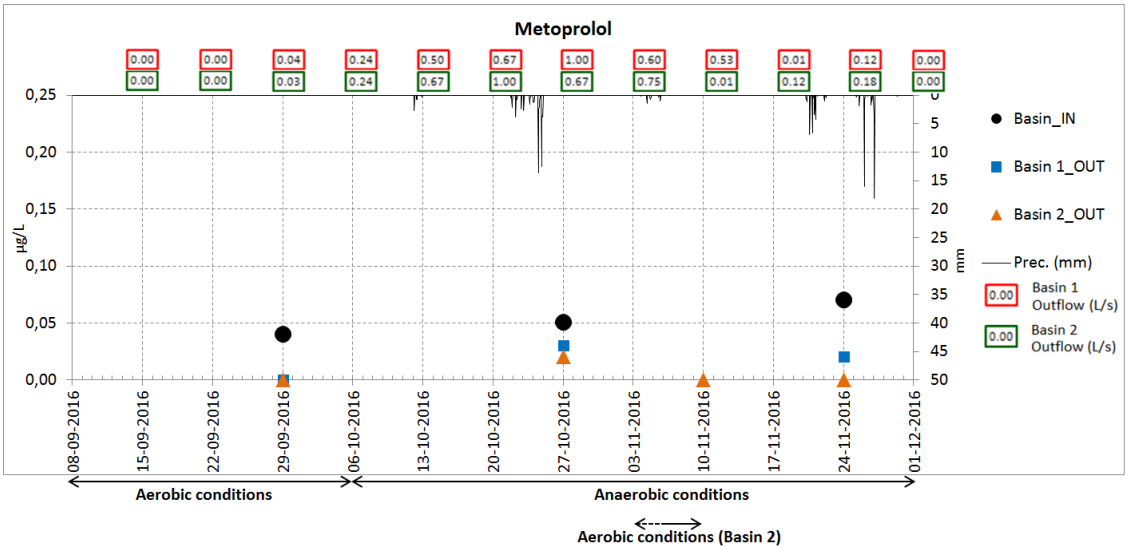

Figure 106 – Metoprolol concentration in water samples obtained during SAT basin experiments

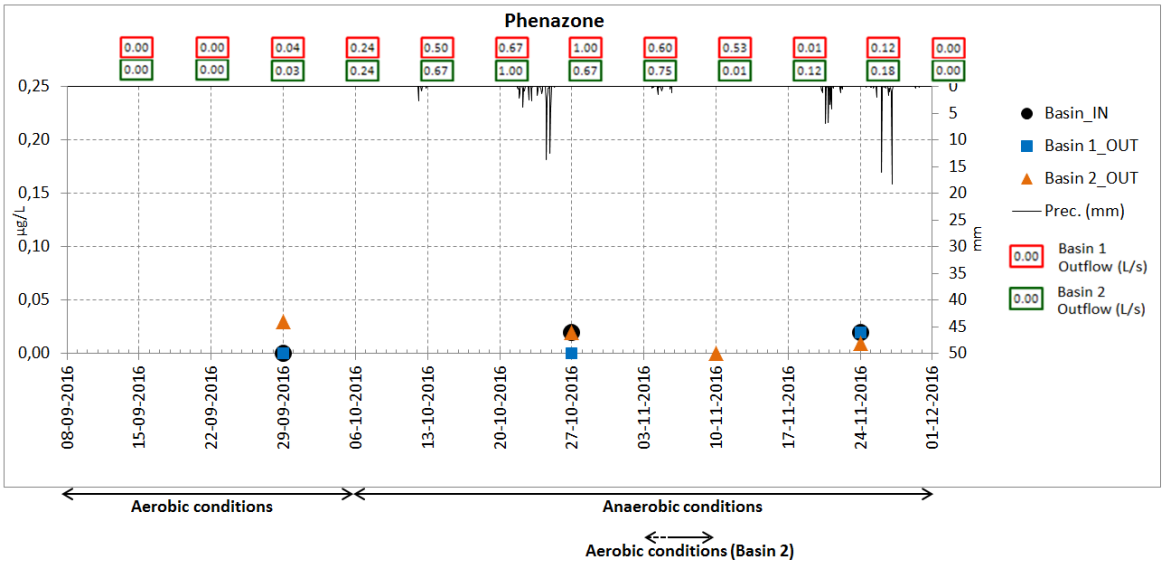

Figure 107 – Phenazone concentration in water samples obtained during SAT basin experiments

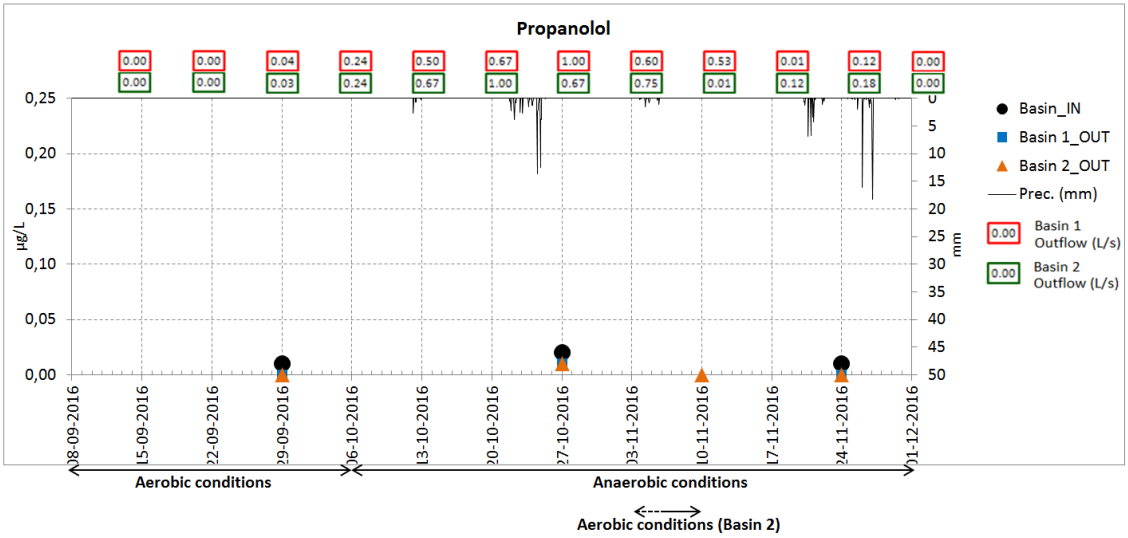

Figure 108 – Propanolol concentration in water samples obtained during SAT basin experiments

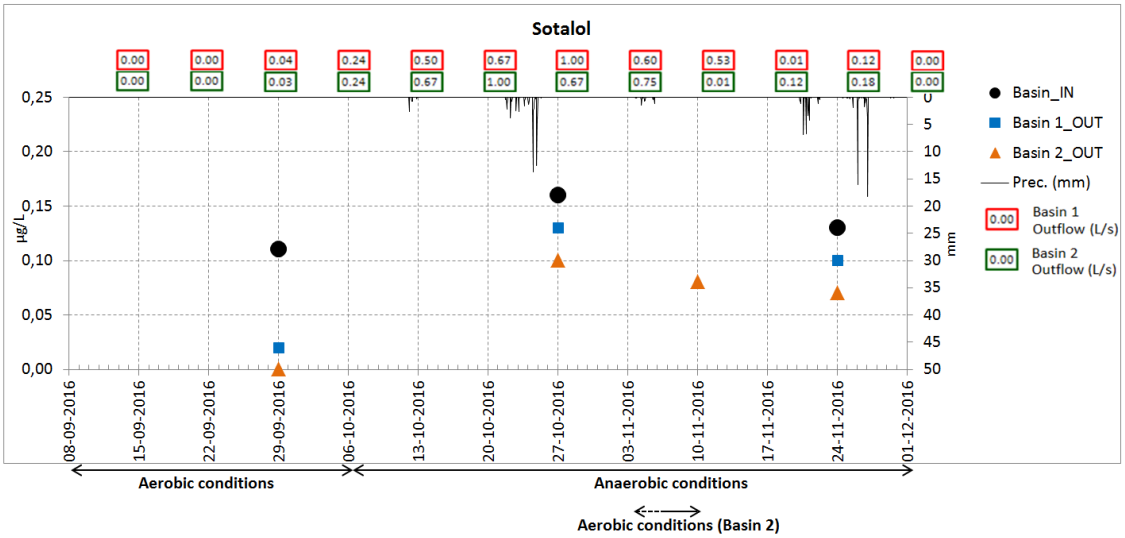

Figure 109 – Sotalol concentration in water samples obtained during SAT basin experiments

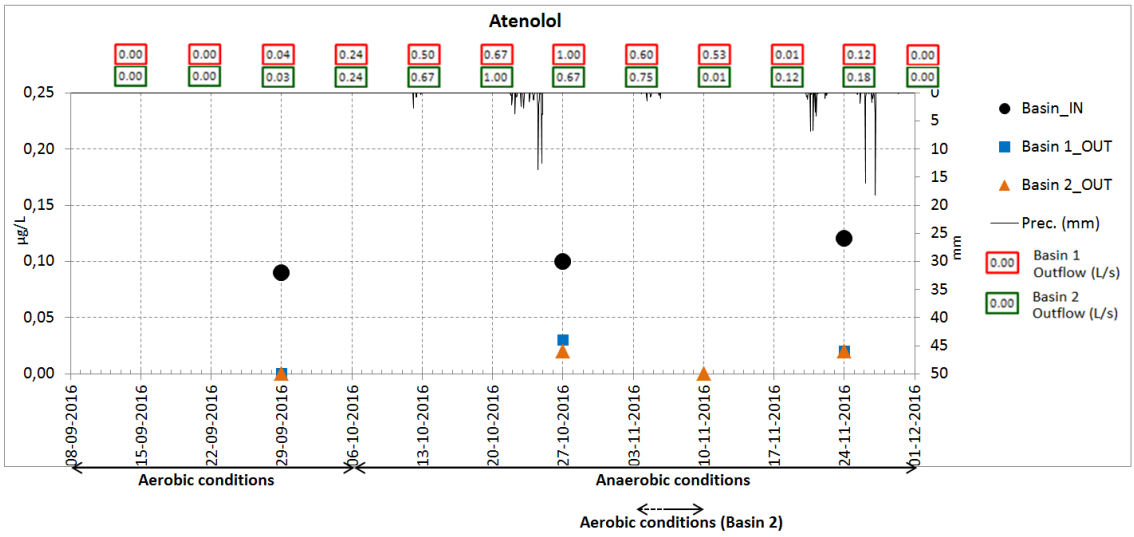

Figure 110 – Atenolol concentration in water samples obtained during SAT basin experiments

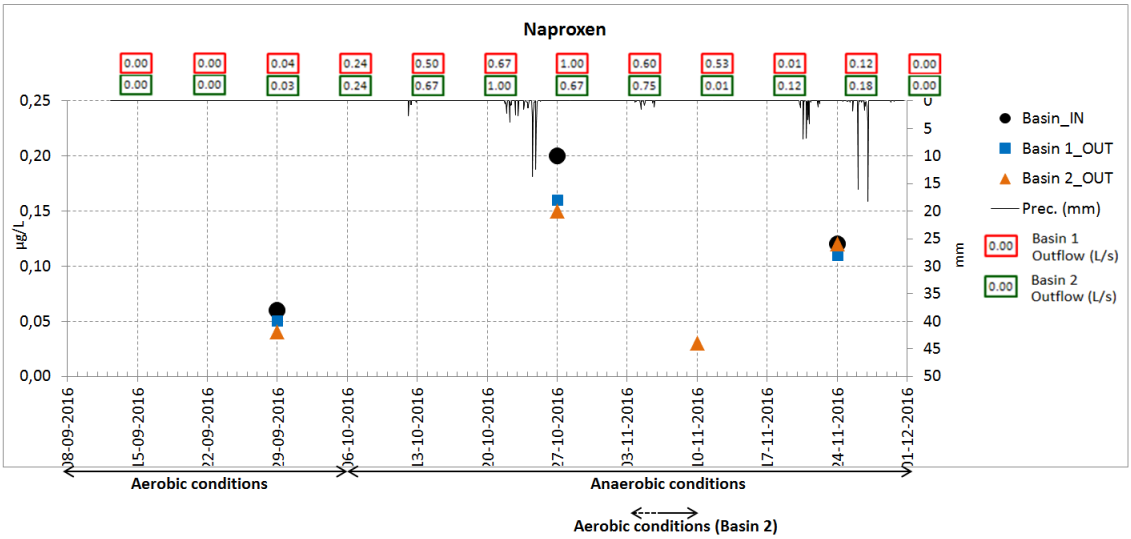

Figure 111 – Naproxen concentration in water samples obtained during SAT basin experiments

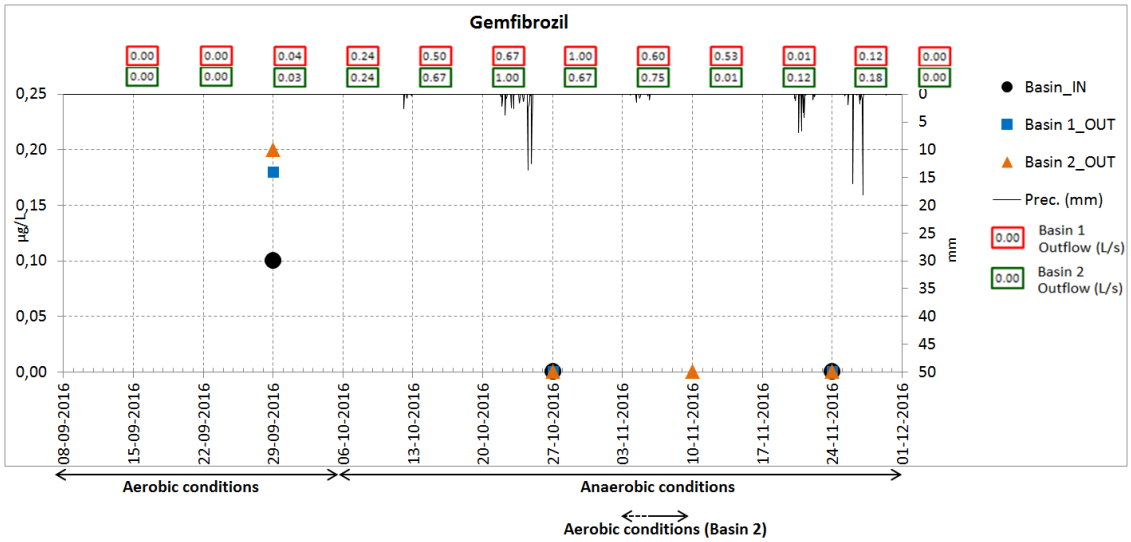

Figure 112 – Gemfibrozil concentration in water samples obtained during SAT basin experiments

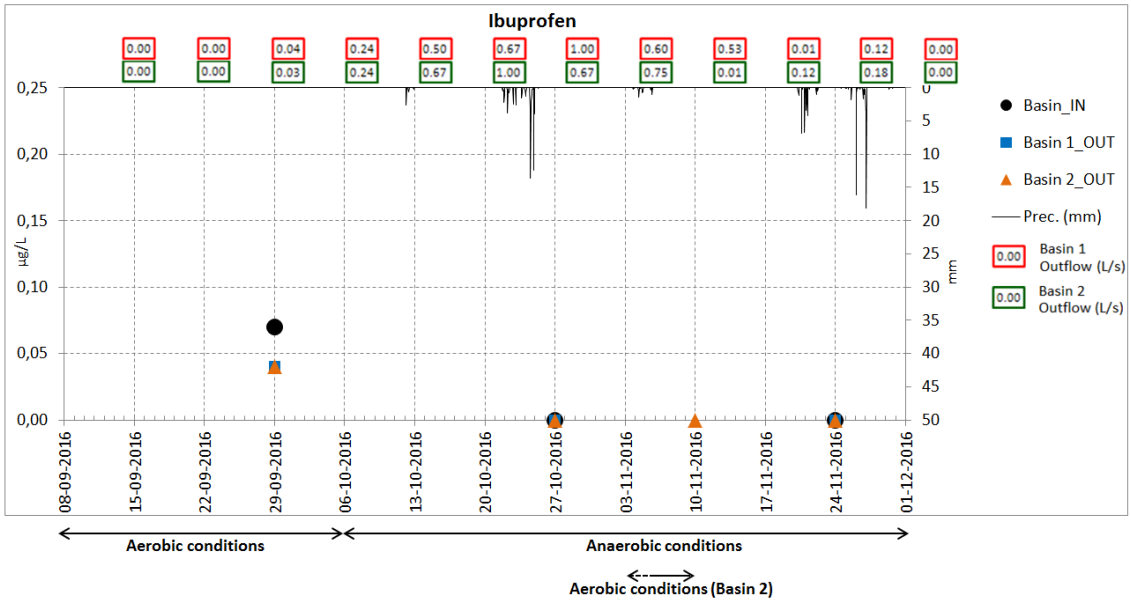

Figure 113 – Ibuprofen concentration in water samples obtained during SAT basin experiments

SAT systems at SB Messines WWTP have shown very interesting ability to remove or minimize several types of contaminants, particularly pharmaceuticals, nitrogenous compounds, suspended solids, as well as phosphates and possibly metals. Besides the quality of the infiltrated water, the performance of these systems also depend on a number of factors, namely the soil layers permeability and the hydraulic load, both determining the time for soil-water equilibrium, as well as the soil mineralogy, organic matter content, pH and redox conditions and microbial activity, all determining the biodegradation and sorption processes.

PT2_6: Cerro do Bardo Infiltration test, April 1st, 2014

Test description

In order to obtain early estimates for the well infiltration rates capacity, an infiltration test with 40,000 L of water was performed on the large diameter well at Cerro do Bardo. The well's characteristics are synthetized in Table 11.

The water for injection was provided by the Municipal Fire-fighters from the city of Silves - *Bombeiros Voluntários de Silves* - with two fire trucks containers of 20,000 L each (Figure 114). The injection rate was 125.20 m^3/h (40 m^3 water injection during a period of approximately 19 minutes) and the groundwater level displacement reached a maximum of 6.38 m in CB well. Water displacement was recorded both manually and with a CTD-Diver (with 5 seconds interval between records) for both the injection and recovery period. Besides the automatic divers, manual records of the water level were taken during injection and recovery period.

Figure 114 – Infiltration test at PT2_6 Cerro do Bardo large well with the support of Silves fire-fighters

Table 20 presents the synthetized characteristics of the injection test.

Table 20 – Injection characteristics

Injected volume (m^3)	40.00
Time of injection (min)	19.26
Injection flow rate (m^3/min)	2.09
Injection flow rate (m^3/h)	125.20
Maximum water displacement (m)	6.38

Methodology for determining injection period volumes and rates

In order to calculate the injection volume and rates the problem was divided in two sections, the injection period and the recovery (or falling-head) period. The injection period consists of the time interval during which water was injected into the well, hence, verifying a water level rate rise in the

well, which depends on the infiltration and injection rate. The recovery period consists of the time after the interruption of the injection flow, in which a water level drop in the well occurs as a consequence of the infiltration.

During the injection period, infiltration rate was calculated based on the observed water displacement and the theoretical water displacement. Considering the well as an impervious volume, and the hydrostatic level at the beginning of the injection period, the total theoretical water level rise for a given time period is calculated according to the following equation (Equation (6)):

$$\textbf{(6)}\quad hc_t = \frac{Va_t}{A}$$

Where:

- hc_t stands for a theoretical water level displacement considering the well as an impervious recipient for a given time period (L);
- Va_t stands for the injected volume of water in the well for a given time period (L^3);
- A stands for the well's surface area (L^2).

In other words, this would be the total water level displacement, in case no infiltration would occur and the well would behave as an impervious recipient. For a given period of time, the observed water level rise in the well multiplied by the area of the well would consist of the well bore storage, and the difference between the theoretical and observed water level provides the infiltrated column of water $(hc_t - h_t)$. Hence, during the injection period, the volume of water infiltrated for a given time period (Vi_i) is calculated by multiplying the area of the well by the difference of the injected column of water between the considered time period (Equation (7)).

$$\textbf{(7)}\quad Vi_i = \left[(hc_{t0} - h_{t0}) - \left(hc_{tf} - h_{tf}\right)\right] \times A$$

where:

- Vi_i stands for infiltrated volume of water during the injection period for a given time period (L^3);
- hc_{t0} and hc_{t1} stands for the theoretical water level at the beginning and ending of the time period considered (calculated assuming a constant injection flow of 125.20 m^3/h, multiplied by the time interval and divided by the well's area) (L);
- h_{t0} and h_{t1} stands for the observed water level for at the beginning and ending of the time period considered (L);
- A stands for the well's area (L^2).

According to the previous considerations, the infiltration rate at a given time for the injection period can be estimated as in equation (8):

$$\textbf{(8)}\quad Ii_t = \frac{Vi_i}{\Delta t \times A}$$

where:

- Ii_t stands for infiltration rate for a given time interval Δt in the injection period (L/T);

- Vi_i stands for infiltrated volume of water during the injection period for a given time period (L^3);
- Δt stands for the time interval for which infiltration is to be calculated (T);
- A stands for the well's area (L^2).

Methodology for determining recovery period volumes and rates

During the recovery period, infiltration volume is estimated based solely on the observed piezometric level decrease for a given period of time (after injection was interrupted) multiplied by the well's surface area as can be seen on equation (9):

$$\textbf{(9)}\quad Vr_i = (h_{tf} - h_{t0}) \times A$$

where:

- Vr_i stands for infiltrated volume of water during the recovery period for a given time period (L^3);
- h_{t0} and h_{tf} stands for the observed water level for at the beginning and ending of the time period considered(L);
- A stands for Area (L^2).

As for infiltration rate, it is calculated by dividing the observed water level decrease in a given time period, by the time period (equation (10)):

$$\textbf{(10)}\qquad Ir_t = \frac{Vr_i}{\Delta t \times A}$$

where:

- Ir_t stands infiltration rate for a given time interval Δt in the recovery period ($L \cdot T^{-1}$);
- Vr_i stands for infiltrated volume of water during the recovery period for a given time period (L^3);
- Δt stands for the time interval for which infiltration is to be calculated (T);
- A stands for the well's surface Area (L^2).

In this case, the well's surface area is 3.14 m^2.

Results

Infiltration rates were estimated based on the water level displacement records in the well, considering both the injection and the recovery periods. Figure 115 shows the water displacement measured manually and with the automatic diver in function of time for the injection and recovery periods. Also, the beginning of the injection period and recovery periods are indicated in the same figure. Time 0 matches the 40 m^3 water injection period, which lasted for 19.26 minutes, corresponding to a flow rate of 125.20 m^3/h or 34.8 L/s. The automatic diver was withdrawn from the well at 441.92 minutes (approx. 7 hours) after the beginning of the injection.

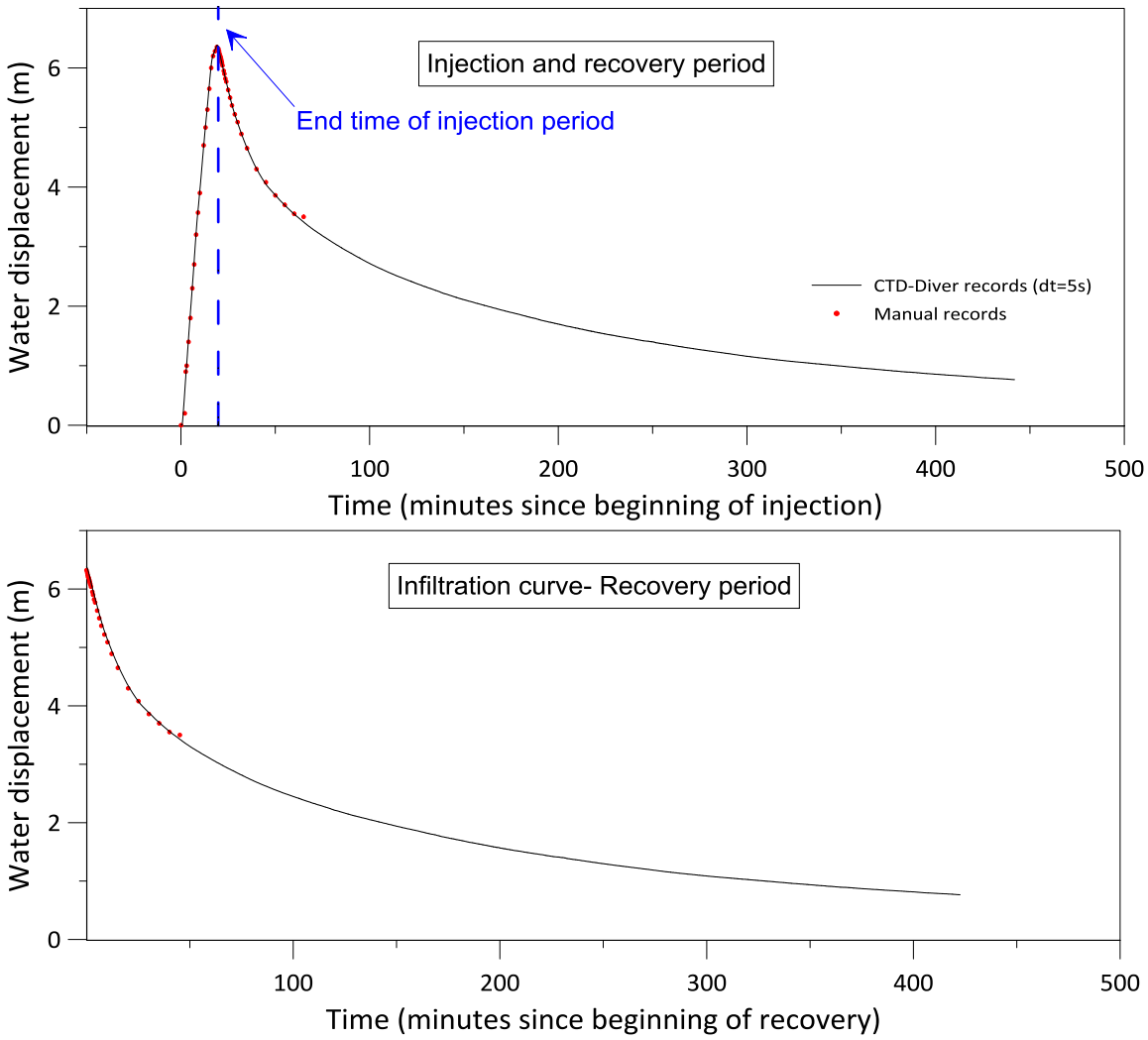

Figure 115 – Manual and CTD records for water displacement in the well as a function of time, since the beginning of the injection test. Top: Water displacement time for both the injection and recovery period. Bottom: infiltration curve for the recovery period in detail

The infiltration rate was estimated based on the water displacement verified in both the injection and recovery periods.

Based on the above mentioned equations, infiltration rates and volumes were estimated for several time periods, in particular for: a) the entire injection period; b) the entire recovery period; c1) for the first 30 minutes of the recovery period decomposed over a 1 minute increment discretization; c2) for the last 10 minutes of the recovery period decomposed over a 1 minute increment discretization; and d) for the first 7 hours of the recovery period (until the diver was withdrawn from the well) decomposed over a 1 hour increment discretization. These results are synthetized in Table 21.

Table 21 – Synthesis of the parameters measured and calculated during the injection and recovery period of the infiltration test

Infiltration Test stage	t_0 (min)	t_f (min)	h_0 (m)	h_f (m)	Δh (m)	Δt (min)	Va - Injected volume (m^3)	Injected volume to fill the well (m^3)	Vi - infiltrated volume (m^3)	I - Infiltration rate (m/day)
a) Injection	0	19.17	0	6.38	6.38	19.17	40	20.04	19.96	477.33
b) Recovery	19.25	441.83	6.38	0.77	5.61	422.6	0	0	17.63	19.12
c1) Recovery period decomposed over 1 minute increment for the first 30 minutes	0	1	6.38	6.29	0.09	1	0	0	0.29	131.04
	1	2	6.29	6.14	0.15	1	0	0	0.46	211.68
	2	3	6.14	6.00	0.14	1	0	0	0.45	204.48
	3	4	6.00	5.86	0.13	1	0	0	0.42	192.96
	4	5	5.86	5.73	0.14	1	0	0	0.42	194.40
	5	6	5.73	5.60	0.13	1	0	0	0.41	187.20
	6	7	5.60	5.47	0.13	1	0	0	0.40	181.44
	7	8	5.47	5.35	0.12	1	0	0	0.38	175.68
	8	9	5.35	5.25	0.10	1	0	0	0.33	149.76
	9	10	5.25	5.15	0.10	1	0	0	0.31	141.12
	10	11	5.15	5.06	0.09	1	0	0	0.29	132.48
	11	12	5.06	4.97	0.09	1	0	0	0.29	132.48
	12	13	4.97	4.88	0.09	1	0	0	0.27	125.28
	13	14	4.88	4.79	0.09	1	0	0	0.27	125.28
	14	15	4.79	4.71	0.08	1	0	0	0.25	115.20
	15	16	4.71	4.63	0.08	1	0	0	0.25	112.32
	16	17	4.63	4.56	0.07	1	0	0	0.23	103.68
	17	18	4.56	4.49	0.07	1	0	0	0.22	102.24
	18	19	4.49	4.42	0.07	1	0	0	0.22	99.36
	19	20	4.42	4.36	0.07	1	0	0	0.21	95.04
	20	21	4.36	4.29	0.06	1	0	0	0.19	87.84
	21	22	4.29	4.24	0.06	1	0	0	0.18	80.64
	22	23	4.24	4.18	0.06	1	0	0	0.18	80.64
	23	24	4.18	4.13	0.05	1	0	0	0.16	74.88
	24	25	4.13	4.08	0.05	1	0	0	0.15	69.12
	25	26	4.08	4.04	0.05	1	0	0	0.15	67.68
	26	27	4.04	4.00	0.04	1	0	0	0.12	56.16
	27	28	4.00	3.96	0.03	1	0	0	0.11	48.96
	28	29	3.96	3.92	0.04	1	0	0	0.12	54.72
	29	30	3.92	3.89	0.03	1	0	0	0.11	48.96
c2) Recovery period decomposed over 1 minute increment for the last 10 minutes	412	413	0.788	0.786	0.002	1	0	0	0.006	2.88
	413	414	0.786	0.783	0.003	1	0	0	0.009	4.32
	414	415	0.783	0.782	0.001	1	0	0	0.003	1.44
	415	416	0.782	0.781	0.001	1	0	0	0.003	1.44
	416	417	0.781	0.78	0.001	1	0	0	0.003	1.44
	417	418	0.78	0.777	0.003	1	0	0	0.009	4.32
	418	419	0.777	0.773	0.004	1	0	0	0.013	5.76
	419	420	0.773	0.772	0.001	1	0	0	0.003	1.44
	420	421	0.772	0.769	0.003	1	0	0	0.009	4.32
	421	422	0.769	0.768	0.001	1	0	0	0.003	1.44
d) Recovery period decomposed over 1 hour increments for 7 hours	0	60	6.38	3.09	3.28	60	0	0	10.32	78.82
	60	120	3.09	2.21	0.88	60	0	0	2.77	21.17
	120	180	2.21	1.70	0.51	60	0	0	1.60	12.22
	180	240	1.70	1.35	0.36	60	0	0	1.12	8.52
	240	300	1.35	1.09	0.26	60	0	0	0.82	6.26
	300	360	1.09	0.91	0.18	60	0	0	0.56	4.30
	360	420	0.91	0.77	0.14	60	0	0	0.43	3.26

- t_0 and t_f (min) – Initial and final time respectively for a given time period;
- h_0 and h_f (m) – initial and final water level displacement respectively for a given time period;

- Δh (m) – Difference between initial and final water level displacement for a given time period;
- Δt (min) – time interval for a given period;
- Va (m^3) – Injected volume of water in the well for a given time period;
- Vs (m^3) – injected volume of water to fill the well, which is stored at the well for a given time period;
- Vi (m^3) – Infiltrated volume of water that has infiltrated for a given time period (Vi = Va – Vs);
- I – Infiltration rate calculated for a given time period.

Estimated infiltration rates for the injection (after the well is filled) and the recovery period are 477.33 and 19.12 m/d. The values indicated for the injection period need to be analysed with caution, since, not only a high flow rate of injection was used, but also a steady state of the injection (i.e. stabilization of the water level displacement) was not achieved. In this case, the infiltration during this period is a rough estimate that may indicate misleading information on the wells infiltration capacity.

The recovery period, or falling-head period, infiltration rate estimates provides an average value of 19.12 m/d, which is indicative of a high infiltration capacity in this system. The decomposition of the recovery period into smaller time period increments (1 minute and 1 hour increment), visible in Figure 116, shows an accentuate decrease on the infiltration rate with time, with higher values in the early stage of the recovery period (211.68 m/d) exponentially decreasing to 1.44 m/d in the last measurements (see Table 21).

The above mentioned exponential decay on the infiltration rate observed in the recovery period could be related with the hydraulic load in the well (i.e. the water level elevation compared to the hydrostatic water level in the beginning of the injection test).

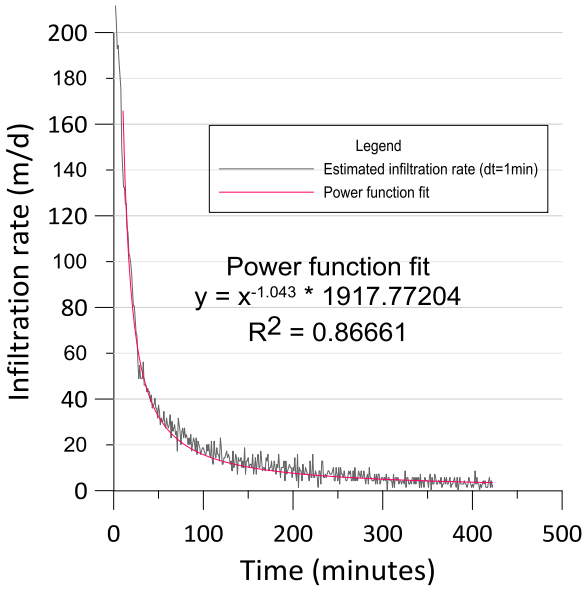

Figure 116 – Estimated infiltration rate during the recovery period for a 1-minute increment step time and the calculated power function fit

The scatter plot between the hydraulic head and the infiltration rate, shown in Figure 117, indicates a positive correlation between the hydraulic load and the injection rate, as expected. Two different stages can be evidenced in this relation, the first one, by lower hydraulic load and the second, for

higher hydraulic loads. In Figure 117a, a polynomial 5th degree fit is found with a squared R value of 0.9913, which, for the observed hydraulic load, presents a good fit with the estimated infiltration rate.

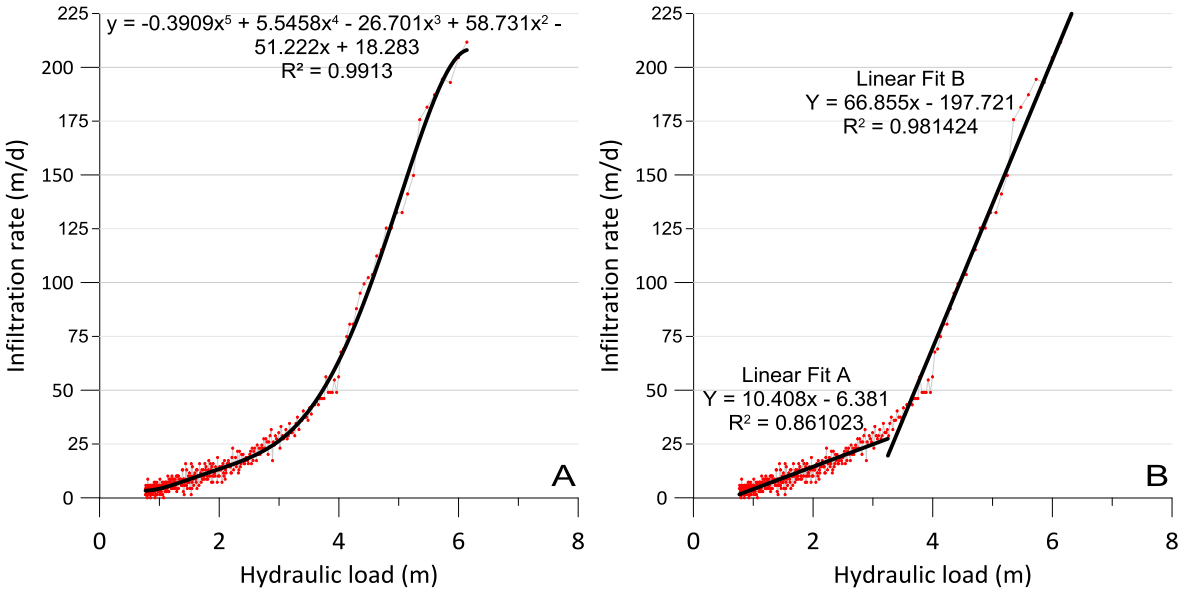

Figure 117 – Scatter plot between hydraulic load and infiltration rate and A: 5th degree polynomial fit; B: Linear fits A and B

The presented equation on the polynomial fit may be used to estimate the infiltration rate as a function of the hydraulic load in the well for future injection tests, assuming there is no clogging effect. Figure 117 b divides the two stages in two linear fits, A and B. The first stage represented by linear fit A, covers hydraulic loads up 3.25 m and the second stage, represented by linear fit B, covers hydraulic loads higher than 3.25 m. These stages can be associated to a double porosity system, wellbore storage or differences in layers permeability or even well skin effects.

In this case, estimating infiltration rate based on a specific hydraulic load in the well would be a more suitable approach. Being so, for hydraulic loads up to 3 m, infiltration rates are expected to be lower than 25 m/d (linear fit A). For loads higher than 3 m, there is a much higher increase on the infiltration rate, with a maximum of 211 m/d, for a hydraulic load of 6.29 m.

PT2_6: Cerro do Bardo tracer test, December 15-16th, 2014

Test description

Based on the results of the previous test, the adequacy of Cerro do Bardo area for MAR was evidenced and a big MAR test was envisaged. To perform this large scale test new monitoring devices (piezometers) had to be constructed. However, a major unknown had to be removed: the groundwater flow direction in the test site.

To answer to this question, a water recharge test was performed with the injection of 250 kg of NaCl salt tracer (in the second day) in CB well, and a time-lapse resistivity survey was performed on three

alignments crossing each other's. Salt was selected as a tracer due to his capability to reduce water resistivity and to enhance the possibility of identifying the water circulation with the geophysical electrical resistivity method.

Methodology for determining the groundwater flowpath

A set of 3 resistivity profiles were performed using the dipole-dipole array before the water injection in the well, to have the resistivity reference pattern. After the end of water injection they were repeated in the 4 subsequent days. The objective was to have more information regarding the water pathways in the area with the time-lapse evolution of the resistivity. Due to a low variation of resistivity with time, data are being reprocessed to have a more accurate input to the outflow modelling of the injected water.

Results

Figure 118 presents a synthesis of the results obtained. Detailed information can be obtained in WP12 deliverables.

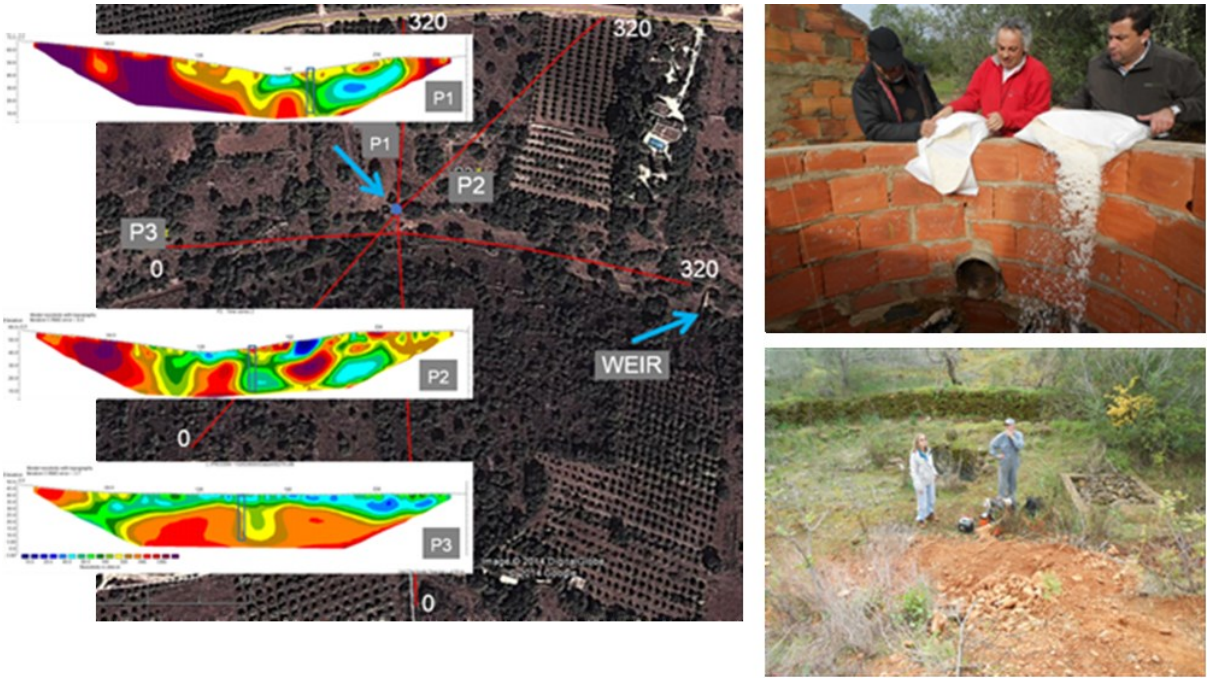

Figure 118 – Geophysical survey in Querença-Silves aquifer at Cerro do Bardo

The results obtained have shown that the natural groundwater flow path would more likely be towards east-southeaster direction. Based on this, two monitoring piezometers were built for the final MARSOL experiment at this DEMO site.

PT2_6: Cerro do Bardo tracer and infiltration large test, April 20-24th, 2016

Preparatory work: pumping test

The preparatory tasks for the development of the large scale infiltration test in Cerro do Bardo included the pumping test performed in CB2 (Figure 119). The test was performed during 24 hours, plus 8 hours of recovery, in February 2016. This test allowed the assessment of the hydraulic characteristics of the local upper unit of Querença-Silves aquifer system. The pump test was performed with an average pumping flow of about 7 m^3/h.

The results of the pumping test clearly showed that the piezometers diameter was overestimated, as the hydraulic permeability and flows are much lower than those found in the main Querença-Silves aquifer, at higher depths. The local hydrogeologic characteristics, transmissivities where calculated with the Cooper and Jacob approach (1946), using the data from the pumping test.

Results show that, locally, the upper unit can be divided in an upper subsystem with transmissivity (T) around 7 m^2/d and a lower subsystem with transmissivities around 3 m^2/d. Considering a saturated thickness of 40 m, the subsystems permeability ranges from 0.2 m/d, in the upper subsystem, to 0.1 m/d in the lower one. These results should, however consider other interpretations, such as lateral anisotropy, the presence of a boundary condition or to the reduction of the saturated thickness, rather than vertical anisotropy.

Nevertheless these permeability results are much inferior to those found in the lower unit, in which the "Águas do Algarve", the biggest water user, relies for public water supply.

Figure 119 shows the results of CB2 during the pumping test from which the local transmissivity was estimated.

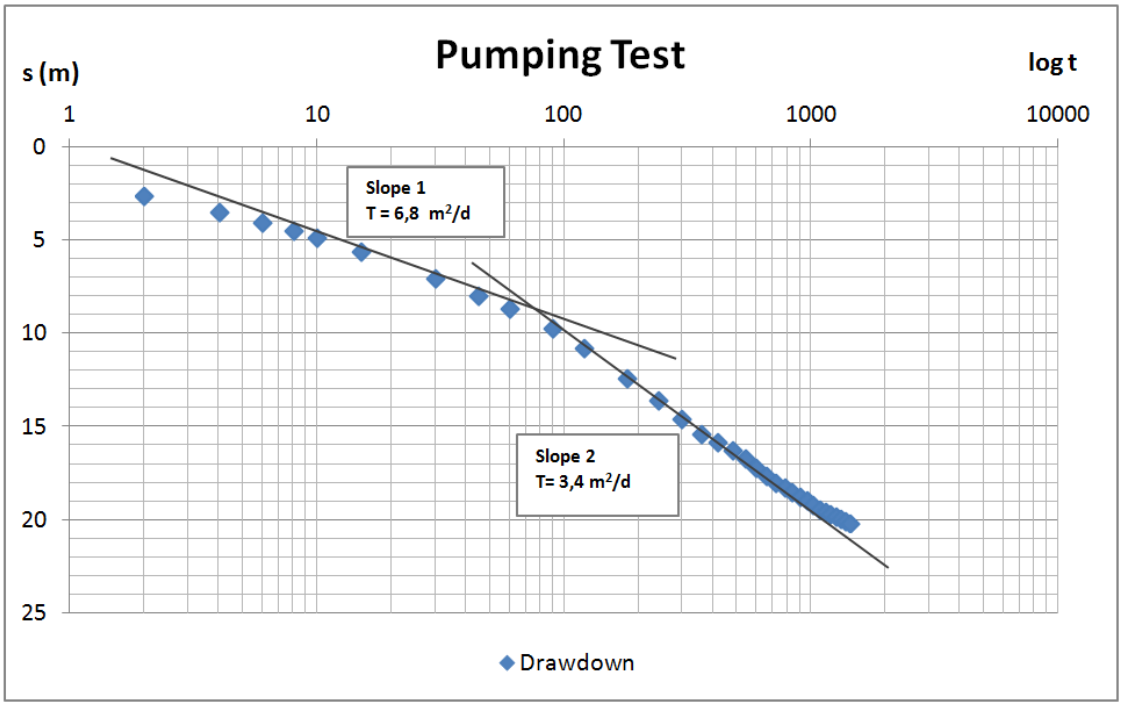

Figure 119 – Interpretation of the pumping period recorded in CB2

Table 22 summarizes the parameters used in the calculation of T and the results of the calculated permeability.

Table 22 – Parameters used in the calculation of T and the results of the calculated permeability

	Slope 1 (upper subsystem)		Slope 2 (lower subsystem)	
Recovery	Δs (m)	4.5	Δs (m)	9
	Q (m^3/d)	166.7	Q (m^3/d)	166.7
	T (m^2/d)	6.8	T (m^2/d)	3.4
	b (m)	40.0	b (m)	40.0
	K (m/d)	0.2	K (m/d)	0.1

These results are extremely relevant in terms of the MAR concept as:

- Most of the private water wells (100 meters depth) in the study area are draining the upper unit of Querença-Silves aquifer, which presents much lower permeability than those of the main Querença-Silves aquifer and main regional groundwater supplier at 200 to 300 meters dept.
- The lower permeability of the upper sector, where the recharge is to be carried out represents a higher residence time, greatly needed for seasonal storage.

Test description

Once the piezometers were built, and thus the monitoring net completed, a large infiltration and tracer test was carried out in CB well. The experiment goal was to assess the overall Cerro do Bardo MAR site infiltration capacity and confirm the main groundwater flow path.

The experiment consisted in inserting water (with a tracer) in CB well, allowing the water to overflow to the stream (through a by-pass existing inside the well at a depth of 1.95 m), until it eventually reached the weir.

The experiment *per si* took place from the 20th to the 24th of April in a total of 90 hours, plus the recovery time (1 week). The infiltration test had a flow rate of approximately 47 L/s, corresponding to a total water amount of 15228 m^3 for the whole period or 4060 m^3/day. Immediately before the start of the recharge in CB well, 1000 kg of NaCl were poured into the well. This tracer corresponds to a concentration of 10256 mg/L if divided by the volume occupied by water in the well:

(Equation (11)):

$$\mathbf{(11)} \qquad Vol_W = \pi\, r^2\, h$$

Where:

- Vol_W stands for the well volume (L^3);
- *r* stands for the well radius (L);
- h stands for the well's maximum water high (L).

Considering that the 1 m radius well has a total depth of 33 m and that the water level reached a maximum value of 1.95 m (the depth of the by-pass inside the well), the volume occupied by water was 97.5 m^3, i.e. 3.14 x (33 m – 1.95 m).

If divided by all the experiment water volume (15228 m^3 = 47 L/s x 90 hours), the tracer concentration would be 65.7 mg/L.

The water for the experiment was abstracted from a local water supply well (SJS2) belonging to Águas do Algarve SA (AdA). This well, built in 2006, was designed to support a continuous flow up to 65 L/s, with just two meters of water level drawdown. Water was thus pumped and then forwarded to CB well through a PVC pipeline along 1360 m distance with a diameter of 200 mm (Figure 120).

Figure 120 – Illustration of the work to install the 1.4 km pipeline from SJS2 well to CB well

Figure 79 shows the relative position of the monitoring net and the SJS2 well, as well as the approximate tracing of the pipeline installed to derive water up to CB well.

Table 23 summarizes the main characteristics of SJS2 and infiltration and tracer test.

The pumping system was equipped with a flowmeter at the head of the pumped well, in order to control pumped water flow. The distance between the infiltration point (CB) and the extraction point (SJS2) was sufficient to guarantee possible cross interference and therefore unreliable results. Furthermore, the water extraction was pumped from the deeper Querença-Silves aquifer, while infiltration took place in the upper unit which guarantees a supplementary security for the feasibility of the infiltration test.

Table 23 – Main characteristics of SJS2 and characteristics during the infiltration test

Well characteristics	SJS2
Total Depth (m)	250
Casing diameter (m)	0-96 m- 356 mm; 96 - 252 - 250 mm
Infiltration test pump depth (m)	80
Q (L/s)	46 to 47
Water level (m)	45

Methodology for determining the groundwater flowpath

The experiment results were analysed using: (1) the data retrieved for the water level and electrical conductivity in the monitoring net (see below) and (2) the geophysical profiles with electrical resistance tomography.

The monitoring net consisted in:

- CTD divers (pressure, electrical conductivity, temperature) in CB well, CB1, CB2 and Mr. Lídio's well.
- Water level manual measurements whenever possible at: CB well, CB1, CB2 and Mr. Fernando's well.
- Manual control of water temperature, electrical conductivity and pH in CB well, CB1, CB2, Mr. Fernando's well, Mr. Luis's well and Mr. Caetano's well (3 times a day).
- Measurement of electrical conductivity at different depths in CB1 and CB2 (once a day).
- The four wells in the surrounding area previously referred, were used as control points, mainly to understand the natural variations of the system during the infiltration test, in order to isolate the infiltration effect in the CB well, CB1 and CB2.

The geophysical profiles were analysed using the same procedure above described for the tracer test of December 2015.

Results

The infiltration and tracer experiment has lasted 90 h plus recovery time, with a flow rate of 47 L/s. The water started to fill the well during the first 3.5 hours (April 20, from 14:07 to 17:35) and then it has overflowed to the stream, through the well by-pass.

The water has never reached the weir since it has infiltrated in the stream bed and into several sinkholes that were identified (Figure 121). Thus, this test allowed having a minimum infiltration value, but much higher infiltration capacity can be expected for this area.

Before finishing the experiment, the flow rate was diminished until it allowed stabilizing the piezometric level in the well (below the by-pass in order to ensure that the water only entered the CB well), and determining the maximum well infiltration capacity. This happened for 14 L/s flow rate, corresponding to a maximum infiltration rate in the well of about 385 m/d (considering the well area of 3.14 m^2). This value is about six times higher than the ones found at Campina de Faro aquifer, but

the latter did not reach the maximum value since the injected volume was lower than the infiltration capacity.

Figure 121 – Sinkholes identified at Cerro do Bardo during the MAR experiment

The remaining 33 L/s (47 L/s – 14 L/s) have left the well through the by-pass and have been disposed in the initially dry stream. This value is in accordance with the average flow rate measurements made in the stream and presented in Table 24.

Table 24 – Flow rate measured in the initial part of the stream formed by the injection water overflow

Date	Hour	Stream section (L/s)
	10:00	
23-04-2016	10:30	36
	18:30	34.8
24-04-2016	07:45	31.9

The water in the stream has further infiltrated into several sink-holes located in the stream floor of this karstic aquifer. Table 25 presents the measurements done in some major sinkholes at different periods.

Table 25 – Infiltration rates measured in the main sinkholes identified

Date	Hour	Sinkhole 1 (L/s)	Sinkhole 2 (L/s)
20-04-2016	17:30		3.20 - 3.32
21-04-2016	10:30		3.4
22-04-2016	11:30	4.60 - 4.68	
22-04-2016	11:40		4.95 - 5.30
23-04-2016	16:30	7.18 - 7.66	8.71 - 9.69
24-04-2016	07:30	5.9	15.26

Several other minor sink-holes are responsible for the infiltration of the remaining water.

Concerning the experiment results obtained from the monitoring piezometers, Figure 122 presents the depth to the water table for CB well, CB1 and CB2.

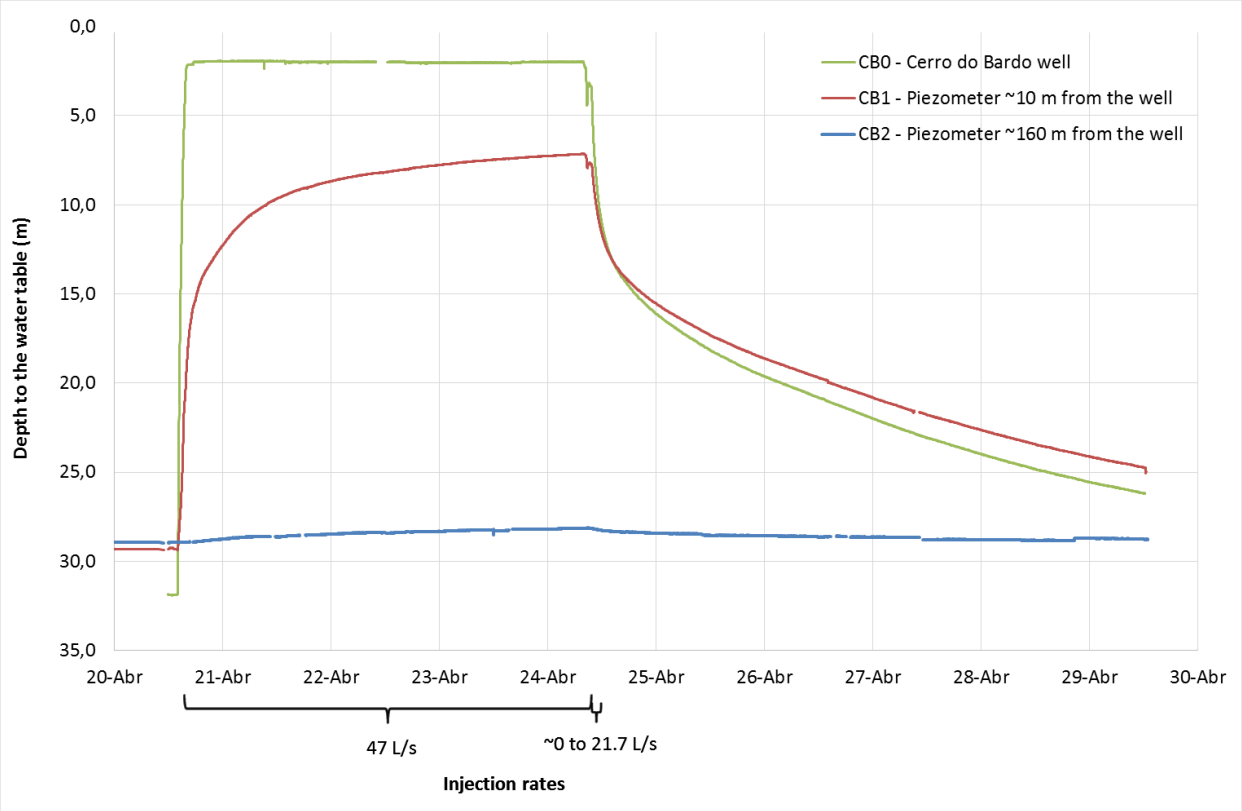

Figure 122 – Depth to the water table in CB well, CB1 and CB2 during the MAR experiment

It is possible to observe the similar response between CB well and CB1, both for the injection and the recovery period. Besides, CB2 also presents an increase of the piezometric level of about 0.8 m.

Figure 123 presents the results obtained for the electrical conductivity (EC) in the same points. It is possible to see that the EC reached a very high value in CB well (also because the probes might have been inside the salt, while it was dissolving) and this values rapidly decreased in CB1. CB2 has showed a very slight increase in its values (starting 10 hours after the beginning of the experiment) from 0.712 mS/cm to 0.752 mS/cm. The tracer has increased the regional level 40 µS/cm during approximately 3 days.

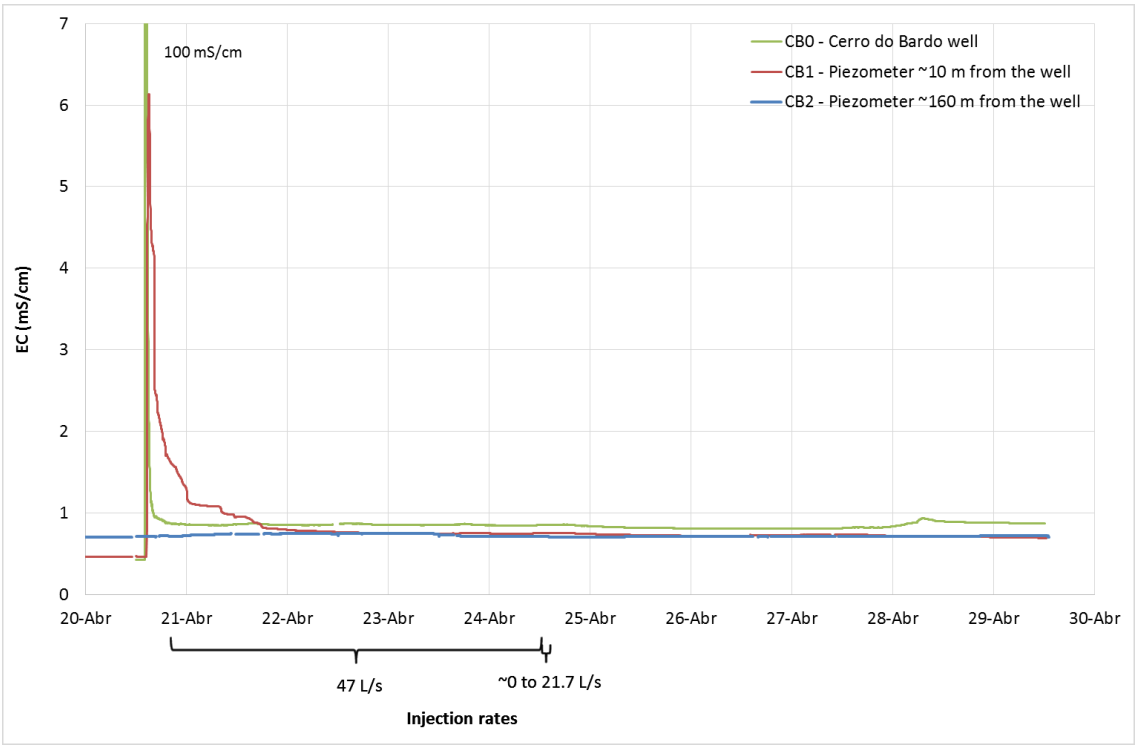

Figure 123 – Water electrical conductivity in CB well, CB1 and CB2 during the MAR experiment

These results, together with the geophysics, allow concluding that the flow direction is towards the weir, i.e. to the E.

The measurements done is the remaining monitoring wells have shown no clear effect on the well's EC, temperature or pH (Figure 124).

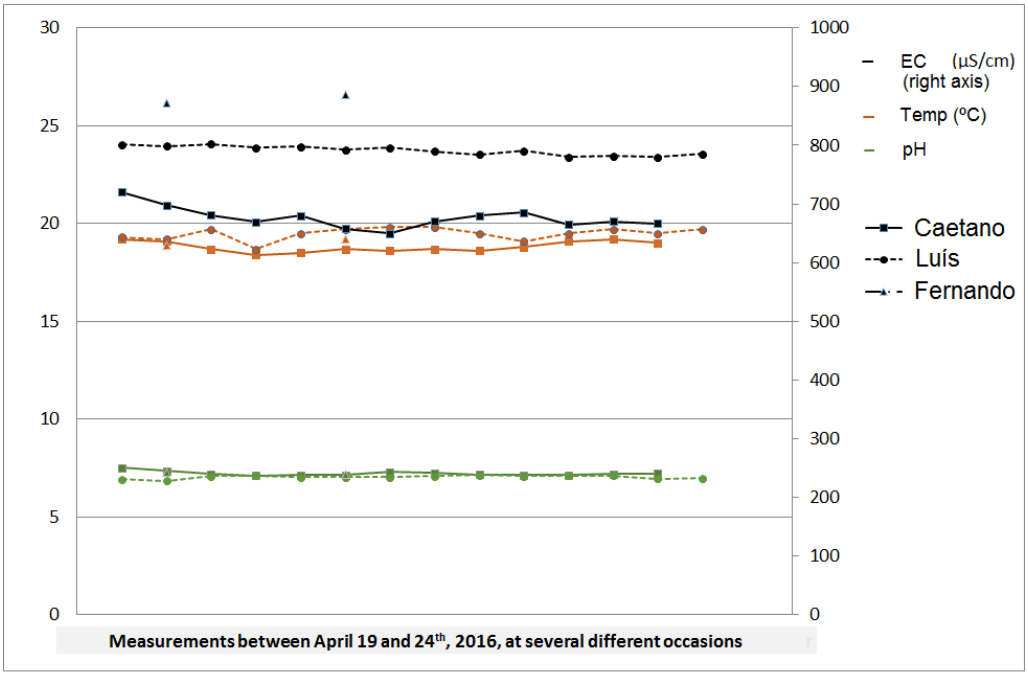

Figure 124 – Variation of EC, T and pH in three wells located in the vicinity of the Cerro do Bardo MAR experiment

In conclusion, this MAR infiltration and tracer test allowed confirming that the Cerro do Bardo DEMO Site:

- Is an adequate area to infiltrate surplus water coming from the three dams, when there is too much of it (wet years) and store it for dry times in Querença-Silves aquifer.
- The DEMO area has an infiltration capacity of at least 4060 m^3/d.
- The flow seems to have an east-southeaster direction.

The results from geophysics, which complement and validate the data from monitoring, are presented in D12.5 and D4.4 within the conceptual model of this site.

2.3 PT3: MELIDES AQUIFER, RIVER AND LAGOON (ALENTEJO)

2.3.1 Introduction and objective

PT3 – Melides aquifer, river and lagoon (Alentejo) aim is to use soil-aquifer-treatment (SAT-MAR) to remove rice field pollutants prior to their discharge in Melides lagoon. Aiming to contribute to solve this problem, and increasing aquifer recharge (MAR), a physical (sandbox) model was built in LNEC pavilions during MARSOL project. The results obtained in these tests have given the necessary knowledge to build in the future an *in situ* SAT-MAR facility.

2.3.2 Motivation for the site selection

Melides watershed and lagoon MARSOL case-study area was selected based on the following background considerations and advantages:

1. This is an area where relevant environmental quality problem (agriculture groundwater contamination), occurs during the summer period due to the rejection of paddy (rice) field contaminating nitrate and pesticide towards Melides coastal lagoon (Leitão *et al.*, 2012).
2. Via infiltrating some of the rejections from the paddy fields waste water in a new MARSOL facility site with appropriate MAR INNO-DEMO solutions an environmental water quality increase is expected.
3. A relevant amount of surface and groundwater data, including climate change water budget and groundwater recharge estimations is available, having been gathered on the Portuguese FCT sponsored PROWATERMAN project (http://www.lnec.pt/organizacao/dha/organizacao/dha/nre/estudos_id/PROWATERMAN).
4. A regional groundwater flow model has been developed by LNEC during PROWATERMAN project, allowing simulating real time aquifer responses, by MARSOL partner LNEC for the Melides aquifer.
5. Following the PROWATERMAN Final Workshop, organized by LNEC in Alentejo both at the University of Évora and in Grândola Municipality, MARSOL project actor APA Ambiente is supporting Melides MARSOL research and case-study objectives.

2.3.3 Geological/hydrogeological setting

The 60.84 km^2 Melides hydrographic basin is located in the coastal region of Alentejo. It may be divided in two different sectors (Monteiro *et al*., 2008; Novo and Oliveira, 2014): the upstream sector, of accidental relief, is developed on low permeability formations of Palaeozoic schists and greywackes; and the downstream sector, of plain relief inducing low to moderate drainage density, which is developed in Cenozoic sandy formations that overlay Jurassic carbonate units, belonging to the Sines aquifer system. The two sectors are separated by the Santo André's fault.

Surface flow dominates in the upstream sector, being reduced in the downstream sector to only a few streams that mainly transport surface flow generated in the upstream sector. Groundwater recharge predominates in the downstream sector. In the downstream sector the connection between the drainage network and the deep carbonate aquifer is made solely by the *Fonte dos Olhos* spring; in the rest of the sector only the upper aquifer is in direct connection with the drainage network that receives the discharge water of the aquifer.

Melides lagoon, located downstream in the hydrographic basin, constitutes a coastal ecosystem partially dependent on groundwater (Lobo Ferreira *et al.*, 2013). It is a receptor of the total amount of pollutant load of surface origin collected by the drainage network of the Ribeira de Melides stream, as it is situated in the downstream part of this hydrographic basin, and also of the pollutant load of groundwater flow that discharges to the surface water network or directly to the lagoon.

2.3.4 Developing the infrastructures

In PT3 it was decided that the planned water quality control would be made using a SAT-MAR prototype basin not placed *in situ* but at a large laboratory scale on a physical (sandbox) model at LNEC (Figure 125).

Figure 125 – LNEC Physical (sandbox) model construction

This sandbox model was divided into three sections (Figure 126) to test the adsorption and degradation capacity of three different soil mixtures. Figure 127 presents a schematic diagram of the sandbox model dimensions.

Figure 126 – LNEC physical (sandbox) model sections, A, B and C

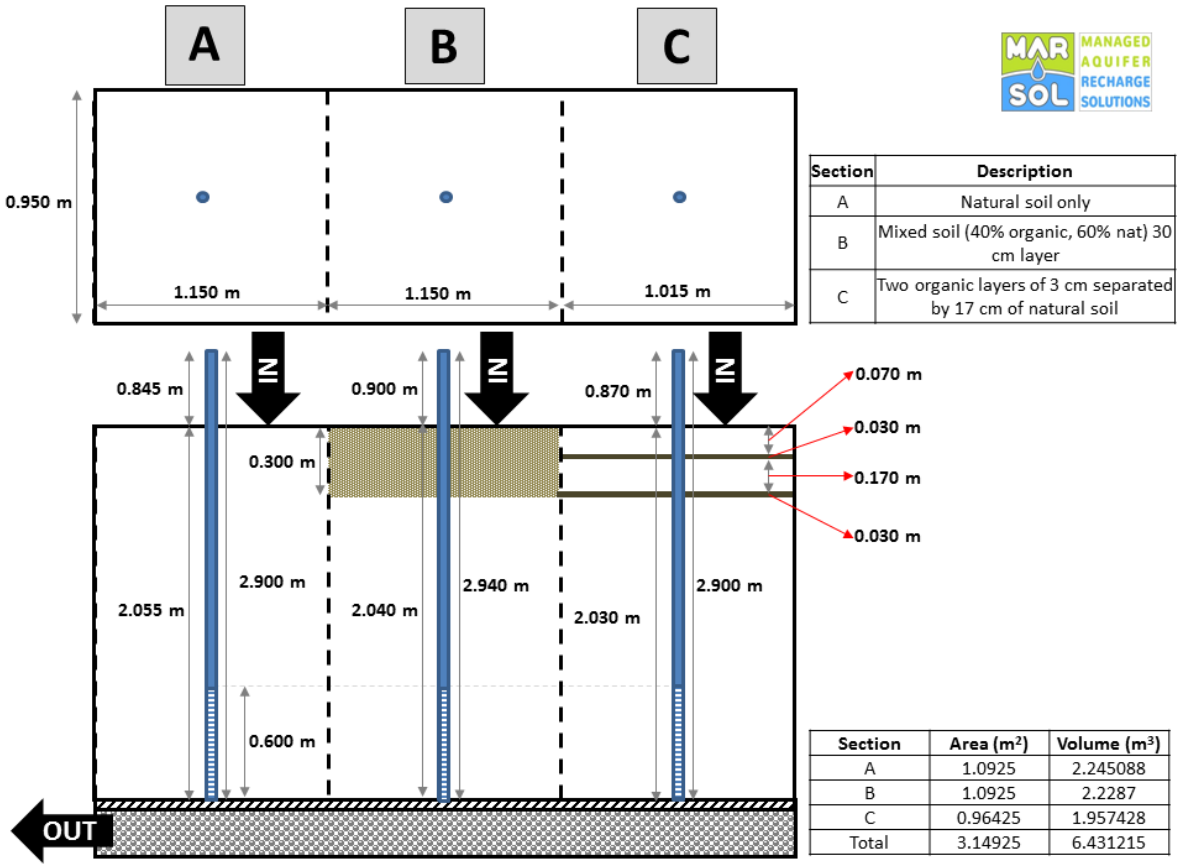

Section	Description
A	Natural soil only
B	Mixed soil (40% organic, 60% nat) 30 cm layer
C	Two organic layers of 3 cm separated by 17 cm of natural soil

Section	Area (m^2)	Volume (m^3)
A	1.0925	2.245088
B	1.0925	2.2287
C	0.96425	1.957428
Total	3.14925	6.431215

Figure 127 – Schematic diagram of the physical (sandbox) model dimensions

2.3.5 Investigation experiments and monitoring

Considering the results from the soil-column experiments conducted at LNEC LASUB facilities in May and June 2014 to determine the hydraulic characteristics of the Melides soils (from a depth of 5 to 20 and 20 to 30 cm layers at the approximate location of the infiltration site), it was concluded that the soil has a permeability value adequate for SAT, with an average Darcy permeability ranging from 0,9 to 4,8 m/d at Melides, the latter for a 20-30 cm layer where permeability increase significantly.

Melides soil was acquired and used to fill the sandbox model, accordingly to the scheme presented in Figure 127.

Two spiked tracer experiments, with fertilizers and hydrocarbons, were done in May/June 2016. In those experiments it was assessed the:

- Water infiltration capacity.
- Water quality in the soil-water, at two depths, 30 cm and 60 cm, using capsules (from PRENART Equipment ApS) to access SAT treatment (Table 26).
- Water quality in the saturated zone (*in situ*: T, EC, pH, redox; chemical parameters: see Table 26).
- Soil at 30 cm and 60 cm (Table 26).

These results have been further developed under WP12, Task 12.5 and are reported in D12.5.

Table 26 – Sampling protocol for the physical (sandbox) model

MAR SOL MANAGED AQUIFER RECHARGE SOLUTIONS

Sampling protocol for the physical (sandbox) model

Sample #1 2016/05/30	# Sampling devices	Water								Soil					
		NO_3^-	NO_2^-	NH_4^+	Ca, Na, Mg, K	SO_4^{2-}	Cl	HCO3	TH	NO_3^-	NO_2^-	NH_4^+	PO_4^{3+}	SO_4^{2-}	TH
Vadose - basin															
Wells	3	x	x	x		x	x	x	x						
Infiltration water	1	x	x	x	x	x	x	x	x						
Soil															

Sample #2 to sample #7	# Sampling devices	Water								Soil					
		NO_3^-	NO_2^-	NH_4^+	Ca, Na, Mg, K	SO_4^{2-}	Cl	HCO3	TH	NO_3^-	NO_2^-	NH_4^+	PO_4^{3+}	SO_4^{2-}	TH
Vadose - basin															
Wells	3	x	x	x		x	x	x	x						
Infiltration water															
Soil															

Sample #8	# Sampling devices	Water								Soil					
		NO_3^-	NO_2^-	NH_4^+	Ca, Na, Mg, K	SO_4^{2-}	Cl	HCO3	TH	NO_3^-	NO_2^-	NH_4^+	PO_4^{3+}	SO_4^{2-}	TH
Vadose - basin	6	x	x	x		x	x	x	x						
Wells	3	x	x	x		x	x	x	x						
Infiltration water															
Soil															

Sample #9 to 17	# Sampling devices	Water								Soil					
		NO_3^-	NO_2^-	NH_4^+	Ca, Na, Mg, K	SO_4^{2-}	Cl	HCO3	TH	NO_3^-	NO_2^-	NH_4^+	PO_4^{3+}	SO_4^{2-}	TH
Vadose - basin															
Wells	3	x	x	x		x	x	x	x						
Infiltration water															
Soil															

Sample #18	# Sampling devices	Water								Soil					
		NO_3^-	NO_2^-	NH_4^+	Ca, Na, Mg, K	SO_4^{2-}	Cl	HCO3	TH	NO_3^-	NO_2^-	NH_4^+	PO_4^{3+}	SO_4^{2-}	TH
Vadose - basin	6	x	x	x	x	x	x	x	x						
Wells	3	x	x	x	x	x	x	x	x						
Infiltration water															
Soil	6									o	o	o	o	o	x

Sample #19 to 20 2016/06/02 and 03	# Sampling devices	Water								Soil					
		NO_3^-	NO_2^-	NH_4^+	Ca, Na, Mg, K	SO_4^{2-}	Cl	HCO3	TH	NO_3^-	NO_2^-	NH_4^+	PO_4^{3+}	SO_4^{2-}	TH
Vadose - basin	6	x	x	x		x	x	x	x						
Wells	3	x	x	x		x	x	x	x						
Infiltration water															
Soil															

Legend: x - samples to IST

o - samples to AmbiPar Control

3. FINAL REMARKS

The development of all three DEMO sites was performed accordingly to the Description of Work. Table 27 presents a synthesis of all experiments done and their timings.

In synthesis, see also Table 28:

In PT1 – Rio Seco and Campina de Faro aquifer system (Algarve) – the main goal is improve the groundwater quality heavily contaminated with nitrates (vulnerable zone), mainly due to agriculture bad practices. For this purpose, surface water surplus generated during strong rain events is being used in several infiltration basins, existing (PT1_1) and constructed during MARSOL (PT1_2), in the Rio Seco river bed to push the nitrate plume towards the sea. Furthermore, to assess the potential impact of water recharge at a regional scale, and its improvement in the groundwater quality status, typical large-diameter wells have been tested as a potential MAR facility (PT1_3). In the future, the water to be used would be collected in the greenhouse roofs during rain events. PT1_1 and PT1_2 sites were built and tested as foreseen and keep functioning. PT1_3 was tested but needs definitive water supply infrastructure, which can be done by the Portuguese Water Authority.

In PT2 – Querença-Silves limestone karstic aquifer system (Algarve) – there are two main sub-areas and two goals: (1) develop a MAR-SAT (managed aquifer recharge – soil aquifer treatment) system to improve the water quality of treated effluents from São Bartolomeu de Messines waste water treatment plant (WWTP) (PT2_4), which discharges into Ribeiro Meirinho river (PT2_5) that in turn recharges the karstic aquifer, and (2) increase groundwater storage at Cerro do Bardo karstic area using wet-years surface water surplus stored in Águas do Algarve water supply Odelouca and Funcho reservoirs to increase the water availability in dry years and facilitate downstream water supply. PT2_4 infrastructures were concluded in July 2016 and experiments successfully ended in December 2016. PT2_6 Cerro do Bardo infrastructures were built and tested as foreseen. Permanent water supply pipe (circa 2 km) can now be done by Águas do Algarve, the water supply company that manages water in the area.

In PT3 – Melides aquifer, river and lagoon (Alentejo) – the main goal is to use soil-aquifer-treatment (SAT-MAR) to remove rice field contaminants prior to their discharge in Melides lagoon. Aiming to contribute to solve this problem, and increasing aquifer recharge (MAR), a physical (sandbox) model was built in LNEC pavilions during MARSOL project. The results obtained with the PT3 sandbox model tests have given the necessary knowledge to build and *in situ* SAT-MAR facility. The results were presented in Deliverable 12.5.

Table 27 – Gantt chart with all the PT experiments performed during MARSOL project

ID	Task Name	Start	Finish (including monitoring period)	Days
1	**PT1: RIO SECO AND CAMPINA DE FARO AQUIFER SYSTEM (ALGARVE)**	01-07-2014	01-12-2016	633d
2	PT1_1: Clogging test in one GABARDINE basin, 1st July 2014	01-07-2014	01-07-2014	1d
3	PT1_1 and PT1_2: Infiltration test in all three basins, 29th and 30th September, 2014	29-09-2014	08-10-2014	8d
4	PT1_2: Tracer test in MARSOL basin, 13th and 14th October, 2014	13-10-2014	20-10-2014	6d
5	PT1_2: Small infiltration test during Mid-Term meeting, 24th June 2015	24-06-2015	26-06-2015	3d
6	PT1_2: Natural recharge episodes	01-09-2015	08-02-2017	377d
7	PT1_3: Infiltration in large wells, 1st October 2014	01-10-2014	01-10-2014	1d
8	**PT2: QUERENÇA-SILVES LIMESTONE KARSTIC AQUIFER SYSTEM (ALGARVE)**	01-04-2014	01-12-2016	698d
9	PT2_4/5: S. Bartolomeu de Messines SAT basins	15-09-2016	30-11-2016	55d
10	PT2_6: Cerro do Bardo Infiltration test, April 1st, 2014	01-04-2014	01-04-2014	1d
11	PT2_6: Cerro do Bardo tracer test, December 15-16th, 2014	15-12-2014	17-12-2014	3d
12	PT2_6: Cerro do Bardo tracer and infiltration large test, April 20-24th, 2016	20-04-2016	27-04-2016	6d
13	**PT3: MELIDES AQUIFER, RIVER AND LAGOON (ALENTEJO)**	10-11-2014	06-06-2016	411d
14	PT3: Physical (sandbox) infiltration and tracer tests	30-05-2016	06-06-2016	6d

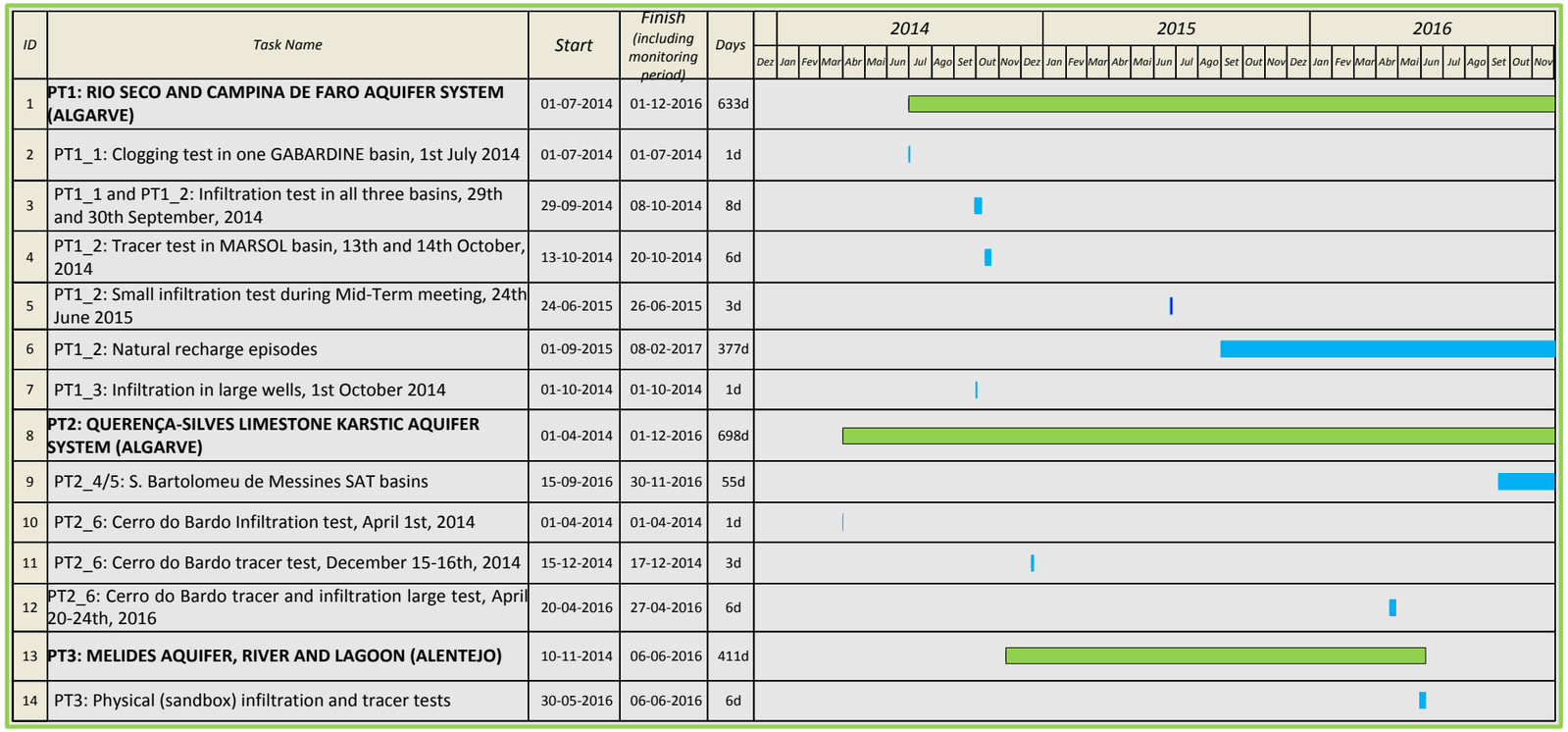

Table 28 – Synthesis of all the PT experiments performed during MARSOL project, their purposes and details

Aim	MAR facility type	Infraestructure		Test		Injection		Infiltration		
		Type	Area	Volume	Period	Flow rate				
Improve the groundwater quality heavily contaminated with nitrates			m^2	m^3		m^3/d	L/s	m/d	m^3/d	m^3/h
Assess the MAR river infiltration basin clogging effect after 7 years	River infiltration basin	Basin	100	-	5 h	103	1,19	1,03	103	4,3
Assess the infiltration potential of the whole MAR river bed infiltration basins system	River infiltration basin	Basin	401	1189,4	38 h	456-518	5,3-6	1,51-1,72	641,6	26,7
Assess the infiltration capacity of MARSol basin; dispersion, velocity	River infiltration basin	Basin	201	-	10 h	375	4,34	1,87	375	15,6
Assess the infiltration capacity of Upstream Gabardine basin	River infiltration basin	Basin	100	-	9 h	250	2,89	2,50	250	10,4
Assess large well's infiltration capacity	Wells	Well	15,9	145,3	249 min	840	9,72	52,83	840	35,0
Improve the water quality of treated effluents and increase groundwater storage										
Improve the water quality of treated effluents from a WWTP	SAT-MAR basins	SAT basin	210	on going	on going	300	3,47	-	-	-
Assess CB well infiltration capacity	Well	Well	3,14	40	19:26 min	3004,8	34,78	956,94	3004,8	125,2
Assess main flow direction	Well	Well	3,14	90	3,48 h	561	6,49	178,66	561	23,4
Assess all area infiltration capacity and main flow direction	Well and karstic pervious site	Well and area	2000	15228	90 h	4060	46,99	2,03	4060	169,2
Improve the water quality using SAT to remove rice field contaminants										
Assess Melides soil permeability and the soil's contaminants retention and/or degradation capacity	SAT physical sandbox model	SAT sandbox model	3,15	6,43	24 h	9,25	0,11	2,94	9,25	0,39

BIBLIOGRAPHY

Almeida, C. (1985) – Hidrogeologia do Algarve Central. Dissertação para obtenção do grau de Doutor em Geologia. Departamento de Geologia da Fac. Cienc. Univ. Lisb. Lisboa, 1985, 333p.

Almeida, C.; Mendonça, J.L.; Jesus, M.R.; Gomes, A.J. (2000) – Sistemas Aquíferos de Portugal Continental, Relatório. INAG, Instituto da Água. Lisboa. Doc. Electr. CD-ROM.

Andrade, G. (1989) – Contribuição para o Estudo da Unidade Hidrogeológica Tôr-Silves. Dissertação para Obtenção do Grau de Mestre em Geologia Económica e Aplicada. Departamento de Geologia da FCUL.

Cooper, H.H. and Jacob, C.E. (1946) – A generalized graphical method for evaluating formation constants and summarizing well field history, Am. Geophys. Union Trans., vol. 27, pp. 526-534.

Diamantino, C. (2009) – Recarga artificial de aquíferos: aplicação ao sistema aquífero da Campina de Faro. Tese de Doutoramento. FCUL.

Diamantino C.; Lobo-Ferreira, J.P.; Leitão T. (2007) – Artificial aquifer recharge experiments in the Portuguese Campina de Faro Case-Study area. In Proceedings XXXV IAH Congress, Groundwater and Ecosystems, Ribeiro, L., Chambel, A., Condesso de Melo, M.T. Eds, 17 a 21 de Setembro de 2007, Lisboa, 10 pp.

Hugman, R.; Stigter, T. and Monteiro, J.P. (2013) – The importance of temporal scale when optimizing abstraction volumes for sustainable aquifer exploitation: a case study in semi-arid South Portugal.Journal of Hydrology. Available online 13 March 2013.

Kessler, H. (1965) – Water balance investigations in the karstic regions of Hungary. In: AIHS-UNESCO Symposium on Hydrology of Fractured Rocks, Dubrovnik, Croatia.

Leitão, T.E.; Oliveira, L.S.; Lobo Ferreira, J.P.; Vilhena, J.; Almeida, A.; Tomé, M.; Pires, A.M. (2012) - Análise Integrada da Qualidade da Água e dos Ecossistemas na Bacia Hidrográfica da Ribeira de Melides. 11.º Congresso da Água – Valorizar a água num contexto de incerteza, organizado pela APRH, Porto, 6-8 de Fevereiro de 2012, 15 pp.

Leitão, T. E.; Mota, R.; Novo, M.; Lobo Ferreira, J. P. C. (2014) - Combined Use of Electrical Resistivity Tomography and Hydrochemical Data to Assess Anthropogenic Impacts on Water Quality of a Karstic Region: A Case Study from Querença-Silves, South Portugal, Environmental Processes. An International Journal, ISSN 2198-7491, Volume 1, Number 1. (2014) 1:43–57, DOI 10.1007/S40710-014-0002-1.

Lobo Ferreira, L.F.; Diamantino, C.; Moinante, M.J.; Oliveira M.M.; Leitão, T.E.; Henriques, M.J., Medeiros, A., Dimitriadis, K., Styllas, M., Soupilas, T., Maheras, P., Anagnostopoulou, C., Tolika, K.,Vafiadis, M., Machairas, C., Sanchez-Vila, X., Barbieri, M., Bensabat, J., Hadad, A., Rabi, A.,Tamimi, A. (2006a) - Deliverable D51: "Test Sites and their characteristics" (18 MG).

Lobo-Ferreira, J.P.C.; Diamantino, C.; Oliveira, M.; Leitão, T.; Moinante, M.J.; Henriques, M.J.; Medeiros, A.; Charneca, N.; Mota, R.; Oliveira, M. (2006b) – First Year Activity Report on Work Package 5.

Lobo Ferreira, J.P., Novo, M.E., Oliveira, L. (2013) – Análise da Contribuição das Fontes Poluentes para a Carga Total de Nitratos e Fosfatos que Afluem à Lagoa de Melides por Transporte Subterrâneo. 11º SILUSBA "A Cooperação para a Água", Maputo, Moçambique.

Lopes, F.M.V. (2006) – A Geologia e a Génese do relevo da Rocha da Pena (Algarve, Portugal) e o seu enquadramento educativo, Dissertação de mestrado, Faculdade de Ciências do Mar e do Ambiente, Universidade do Algarve, Faro, 114 pp.

Manuppella, G. (Coord.) (1992) – Carta Geológica da Região do Algarve, escala 1/100.000, Folha Ocidental, Serv. Geol. Portugal, Lisboa.

Manuppella, G. (coordenação), Ramalho, M.; Rocha, R.; Marques, B.; Antunes, M.T.; PAIS, J.; Gonçalves, F.; Carvalhosa, A. (1993) – Carta geológica da região do Algarve, folha Ocidental, na escala 1:100 000. Serviços Geológicos de Portugal.

Mendonça L.; Almeida C. (2003) – Exploitation of groundwater resources: the example of aquifer system Querença-Silves. Recursos Hídricos Journal 24(3):53–61, In: e-geo.ineti.pt/edicoes_online/obras/costa_almeida/tp067.pdf. (in Portuguese: A Exploração de Recursos Hídricos Subterrâneos: O Exemplo do Sistema Aquífero Querença-Silves).

Monteiro, J.P.; Vieira, J.; Nunes, L.; Younes, F. (2006) – Inverse Calibration of a Regional Flow Model for the Querença-Silves Aquifer System (Algarve-Portugal). Integrated Water Resources Management and Challenges of the Sustainable Development. International Association of Hydrogeologists, IAH. Marrakech. pp 44, doc. Elect. CD-ROM - 6pp.

Monteiro, J.P.; Ribeiro, L.; Reis, E.; Martins, J.; Matos Silva, J. (2007) – Modelling Stream-Groundwater Interactions in the Querença-Silves Aquifer System. XXXV AIH Congress. Groundwater and Ecosystems. Lisbon. Portugal. pp 41-42, doc. Elect. in CD Rom. 10pp.

Monteiro, J. P.; Chambel, A.; Martins, J. (2008) - Conceptual and Numerical Flow Model of the Sines Aquifer System (Alentejo, South Portugal). International Groundwater Symposium. International Association of Hydraulic Engineering and Research (IAHR). Istanbul-Turkey. p.38 (abstract) and doc. elect. CD-Rom 9pp

Novo, M.E.; Oliveira, L.G.S. (2014) – Uso de cenários de alterações climáticas para previsão do estado de aquíferos e EDAS. Caso de Estudo: Melides. Revista Recursos Hídricos. Associação Portuguesa dos Recursos Hídricos. Volume 35, Nº 2, novembro 2014.

Nunes, G.; Monteiro J.P.; Martins, J. (2006) – Quantificação do Consumo de Água Subterrânea na Agricultura por Métodos Indirectos – Detecção Remota. IX Encontro de Utilizadores de Informação Geográfica (ESIG). 15 - 17 de Novembro, Tagus Park, Oeiras. Doc. Electrónico em CD-ROM. 15pp.

Oliveira L.S. (2007) – Soluções para uma gestão adequada de bacias hidrográficas e de sistemas aquíferos, em cenários de escassez hídrica extrema: Aplicação ao sistema aquífero Querença-Silves (Algarve) no âmbito da Acção de Coordenação ASEMWaterNet. Dissertação de Mestrado apresentada no IST.

Oliveira, M.M.; Oliveira L.S.; Lobo Ferreira J.P. (2008) – Estimativa da recarga natural no sistema aquífero de Querença-Silves (Algarve) pela aplicação do modelo BALSEQ_MOD. In 9.º Congresso da Água - Água: desafios de hoje, exigências de amanhã, Cascais (Portugal), 2 - 4 Abril 2008, CD.

Oliveira M.M.; Oliveira L.S. (2012) – Water, aquatic ecosystems and human activity project PROWATERMAN. 5th Thematic Report. Recharge and direct runoff assessment of Querença-Silves aquifer system catchment area. Report 180/2012-NAS. LNEC, pp. 108. In Portuguese: Água, Ecossistemas Aquáticos e Atividade Humana. Projeto PROWATERMAN. Quinto Relatório Temático - Estimativa da recarga e do escoamento direto na área de drenagem do sistema aquífero Querença-Silves.

Oliveira L.G.S.; Leitão T.E.; Lobo Ferreira J.P.; Oliveira M.M.; Novo M.E. (2011) – Água, Ecossistemas Aquáticos e Actividade Humana – Projecto PROWATERMAN. Terceiro Relatório Temático – Resultados Quantitativos e Qualitativos das Campanhas de 2011 e Balanços Hídricos. Referência do Projecto n.º PTDC/AACAMB/105061/2008, 2011, 99 pp.

Reis E.; Gago C.; Borges G.; Matos M.; Cláudio A.; Mendes E.; Silva A.; Serafim J.; Rodrigues A.; Correia S. (2007) – Contribution to water budget evaluation of the main aquifer systems of Algarve. Ministry of Environment and Regional Development. CCDR, pp 41. In Portuguese: Contribuição para o cálculo do balanço hídrico dos principais sistemas aquíferos do Algarve.

Salvador, N.; Monteiro, J. P.; Hugman, R.; Stigter, T. Y.; and Reis, E. (2012) – Quantifying and modelling the contribution of streams that recharge the Querença-Silves aquifer in the south of Portugal, Nat. Hazards Earth Syst. Sci., 12, 3217-3227, doi:10.5194/nhess-12-3217-2012.

Stigter, T.Y.; Carvalho Dill, A.M.M. (2000) – Limitações do Modelo DRASTIC - Aplicação a duas regiões algarvias contaminadas por nitratos. 5º Congresso da Água, "A água e o desenvolvimento sustentável. Desafios para o novo século", organized by APRH. Lisboa, Culturgest, 25 a 29 September 2000, 12 pp.

Stigter, T.Y. (2005) – Integrated Analysis of Hydrogeochemistry and Assessment of Groundwater Contamination Induced by Agricultural Practices. PhD dissertation presented to Technician University of Lisbon.

Stigter, T.Y.; Monteiro, J.P.; Nunes, L.M.; Vieira, J.; Cunha, M.C. ; Ribeiro, L.; Nascimento, J. and Lucas, H. (2009) – Screening of sustainable groundwater sources for integration into a regional drought-prone water supply system. Hydrol. Earth System Sci. 13, 1–15.

Terrinha, P. (1998) – Structural Geology and Tectonic Evolution of the Algarve Basin, South Portugal, Ph.D., University of London, London, 430 pp., 1998.

Vieira, J.; Monteiro, J. P. (2003) – Atribuição de propriedades a redes não estruturadas de elementos finitos triangulares (Aplicação ao Cálculo da Recarga de Sistemas Aquíferos do Algarve). In: Ribeiro, L. and Peixinho de Cristo, F. (eds.) As Águas Subterrâneas no Sul da Península Ibérica. Assoc. Intern. Hidrog. APRH publ., pp183-192.

Vilanova, E.; Miret, M., Molinero, J. and Sprenger, C. (2015) Decision trees for MAR impact evaluateio: Identification of optimum conditions to face emerging pollutants removal in MAR systems. D12.1 report. DEMEAU FP7 (project nº 308339).